

**EVALUATION OF THIN FILM NANOCOMPOSITE MEMBRANE
INCORPORATED WITH CARBON-BASED QUANTUM DOTS**

ERIC SEOW KAI JUN


**A project report submitted in partial fulfilment of the
requirements for the award of Bachelor of Engineering
(Honours) Chemical Engineering**

**Lee Kong Chian Faculty of Engineering and Science
Universiti Tunku Abdul Rahman**

May 2021

DECLARATION

I hereby declare that this project report is based on my original work except for citations and quotations which have been duly acknowledged. I also declare that it has not been previously and concurrently submitted for any other degree or award at UTAR or other institutions.

Signature : 

Name : Eric Seow Kai Jun

ID No. : 1603117

Date : 03 May 2021

APPROVAL FOR SUBMISSION

I certify that this project report entitled “**EVALUATION OF THIN FILM NANOCOMPOSITE MEMBRANE INCORPORATED WITH CARBON-BASED QUANTUM DOTS**” was prepared by **ERIC SEOW KAI JUN** has met the required standard for submission in partial fulfilment of the requirements for the award of Bachelor of Engineering (Honours) Chemical Engineering at Universiti Tunku Abdul Rahman.

Approved by,

Signature

:



Supervisor

:

Ir. Dr. Chong Woon Chan

Date

:

03 May 2021

The copyright of this report belongs to the author under the terms of the copyright Act 1987 as qualified by Intellectual Property Policy of Universiti Tunku Abdul Rahman. Due acknowledgement shall always be made of the use of any material contained in, or derived from, this report.

© 2021, Eric Seow Kai Jun. All right reserved.

ACKNOWLEDGEMENTS

I would like to express my sincere gratitude to my research supervisor, Ir. Dr. Chong Woon Chan for her invaluable advice, guidance, and her patience throughout this final year project. Without her guidance and supervision, this study would not have been possible.

Besides, I would like to express my gratitude to my loving parents and friends for the motivation and encouragement towards the completion of the project.

ABSTRACT

Water crisis is a severe global matter. In order to mitigate this matter, filtration with conventional polymeric membrane have been developed as it offers great flexibility, accessibility, and is cost-effective. However, conventional filtration membranes suffer from limitations such as membrane fouling. In this study, the fabrication method, characteristic and performance of carbon-based quantum dots incorporated thin film nanocomposite (TFN) nanofiltration (NF) and reverse osmosis (RO) membranes from previous works were evaluated. The carbon-based quantum dots included in this review are carbon quantum dots, graphene quantum dots and graphene oxide quantum dots. The introduction of functionalized carbon-quantum dots was found to have significant effect on the membrane characteristic and performance. The studies showed good compatibility of the quantum dots with a wide variety of amine and acyl chloride monomers. In addition, carbon-based quantum dots had significant effects on the membrane characteristics. The surface roughness was inconsistent across the reviewed journals mainly due to the difference of the size of the quantum dot. Besides, oxygen-containing functional groups were observed after the introduction of carbon-based quantum dots which indicated the improved hydrophilicity. The membrane flux was improved significantly ranging from 1.5 to 6.8 times with a little amount of carbon-based quantum dots. Furthermore, the addition of carbon-based quantum dots into the PA matrix also helped to overcome the conventional limitation of filtration membrane, which is membrane fouling. Moreover, the surface charge of the membranes also increased which enhanced the membrane antifouling properties. All in all, it shows that carbon-based quantum dots are suitable to be incorporated into TFN membranes in terms of filtration performance, regardless of the type of filtration process. Nevertheless, most of the previous studies included in this work are limited to laboratory scale, where the consideration for industrial application such as the large-scale synthesis of carbon-based quantum dots and fabrication of TFN membranes, as well as the maintainability of the membrane have not been investigated fully.

TABLE OF CONTENTS

DECLARATION		i
APPROVAL FOR SUBMISSION		ii
ACKNOWLEDGEMENTS		iv
ABSTRACT		v
TABLE OF CONTENTS		vi
LIST OF TABLES		viii
LIST OF FIGURES		ix
LIST OF SYMBOLS / ABBREVIATIONS		xii
 CHAPTER		
1	INTRODUCTION	1
	1.1 Background	1
	1.2 Problem Statement	4
	1.3 Aims and Objectives	5
	1.4 Importance of Study	5
	1.5 Scope and Limitation of Study	7
	1.6 Outline of the Study	7
2	LITERATURE REVIEW	8
	2.1 Properties of Carbon-based Quantum Dots	8
	2.1.1 Structural Properties	8
	2.1.2 Optical Properties	9
	2.2 Carbon-based Quantum Dots Synthesis Methods	13
	2.2.1 Top-down Methods	14
	2.2.2 Bottom-up Methods	16
	2.3 Application of Carbon-based Quantum Dots	24
	2.4 Nanofiltration and Reverse Osmosis	25
	2.4.1 Retention Mechanisms of Nanofiltration	27
	2.4.2 Retention Mechanisms of Reverse Osmosis	29
	2.5 Thin Film Composite Membranes	30

2.5.1	Thin Film Composite Membrane Fabrication	30
2.6	Thin Film Nanocomposite Membrane Modification	36
2.6.1	Interfacial Polymerization (IP)	36
2.6.2	Grafting Polymerization	37
3	METHODOLOGY AND WORK PLAN	47
3.1	Research Methodology	47
3.2	Work Plan	47
3.2.1	Investigation Phase	48
3.2.2	Interpretation Phase	50
3.2.3	Presentation Phase	52
4	RESULTS AND DISCUSSION	53
4.1	Incorporation of Carbon-based Quantum Dots Nanoparticles in Membrane	53
4.2	Carbon-based Quantum Dots Modified Thin Film Nanocomposite (TFN) Membranes	54
4.2.1	Preparation of Carbon-based Quantum Dots Nanofiltration Membrane	54
4.2.2	Preparation of Carbon-based Quantum Dots Reverse Osmosis Membrane	61
4.2.3	Others Methods	64
4.3	Characterization of Carbon-based Quantum Dots Incorporated Thin Film Nanocomposite (TFN) Membranes	66
4.3.1	Surface Morphology Study	66
4.3.2	Functional Groups Characterization	71
4.3.3	Water Contact Angle and Surface Charge	75
4.4	Effect on Performance	82
4.4.1	Nanofiltration	82
4.4.2	Reverse Osmosis	86
	CONCLUSIONS AND RECOMMENDATIONS	96
5.1	Conclusions	96
5.2	Recommendations for Future Work	97
	REFERENCES	98

LIST OF TABLES

Table 2.1:	Summary of the Advantages of Carbon-based Quantum Dots (Singh et al., 2018)	13
Table 2.2:	Types of Amino Acids and the Respective Colour and Diameter of CQDs (Wei et al., 2014)	18
Table 2.3:	Comparison Between Different Synthesis Methods (Singh et al., 2018; Chen et al., 2018)	21
Table 2.4:	Quantum Yield of Carbon-based Quantum Dots from Different Synthesis Methods	23
Table 2.5:	General Comparison between Membrane Processes (Shon et al., 2013; Abdel-Fatah, 2018)	27
Table 2.6:	Different Monomers for TFC Membrane Synthesis (Lau et al., 2012)	33
Table 2.7:	Interfacial Polymerization Technique Used in Preparing Polyamide Thin Film Nanocomposite (PA TFN) Membranes	43
Table 2.8:	Grafting Polymerization Techniques Used in Preparing Polyamide Thin Film Nanocomposite (PA TFN) Membranes	44
Table 3.1:	Differences between Qualitative and Quantitative Research Approaches (Apuke, 2017)	51
Table 4.1:	Overall Comparison of the Incorporation Methods of Carbon-based Quantum Dots (Fang, Xu and Wu, 2013)	65
Table 4.2:	Surface Roughness of TFC and TFN Membranes Obtained from AFM	68
Table 4.3:	Chemical Composition of the TFN Membranes Determined from the XPS Spectra (Sun and Wu, 2018)	72
Table 4.4:	XPS Analyses of the TFC and TFN Membranes	73
Table 4.5:	Separation Performance of Carbon-based Quantum Dots Incorporated TFN NF Membranes	89
Table 4.6:	Separation Performance of Carbon-based Quantum Dots Incorporated TFN RO Membranes	94

LIST OF FIGURES

Figure 1.1:	Schematic Representation of Membrane Barrier Performances (Ostarcevic et al., 2018)	2
Figure 2.1:	Structure of a Typical Carbon-based Quantum Dots	8
Figure 2.2:	Absorbance of (a) CQDs (Wang and Hu, 2014), (b) GQDs (Tabish and Zhang, 2019), and (c) GOQDs (Lu et al., 2017) at Different Wavelength	10
Figure 2.3:	Aqueous Solution of CQDs Passivated with PEG _{1500N} Excited at Different Wavelength (Wang et al., 2015)	11
Figure 2.4:	Photoluminescence Colour of GQDs with Different Sizes at 365 nm UV Light (Li et al., 2015a)	11
Figure 2.5:	Summary of the Synthetic Methods of Carbon-based Quantum Dots (Singh et al., 2018)	14
Figure 2.6:	Comparison of Schematic Spectrum between Different Membrane Processes (Maddah et al., 2018)	26
Figure 2.7:	Interaction Between MPD and TMC to Form PA Selective Layer (Lau et al., 2012)	31
Figure 2.8:	Rejection of Different Salts by the Different Modified Membranes (Zhong et al., 2012)	38
Figure 3.1:	Illustration of the General Work Plan of This Study	48
Figure 3.2:	Main Page of Mendeley Desktop	50
Figure 4.1:	Typical Carbon-based Nanoparticles Incorporated Thin Film Nanocomposite Membrane (Zhao and Chung, 2018)	54
Figure 4.2:	Schematic Diagram of the Methods to Fabricate the CQDs-NH ₂ -modified TFN Membranes (Guo et al., 2021)	55
Figure 4.3:	Schematic Diagram of the Preparation of TFN NF Membrane (Yang et al., 2020)	55
Figure 4.4:	The Severity of Concentration Polarization on Different Membrane Surfaces (Shao et al., 2020)	56
Figure 4.5:	Illustration of the Preparation of GOQDs Incorporated TFN Membranes (Zhang et al., 2017)	57

Figure 4.6:	General Flow of the Preparation of the GQDs Incorporated TFN Membranes (Bi et al., 2018)	58
Figure 4.7:	Preparation of L-aspartic Acid Functionalized GQDs incorporated TFN Membranes (Wu et al., 2021)	59
Figure 4.8:	Illustration of (a) Rubber Rolling IP and (b) Vacuum Filtration-Assisted IP (Xie et al., 2012)	60
Figure 4.9:	Illustration of a Spinning Machine (Fried, 1997)	62
Figure 4.10:	Schematic Diagram of the Fabrication of the TFN RO Membrane Through Vacuum Filtration IP Process (Song et al., 2016)	62
Figure 4.11:	Illustration of IP Reaction Between MPD and TMC (Shen et al., 2020)	63
Figure 4.12:	SEM Images of the Surface of Membranes with Different CQDs Loading: (a) 0 wt%, (b) 10 wt%, and (c) 30 wt%; the Cross-sectional Image of the Membranes With 10 wt% CQDs Loadings (d and e) (Yuan et al., 2018)	66
Figure 4.13:	SEM Images of the Surface of (a) PES Substrate, (b) Unmodified TMC Membrane, (c) TFN-NCQD Membrane; (d) TEM Image of the Surface of TFN-NCQD (Guo et al., 2021)	68
Figure 4.14:	SEM Images of the Surface of (a) TFC and (b) GOQDs-TFN Membranes (Zhang et al., 2017)	69
Figure 4.15:	SEM Images of the Surface of (a) TFC Membrane and (b) GQDs Incorporated TFN Membranes (Liang et al., 2020)	70
Figure 4.16:	(a) FTIR and (b) XPS Spectra of the TFC and Functionalized CQDs Incorporated TFN Membranes (Sun and Wu, 2018)	72
Figure 4.17:	XPS Spectra of TFC and Na-CQDs Incorporated TFN Membranes (He, Zhao and Chung, 2018)	73
Figure 4.18:	(a) FTIR and (b) XPS Spectra of TFC and GOQDs Incorporated TFN Membranes (Zhang et al., 2017)	74
Figure 4.19:	FTIR Spectra of the PI Substrate and the GQDs Incorporated TFN Membranes (Li et al., 2019b)	75
Figure 4.20:	Water Contact Angles of TFN Membranes at Different CQDs Loading (Yuan et al., 2018)	76
Figure 4.21:	Water Contact Angles of TFN Membranes with Different CQDs Loadings (Yang et al., 2020)	77

Figure 4.22:	Zeta Potential Analysis Results for the TFN and the Commercial Membranes (Yang et al., 2020)	78
Figure 4.23:	Zeta Potential Analysis Results of the Membranes at Different Stages (Shao et al., 2020)	78
Figure 4.24:	Water Contact Angle of TFC and GOQDS Incorporated TFN Membranes (Zhang et al., 2017)	79
Figure 4.25:	Water Contact Angle of TFN Membranes With Different GQDs Loadings (Bi et al., 2018)	80
Figure 4.26:	Zeta Potential Analysis Results of TFN Membranes Incorporated With Different GQDs Loadings (Bi et al., 2018)	81
Figure 4.27:	Zeta Potential Analysis Results of the Membranes at Different pH Values (Xu et al., 2021)	81
Figure 4.28:	(a) Pure Water Flux and (b) Salt Rejection of the TFC and TFN Membranes at 0.6 MPa (Sun and Wu, 2018)	83
Figure 4.29:	Salt Rejection of the Pristine TFC and GOQDs Incorporated TFN Membrane (Zhang et al., 2017)	84
Figure 4.30:	Water fluxes of the Membranes with Different GQDs Loadings (Bi et al., 2018)	85
Figure 4.31:	Salt Rejection of TFN Membranes Incorporated with GQDs-NH ₂ (Xu et al., 2021)	85
Figure 4.32:	Effects of (a) CQDs Content and (b) Deposition Time on Water Flux and NaCl Salt at 2000 ppm and 225 psi (Li, Li and Zhang, 2017b)	86
Figure 4.33:	(a) Pure Water Permeability and (b) Salt Permeability of Different Membranes (Gai, Zhao and Chung, 2019)	87
Figure 4.34:	Water Flux and Salt Rejection of the Pristine TFC and GOQDs Incorporated TFN Membranes in Extensive RO Test (Song et al., 2016)	88
Figure 4.35:	(a) Antifouling Behaviour and (b) Fouling Resistance of the TFC and TFN Membranes (Song et al., 2016)	88

LIST OF SYMBOLS / ABBREVIATIONS

A	Constant
B	Salt permeability constant
J	Flux, ($\text{L}\cdot\text{m}^{-2}\cdot\text{h}^{-1}$)
J_i	Flux, ($\text{g}\cdot\text{cm}^{-2}\cdot\text{s}^{-1}$)
P	Permeability, ($\text{L}\cdot\text{m}^{-2}\cdot\text{h}^{-1}$)
R	Membrane solute rejection, (%)
r_p	Pore radius, (nm)
r_s	Solute radius, (nm)
R_t	Total fouling rate
ΔP	Pressure difference across the membrane
$\Delta\pi$	Osmotic pressure differential across the membrane
ρ_i	Density of water, (g/cm^3)
σ	Reflection coefficient
4AAP	4-Aminoantipyrine
AFM	Atomic force microscopy
AGQDs	L-aspartic acid functionalized graphene quantum dots
ALG	Sodium alginate
AMPS	2-Acrylamido-2-methylpropanesulfonic acid
AP	Silver phosphate
APDEMS	Silane coupling agent
APT EOS	γ -Aminopropyltriethoxysilane
BTAC	1,2,4,5-Benzenetetracarboxylic acyl chloride
CA	Cellulose acetate
CCQDs	Carboxylic carbon quantum dots
CDIL	Carbon quantum dots-based ionic liquid
CFIC	5-chloroformyloxy-isophthaloyl chloride
CHI	Chitosan
CHMA	1,3-Cyclohexanebis (methylamine)
CL	Chemiluminescence
CMPI	2-Chloro-1-methylpyridinium iodide
CNTs	Carbon nanotubes

CQDs	Carbon quantum dots
CQDs-NH ₂	Amino-rich carbon quantum dots
CSA	10-Camphorsulfonic acid
DABA	3,5-Diamino-N-(4-aminophenyl) benzamide
DBPs	Disinfection by-products
DETA	Diethylenetriamine
DI	Deionized
DMC	Methacryloethyl trimethyl ammonium chloride
DMF	N, N-dimethylformamide
DNA	Deoxyribonucleic acid
DSCs	Dye-sensitized solar cells
EB	Electron Beam
ECL	Electrochemiluminescence
ED	Electrodialysis
EDA	Ethylenediamine
EDC	1-(3-Dimethylaminopropyl)-3-ethylcarbodiimide hydrochloride
EDTA	Ethylene diamine tetra-acetic acid
FESEM	Field emission scanning electron microscopy
FRR	Flux recovery rate
FTIR	Fourier transform infrared spectroscopy
GO	Graphene oxide
GOQDs	Graphene oxide quantum dots
GQDs	Graphene quantum dots
GQDs-NH ₂	Amino-functionalized graphene quantum dots
HC	Hydrothermal carbonisation
HDA	1,6-Hexanediamine
HF	Hollow fibre
HOMO	Highest occupied molecular orbital
HTC	Cyclohexane-1,3,5-tricarbonyl chloride
ICIC	5-Isocyanato-isophthaloyl chloride
IDPI	Isophorone diisocyanate
IP	Interfacial polymerization
IPA	Isopropanol

IPC	Isophthaloyl chloride
LbL	Layer-by layer
LUMO	Lowest unoccupied molecular orbital
MDEOA	Methyl-diethanolamine
MF	Microfiltration
mm-BTEC	mm-Biphenyl tetraacyl chloride
MMPD	m-Phenylenediamine-4-methyl
MPD	m-Phenylenediamine
MWCNT	Multi-walled carbon nanotubes
MWCO	Molecular weight cut off
Na-CQDs	Na ⁺ functionalized carbon quantum dots
NCQDs	Amino carbon quantum dots
NF	Nanofiltration
N-GOQDs	Nitrogen-doped graphene oxide quantum dots
NHS	N-hydroxysuccinimide
NMP	N-methyl pyrrolidone
NOM	Natural organic matter
NPs	Nanoparticles
om-BTEC	om-Biphenyl tetraacyl chloride
op-BTEC	op-Biphenyl tetraacyl chloride
PA	Polyamide
PAA	Polyamic acid
PAN	Polyacrylonitrile
PDA	Polydopamine
PEEKWC	Poly(ether ether ketone)
PEG	Poly(ethylene glycol)
PEG-200	Poly(ethylene glycol)
PEI	Polyetherimide
PEK-C	Cardo polyetherketone
PES	Polyethersulfone
PHGH	Polyhexamethylene guanidine hydrochloride
PI	Polyimide
PIP	Piperazine
PK	Polyketone

PL	Photoluminescence
PLAL	Pulsed laser ablation in liquid
PPD	p-Phenylenediamine
PSf	Polysulfone
PWP	Pure water permeability
RO	Reverse osmosis
SCQDs	Sulfonated carbon quantum dots
SDS	Sodium dodecyl sulfate
SEM	Scanning electron microscopy
SPES-NH ₂	Sulfonated cardo poly (arylene ether sulfone)
sPPSU	Sulfonated polyphenylenesulfone
SRNF	Solvent resistant nanofiltration
TA	Tannic acid
TDS	Total dissolved solid
TEM	Transmission electron microscopy
TEOA	Triethanolamine
TEPA	Tetraethylenepentamine
TETA	Triethylenetetramine
TFC	Thin film composite
TFN	Thin film nanocomposite
TMC	Trimesoyl chloride
UCPL	Up-conversion photoluminescence
UF	Ultrafiltration
VSA	Vinylsulfonic acid sodium salt
XPS	X-ray photoelectron spectroscopy
γ -AlOOH	Boehmite

CHAPTER 1

INTRODUCTION

1.1 Background

Water crisis is getting serious and affecting about 30% of the world population every year. It has been listed as the top global risk since 2012 due to the potential impacts it could cause (World Economic Forum, 2020). Recent years, the increase of human population, climate change and contamination of natural water source have further deteriorated the situation (Lee, Arnot and Mattia, 2011). Thus, advanced water treatment technology such as membrane filtration has become more important. Membrane filtration is a process that utilised pressure as the driving force. While relatively clear water are allowed to pass through the membrane, the passage of pollutants such as nutrients and inorganic metal ions are restricted (Shon et al., 2013). The extensive studies on membrane development and fabrication have led to a wide variety of membranes and also reduce the cost of membrane. Hence, the installation of membrane separation system has become more popular in the industry (Baker, 2012b).

Typically, membrane systems such as reverse osmosis (RO), ultrafiltration (UF), microfiltration (MF), and electrodialysis (ED) are used in water treatment processes. Among these membrane processes, RO and NF membrane technology is the most commonly applied technology for desalination (Ostarcevic et al., 2018). As illustrated in Figure 1.1, these membranes are capable to reject pathogens, bacteria, particles, as well as dissolved ions. On one hand, RO membranes are able to reject wider range of substances compared to NF membranes due to the dense membrane structure. On the other hand, NF membranes are able to operate under lower pressure at the cost of the passage of monovalent ions. Generally, NF membranes have pore sizes between UF and RO membranes, ranging from 0.1 to 1 nm. Therefore, more substances such as organic molecules, viruses, multivalent ions can be removed more effectively compared to UF or MF membranes due to the smaller pore size of NF membranes. Generally, monovalent ions and water are the only substances that are allowed to pass through NF membranes (Ostarcevic et al.,

2018). Figure 1.1 compares the performances of different membrane separation processes.

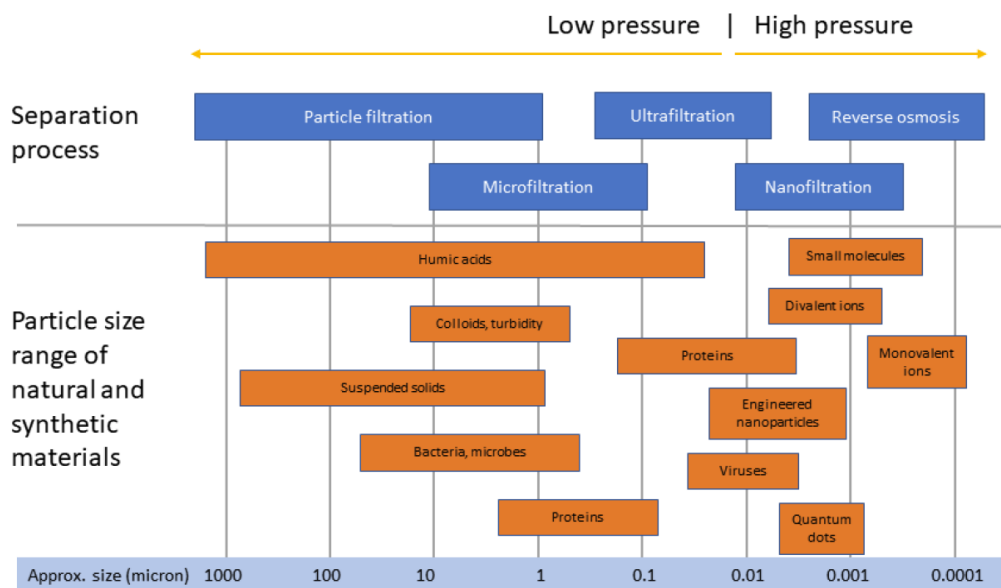


Figure 1.1: Schematic Representation of Membrane Barrier Performances (Ostarcevic et al., 2018)

Currently, thin film composite (TFC) polyamide membranes are dominating the membrane market. The commonly used methods to fabricate TFC membranes are interfacial polymerization, surface grafting, physical coating and layer-by-layer assembly (Zhang et al., 2017). Although NF and RO membranes are capable of rejecting the substances as illustrated in Figure 1.1, it is subjected to limitations such as fouling, degradation and low permeability. Thus, the development of novel TFC membranes on improving the performances such as permeability and antifouling properties are necessary.

Over the years, various studies have been performed to enhance the performances of TFC membranes especially the top polyamide (PA) layer. A whole new class of nanocomposite membranes, namely thin film nanocomposite (TFN) membrane has been produced by using the nanotechnology. Most of the TFN membranes possess improved separation, sorption capacity as well as improved thermal, mechanical and chemical stability. Jeong et al. (2007) was the first in developing TFN membrane. Zeolite NaA nanoparticles were incorporated into the PA selective layer, showing an

improved permeability of the membrane. By incorporating nanofillers into the PA layer, different properties and performances of TFN membranes can be significantly enhanced and optimised depending on the type and amount of nanofillers. For instance, silver nanoparticles were embedded into a PA thin film layer by Lee et al. (2007) to improve the antibiofouling properties while Mendret et al. (2013) successfully embedded titanium oxide/aluminium oxide ($\text{TiO}_2/\text{Al}_2\text{O}_3$) composite into the PA layer to enhance the hydrophilicity and flux stability.

Carbon-based nanoparticles have drawn great attention from the researchers as they are low cost and possess high mechanical and chemical stability. Graphene oxide (GO) and carbon nanotubes (CNTs) are the mostly studied carbon-based nanoparticles due to their oleophilic, hydrophobic, huge specific surface area and one-dimensional structure (Al-anzi and Siang, 2017). Many studies have been reported by the researchers regarding the advantages of embedding CNTs into membranes. These advantages include improved mechanical properties (Bai et al., 2017), enhanced thermal stability (Namasivayam and Shapter, 2017), enhanced electrical conductivity (Sarno et al., 2013) and improved oleophobicity and hydrophilicity (Zhang et al., 2016b). On the other hand, the incorporation of graphene oxide nanoparticles into the PA layer have been reported to have positive effect on the performance of the membranes. These include enhanced antifouling properties, hydrophilicity and water flux (Lai et al., 2019, 2018).

Recently, carbon-based quantum dots such as carbon quantum dots (CQDs), graphene quantum dots (GQDs), and graphene oxide quantum dots (GOQDs) as an effective nanofiller has gained great attention from researchers due to its unique properties (Zhao and Chung, 2018). Substantial amounts of carboxyl, hydroxyl and epoxy groups are found at the surfaces and basal layers of the quantum dots (Wang and Hu, 2014). These groups are responsible for their unique properties such as great water solubility and leads to better membrane properties when embedded into the PA selective layer. Besides, other favourable properties such as antifouling, antimicrobial, rich chemistry and small sizes also indicates their potential to improve the performance of TFN membranes (Zhao and Chung, 2018). These properties also allow carbon-based

quantum dots to have outstanding dispersibility in polymer matrices and polar solvents which is crucial for the formation of membrane.

1.2 Problem Statement

According to Kolbasov et al. (2017), more than 4 billion people over the world will live with insufficient clean water source by the year 2025. Although NF and RO technology has been widely employed in water and wastewater treatment, typical membrane limitations are still commonly encountered. The long persistent problems of filtration membranes include membrane fouling, low permeability and short membrane lifetime.

Membrane fouling is a common problem faced by every membrane separation process. The fouling mechanism of NF is more complex as the fouling take place at nanoscale which makes it harder to address (Van der Bruggen, Mänttari and Nyström, 2008). The negative impacts are noticeable, including the need for membrane cleaning and pre-treatment, restricted recoveries, feed loss, and low membrane stability. Moreover, frequent membrane fouling will shorten the membrane lifetime as frequent physical or chemical cleaning is needed. Not to mention that frequent chemical cleaning will increase the operating cost by a large amount. Therefore, resolving the fouling issue will lead to better permeate yield and reduce the need for cleaning (Van der Bruggen, Mänttari and Nyström, 2008). Next, to achieve high rejection of salt solution, the interfacial polymerization technique is often modified. However, the thickness of the PA layer would exceed 100 nm which yields a low permeability (Hao et al., 2020).

Recently, the potential of TFN membranes were widely explored to address the mentioned issues. Among the studies, graphene oxide (GO), CNT, carbon dots and metal oxide are the mostly studied nanomaterials in the modification of TFN membranes. However, the development of TFN membranes is still a challenging topic. The major problems are is that some of the nanomaterials either have poor compatibility to the PA matrix as well as poor dispersibility or it is too expensive (Sun and Wu, 2018). Poor dispersibility and compatibility would lead to poor performance of the membrane For instance, metal oxide such as titanium oxide (TiO_2) have poor interaction with the PA matrix which would need an extra organic monolayer (Rajaeian et al., 2013).

Furthermore, according to Sun and Wu (2018), the poor compatibility of some nanomaterials to the PA matrix would lead to nonselective interface void which could potentially decrease performance stability and solute selectivity. For CNTs and GO, although it has many benefits from the aspect of improving the membrane performance such as hydrophilicity, enhanced flux and others, it is still too expensive and relatively hard to produce at large capacity (Woo et al., 2019).

Various researches have been conducted in carbon-based quantum dots incorporated TFN membranes over the past decade. However, it is not well compared and evaluated in any of the previous work. Therefore, this work serves to compile and evaluate the membrane fabrication methods, characteristics, and the improvements on the membrane performance due to the addition of carbon-based quantum dots into RO and NF TFN membranes.

1.3 Aims and Objectives

The aim of this project is to evaluate the performance of thin film nanocomposite (TFN) nanofiltration and reverse osmosis membrane incorporated with carbon-based quantum dots such as CD, GQD, and GQD. The objectives of this project include:

- i. To discuss and compare the fabrication method of TFN membranes.
- ii. To investigate the characteristics of TFN membranes incorporated with carbon-based quantum dots in terms of surface hydrophilicity, charge and morphology.
- iii. To evaluate the performance of TFN membranes incorporated with carbon-based quantum dots in terms of pure water permeability, salt rejection, and anti-fouling properties.

1.4 Importance of Study

Carbon-based quantum dots such as CQDs, GQDs, and GOQDs can be synthesized through various cost-effective and simple methods. They are rich with oxygen-containing functional groups such as epoxy, carboxyl, and hydroxyl groups which results in the high hydrophilic properties. Besides, due to the smaller size of quantum dots compared to normal carbon or graphene, they have larger surface area which allows them to improve the membrane

performance more effectively. Furthermore, they have low cytotoxicity, high mechanical and chemical stability, and cost-effective (Li et al., 2013; Wang and Hu, 2014). With their unique properties, the incorporation of carbon-based quantum dots has been studied extensively in recent years.

Although experimental works are important to discover the potential of different materials, theoretical analysis is just as important to deliver fundamental knowledge, properties, characteristics, mechanism, as well as the potential application. In order to aid the researchers to improve their understanding while performing their studies, it is vital to have a study that gives detailed cumulative findings and analysis as they are able to provide the information of interest. Various studies have reported the important role of carbon-based quantum dots in the modification of TFN membranes, which have numerous applications particularly in clean water production (Li, Li and Zhang, 2017a; Fathizadeh et al., 2019; Xu et al., 2021). Hence, it is necessary to investigate and develop more understanding on these membranes to overcome the conventional membrane limitations such as low rejection or membrane fouling.

Moreover, there are plenty of variation of carbon-based quantum dots reported in previous studies, for example functionalized carbon-based quantum dots and carbon-based quantum dots with metal or metal oxide composites. Different types of carbon-based quantum dots bring different degree of impact on the membrane performance, depending on the interaction of that particular quantum dots with the membrane materials.

In summary, this study is essential to evaluate the improvement on the membrane performance through the incorporation of carbon-based quantum dots and provide a well-defined structure of the effect of carbon-based quantum dots on membrane hydrophilicity, selectivity, antifouling properties and the characteristics. This could contribute in future development on breaking the typical membrane limitations like permeability/selectivity trade-off and fouling.

1.5 Scope and Limitation of Study

There are several factors that could affect the performance of the carbon-based-quantum dots incorporated membranes such as the membrane fabrication method, the quantum dots synthesis method, testing condition, and operating condition. Due to the time limitation of this study, the scope only involved NF and RO TFN membranes. These membranes will be the focus in this study to compare their performance, characteristic, as well as the fabrication method. The carbon-based quantum dots of interest include CQDs, GQDs and GOQDs. In summary, this study focuses on the improvement through the addition of carbon-based quantum dots in terms of the membrane fabrication method, characteristics and performances.

1.6 Outline of the Study

Chapter 1 includes a brief overview of NF and RO TFN membranes and some of the commonly used nanoparticles especially carbon-based quantum dots. The problem statement and objectives of the study have also been discussed. Next, relevant reviews of carbon-based quantum dots incorporated TFN membranes are reviewed in Chapter 2. Then, Chapter 3 demonstrates the methodology of data gathering and conducting the review. Subsequently, the relevant data from previous studies are evaluated and discussed in Chapter 4. Lastly, the final evaluation and justification are concluded in Chapter 5, as well as recommendation for future studies.

CHAPTER 2

LITERATURE REVIEW

2.1 Properties of Carbon-based Quantum Dots

Recently, carbon-based materials such as carbon and graphene have gain tremendous attention in membrane technology, particularly its derivatives such as carbon quantum dots (CQDs), graphene quantum dots (GQDs), and graphene oxide quantum dots (GOQDs). Figure 2.1 shows the illustration of the structure carbon-based quantum dots.

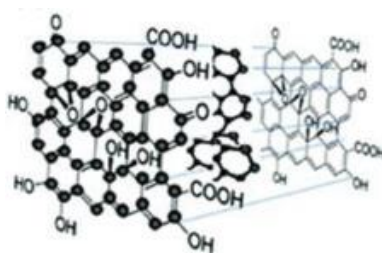


Figure 2.1: Structure of a Typical Carbon-based Quantum Dots

2.1.1 Structural Properties

CQDs have arisen as a new class of nanocarbons in recent years. (Wang and Hu, 2014). Their unique advantages compared to the other well developed nanocarbons have led to the wide-ranging researches and studies by the researchers. Generally, the diameter of CQDs is less than 10 nm. It is a quasi-spherical nanoparticle (NPs) and can either be amorphous or crystalline subject to the carbon clusters. Furthermore, CQDs is significantly size dependent, which makes its modulated electronic structure more unique from other carbonaceous materials. It has outstanding aqueous solubility due to the functional groups such as carboxyl and hydroxyl attached to the surface of CQDs. In the work of Cong and Zhao (2018), the effects of different functional groups on the lowest unoccupied molecular orbital (LUMO) and the highest occupied molecular orbital (HOMO) were shown. The LUMO and HOMO levels are raised by electron donating groups and shifted down by electron withdrawing groups in the different functional groups.

On the other hand, GQDs are also gaining increasing attention due to their low cytotoxicity, great solubility, and stable fluorescence (Li et al., 2013). Besides, GQDs are quasi-spherical NPs which involves crystalline and amorphous fragments (Li et al., 2015a). Typically, the diameter of GQDs is less than 100 nm which is significantly larger than CQDs (Tabish and Zhang, 2019). Additionally, GQDs normally possess graphene lattices in its dots which are comparable to the structure of single or multi-layered graphene. As for GOQDs, it shares the same chemical structure with graphene oxide (GO) but exhibit a smaller size, ranging from 0.5 to 32.7 nm. It possesses outstanding hydrophilicity due to the presence of different oxygen-containing functional group such as carboxyl, hydroxyl and epoxy (He et al., 2015). Similar to GQDs, it was reported that GOQDs have lower cytotoxicity than GO sheets (Nurunnabi et al., 2013; Zeng et al., 2016). Besides, the small average diameter of GOQDs makes them attractive in membrane technology.

2.1.2 Optical Properties

2.1.2.1 Absorbance

Carbon-based quantum dots normally show great optical absorption at similar region which is around 260 to 320 nm (UV region) with extending tail to the visible region as illustrated in Figure 2.2. They are able to absorb carbon effectively especially in shorter wavelength due to the π - π^* transition of the carbon-carbon double bonds and the n - π^* transition of the carbon-oxygen double bonds (Wang and Hu, 2014; Lu et al., 2017; Tabish and Zhang, 2019).

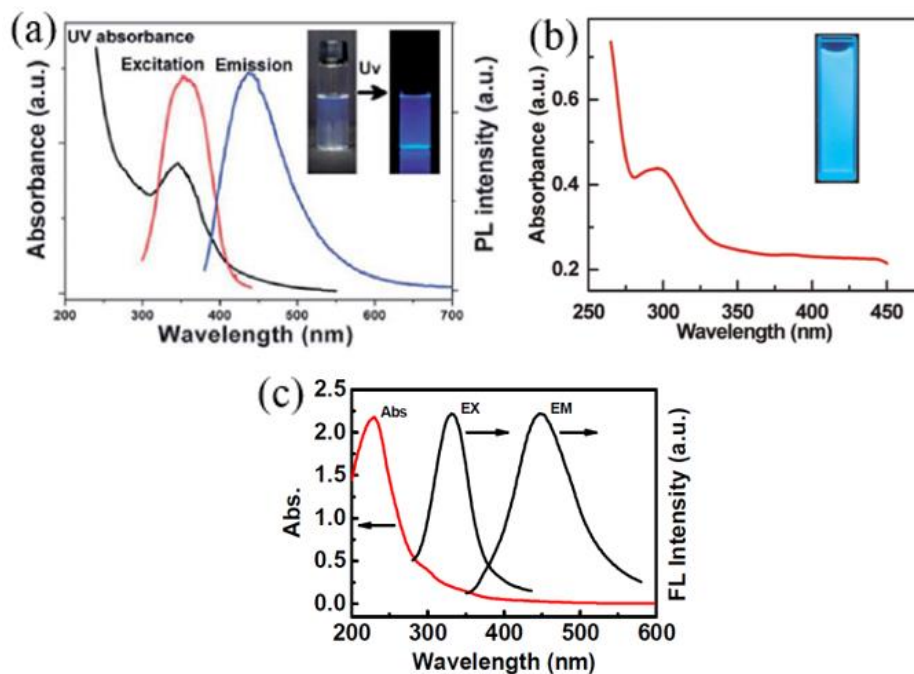


Figure 2.2: Absorbance of (a) CQDs (Wang and Hu, 2014), (b) GQDs (Tabish and Zhang, 2019), and (c) GOQDs (Lu et al., 2017) at Different Wavelength

2.1.2.2 Photoluminescence

Either from the aspect of practical application or elementary research, photoluminescence (PL) is the most attractive property of carbon-based quantum dots. The PL of carbon-based quantum dots is distinctly dependent on the emission wavelength and intensity. Figure 2.3 shows the capability of CQDs to emit different colours when it is excited at different wavelength. In other words, the PL properties of the CQDs can be adjusted via modification (Wang and Hu, 2014). According to (Li et al., 2010), the size of CQDs also affects the emission. It was proposed that smaller CQDs give shorter wavelength emission and vice versa. For instance, small CQDs emits UV light and large CQDs emits near-infrared light. Meanwhile, GQDs and GOQDs possess similar PL property to CQDs. Li et al. (2015a) and Lu et al. (2017) suggested that the PL intensity of GQDs and GOQDs are affected by the surface functional groups, pH values as well as its size. On top of that, the reduction or oxidation of the functional groups are able to affect the PL intensity too. Figure 2.4 shows the effect of the size of GQDs on the PL colour at a wavelength of 365 nm.

However, there are different explanation for the exact mechanism of PL (Singh et al., 2018). Cong and Zhao (2018) claimed that “the PL originates from the emissive surface energy traps upon stabilization, since surface passivation is often indispensable for photoluminescent quantum dots with high quantum yield”. On the other hand, Cao, Meziani and Sahu (2013) claimed that radiative recombination of the holes and surface-confined electrons is responsible for the phenomenon. Hence further investigation is required to study the exact mechanism of PL.

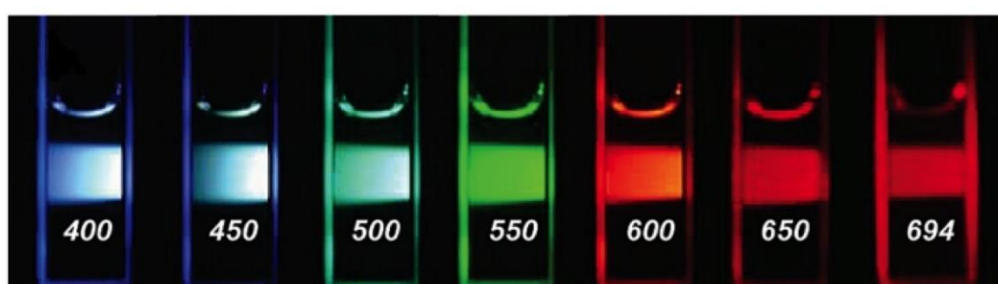


Figure 2.3: Aqueous Solution of CQDs Passivated with PEG_{1500N} Excited at Different Wavelength (Wang et al., 2015)

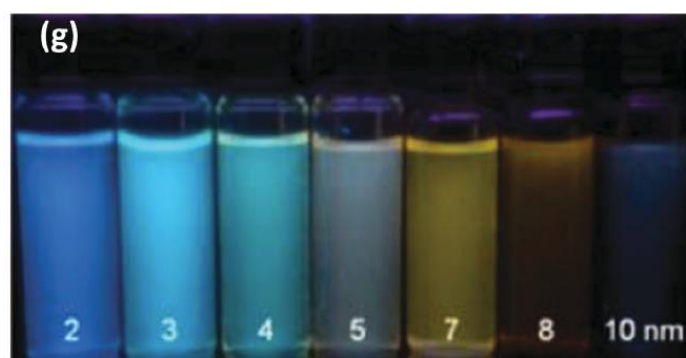


Figure 2.4: Photoluminescence Colour of GQDs with Different Sizes at 365 nm UV Light (Li et al., 2015a)

2.1.2.3 Chemiluminescence

Oxidants such as cerium (IV) and potassium permanganate, KMnO_4 are able to infuse holes into the carbon-based quantum dots. The increased hole population step up the electron hole annihilation which leads to the release of energy in chemiluminescence (CL) form.

For CQDs, it was found that the CL intensity is affected by the temperature and concentration of CQDs (Wang and Hu, 2014). Furthermore, a phenomenon was observed when CQDs are prepared in a strong alkaline solution where it shows outstanding electron donating and accepting ability. The combination of both the chemical reduction and holes generated by thermally exciting is proposed to be responsible for this phenomenon. The excellent performance of CQDs as electron donor and acceptor make it potentially applicable in catalysis and optronic (Wang and Hu, 2014).

On the other hand, it was reported by Amjadi, Manzoori and Hallaj (2014) that the CL intensity of GQDs was significantly higher than CQDs. The chemical reaction between GQDs and cerium (IV) results in the formation of excited-state GQDs through the electron hole annihilation which have led to the CL emission. It is worth noting that the deoxygenation of the solution had reduced the CL intensity which indicates the effect of dissolved oxygen on the CL. Furthermore, temperature is also another factor which will affect the CL. As the temperature increases, the electrons are excited into the higher energy levels.

2.1.2.4 Up-conversion Photoluminescence

The up-conversion photoluminescence (UCPL) of carbon-based quantum dots is an anti-Stokes emission which means that the excitation wavelength is longer than the emission wavelength. It is responsible to the multi-photon activation process where two or more photons are absorbed concurrently (Wang and Hu, 2014). This is especially great for designing highly efficient catalyst and cell imaging with two-photon luminescence microscopy. However, it was still unclear that multi-photon activation process is the only process that is accountable for the UCPL of CQDs. Wen et al. (2014) argued that the UCPL of CQDs actually originates from the normal fluorescence. It was excited in the monochromator of the fluorescence spectrophotometer by the escaping component from the second diffraction which leads to the UCPL. It is proposed that the UCPL of most CQDs is undetectable and can be determined by computing the excitation intensity dependence of the fluorescence.

Nevertheless, the studies on the UCPL of GQDs and GOQDs are relatively rare. Shen et al. (2011) reported that the upconverted emission peaks changed from 390 to 468 nm while the excitation wavelength shifted from 600 to 800 nm. Table 2.1 summarises the advantages of carbon-based quantum dots from different aspects.

Table 2.1: Summary of the Advantages of Carbon-based Quantum Dots (Singh et al., 2018)

Aspects	Description
Cost & Availability of Precursors	Relatively inexpensive and abundant.
Luminescence	Greater luminescence than other quantum dots.
Electronic Properties	Great electron donor and acceptor.
Chemical Stability	More stable than metallic or traditional quantum dots.
Aqueous Stability	More stable than organic dyes and cadmium-based quantum dots.
Photostability	More stable than traditional quantum dots and organic dyes.
Biological	Low toxicity, good biocompatibility and hydrophilicity.

2.2 Carbon-based Quantum Dots Synthesis Methods

Generally, the synthetic methods of carbon-based quantum dots are categorised into top-down and bottom-up path. The former destroys or disperses macromolecule into smaller sized quantum dots either by chemical or physical. In contrast, the latter is primarily the carbonisation and polymerization of non-conjugated small molecules into quantum dots through chemical reactions (Wang et al., 2019). Figure 2.5 summarises the synthetic methods of carbon-based quantum dots.

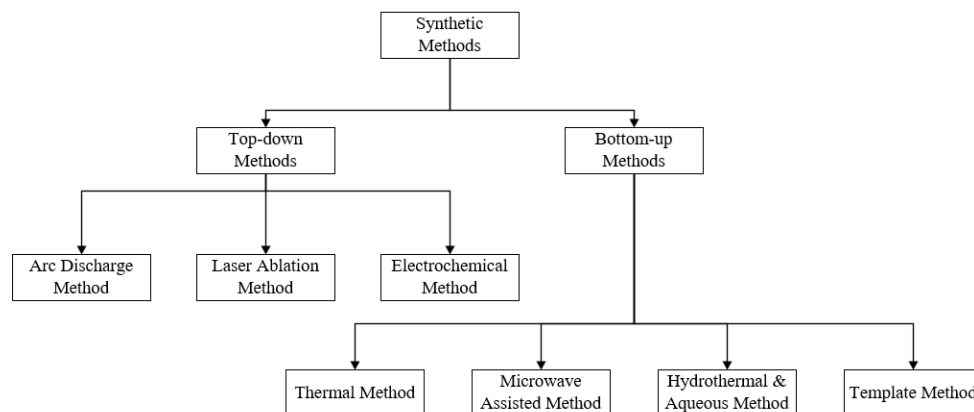


Figure 2.5: Summary of the Synthetic Methods of Carbon-based Quantum Dots (Singh et al., 2018)

2.2.1 Top-down Methods

2.2.1.1 Arc Discharge Method

Arc discharge is a method where carbon atoms that are broken down from the precursors are rearranged in the anode. Gas plasma which is produced in a confined reactor is the driving force of the process (Arora and Sharma, 2014). To generate a plasma with high energy, high temperature is needed in the reactor. It can achieve up to 4000 K by electric current (Wang et al., 2019).

The arc discharge method is applicable to synthesize CQDs from crude material such as crude carbon nanotube soot. It was first oxidized with 3.3 M of nitric acid and extracted with basic solution with a pH of 8.4. As a result, a stable product in dark coloured was obtained. Gel electrophoresis was conducted afterward to get rid of the impurities (Roy et al., 2015).

The CQDs synthesized from the arc discharge method have good solubility in water. However, the formation of large carbon particles with various sizes would significantly reduce the specific surface area of CQDs. This could in turn restrain the number of active reaction sites during the electrocatalytic process (Wang et al., 2019).

2.2.1.2 Laser Ablation Method

Laser ablation is a method where the surface of the target is irradiated with a high-energy laser to a thermodynamic state. The target heats up quickly and

vaporise into a plasma state as high pressure and temperature are generated. The vapour then crystallises and nanoparticles are formed (Sun et al., 2006).

Due to the complex procedures and long passivation times, simpler methods are highly desired. Hu et al. (2009) reported a one-step synthetic method where the surface modification can be achieved together with the formation of CQDs with tuneable PL by selecting suitable solvents. Moreover, Li et al. (2011a) described a simple procedure to produce CQDs with tuneable and visible PL where nano-carbon materials are being used as the precursor and simple solvent as liquid medium. Furthermore, GQDs was synthesized in the work of Russo et al. (2016) through a single-step femtosecond laser ablation of GO dispersion. By manipulating the ablation time and laser power, different sizes of GQDs can be obtained. Besides, Kang et al. (2019) reported another simple method to prepare both GQDs and GOQDs through pulsed laser ablation in liquid (PLAL) method. The as-produced GQDs and GOQDs show notably different optoelectronic properties. This phenomenon can be attributed to the presence of oxygen-containing functional groups on the surface, such as hydroxyl and carboxyl groups.

Laser ablation has several advantages such as its effectiveness and it produce carbon-based quantum dots with good solubility in water and good PL characteristics. However, laser ablation needs high amount of carbon material to prepare the carbon targets which could increase the cost (Wang et al., 2019).

2.2.1.3 Electrochemical Method

Electrochemical method is a simple approach as CQDs can be synthesized at normal pressure and temperature conditions (Wang et al., 2019). It is also a common method that is widely used to prepare GQDs (Tabish and Zhang, 2019). Various studies and researches have been done on this method due to the effortlessness in tuning the PL properties and particle size (Anwar et al., 2019; Deng et al., 2014).

Hou et al. (2015) proposed a simple and inexpensive approach to produce CQDs with good photostability. CQDs were produced through the electrochemical carbonisation of urea and sodium citrate with an average size of 2.4 nm. The CQDs prepared are especially great for sensing mercury ions in

wastewater. Aside from that, a one-step electrochemical tailoring method where the synthesis of GQDs at large scale can be done is suggested by Deng et al. (2015). The as prepared GQDs have different sizes as well as emission colour and possess intrinsic peroxidase-like activity in glucose detection. Besides, Chang and Wu (2013) demonstrated the preparation of size-tuneable GQDs by using multi-walled carbon nanotubes (MWCNT) in propylene carbonate solution.

By using electrochemical method, GQDs are able to be synthesized effectively even if the starting materials are different. Nonetheless, the preparation method is relatively complex and has low product yields (Tabish and Zhang, 2019).

2.2.2 Bottom-up Methods

2.2.2.1 Thermal Method

Recently, the researches and studies on the synthesis of carbon based quantum dots from thermal method are increasing as it is highly effective and inexpensive (Guo et al., 2016; Li et al., 2012a). Besides, this method has simple procedure, short reaction time, scalable generation, and is able to be used with a wide variety of precursors (Tajik et al., 2020).

Similar to the electrochemical method, the PL properties of the as-prepared CQDs can be tuned according to applications by selecting appropriate carbon source, passivating agents and solvent. This method offers great control of the optical properties and morphology of CQDs (Wang et al., 2015). Bourlinos et al. (2008) was the first in reporting the method. In their studies, the CQDs prepared were either hydrophilic or organophilic. CQDs were synthesized through a one-step thermal carbonisation of carbon precursors which have low melting point. There are two approach in the studies which are the citrate approach and the 4-aminoantipyrine approach. In the first approach, organophilic CQDs were synthesized by pyrolyzing octadecyl ammonium citrate directly in air for two hours at a temperature of 300 °C. The products were then washed repeatedly with ethanol and acetone and dried. Meanwhile, the hydrophilic CQDs were synthesized by hydrothermally heating up diethylene glycol ammonium citrate in an autoclave for two hours at a

temperature of 300 °C. The products were washed repeatedly with acetone. In the second approach, 4-aminoantipyrine (4AAP) was pyrolyzed in the air at a similar condition as the first approach. The CQDs prepared from both approaches have great dispersibility in aqueous and organic solvents and emit visible light when excited with different excitation wavelength (Bourlinos et al., 2008).

In the study performed by Ma et al. (2015), synthesized nitrogen-doped GQDs through direct carbonization of ethylene diamine tetra-acetic acid (EDTA) at 260 to 280 °C in a sand bath. The resulting materials from the EDTA decarboxylation are able to combine with each other and form a graphite-like structures. Consequently, it is converted into diverse graphitic carbon nitrides at high temperature. It was reported that the GQDs produced through this method possess low cytotoxicity, high fluorescence, and decent pH stability, which makes them a good candidate for optoelectronic and bio-labelling application.

2.2.2.2 Microwave Assisted Method

Microwave assisted method is a method that has been broadly practised in the chemical synthesis industry. The method heats up the carbon precursors faster and easier compared to other methods. The preparation procedures are simplified and CQDs can be obtained in minutes with an improved yield (Zuo et al., 2016). In this method, heat is replaced by microwave to heat up the carbon precursors. Various researches and studies on the microwave assisted method are done due to the simplicity of the procedure and rapidness of the method (Schwenke, Hoepfner and Schubert, 2015; Rai et al., 2017; Shen et al., 2018; Jiang et al., 2018).

Zhu et al. (2009) reported a microwave assisted method for the synthesis of CQDs with electrochemiluminescence (ECL) properties. The method is simple and economical. CQDs were prepared by heating of the mixture of poly(ethylene glycol) (PEG-200), distilled water and saccharide in a microwave oven for two to ten minutes. On the other hand, Wei et al. (2014) demonstrated a procedure to prepare nitrogen-doped CQDs with tuneable multicolour luminescent display via the microwave assisted Maillard reaction. The reported method took about 35 minutes to synthesize CQDs with high quantum yield

from amino acids and glucose. The physicochemical and luminescence properties are governed by the selection of amino acids. Table 2.2 summarises the types of amino acid and the respective colour and diameter of CQDs synthesized. The studies also found that the diameter of CQDs have a positive effect on the excitation wavelength.

Table 2.2: Types of Amino Acids and the Respective Colour and Diameter of CQDs (Wei et al., 2014)

Type of Amino Acids	Colour of CQDs	Diameter (nm)
Tryptophan	Blue	2.88
Leucine	Green	3.78
Aspartic acid	Yellow	4.93

Moreover, Li et al. (2012b) have described a microwave assisted method where GQDs with 2 colour (greenish-yellow and bright blue) ECL were prepared through the cleavage of GO in acidic condition. The as-prepared GQDs were produced at low cost with outstanding solubility and low cytotoxicity. Other than that, Zhang et al. (2016a) demonstrated a one-step microwave assisted pyrolysis of NH_4HCO_3 and aspartic acid. Firstly, aspartic acid and NH_4HCO_3 were added into 20 mL of deionized water. The mixture was then microwave-irradiated for 10 minutes to produce GQDs. The resulting GQDs possess strong blue FL with a quantum yield of 14%. Besides, the GQDs are sensitive to the pH of the environment which indicates the potential as optical pH sensors. Due to its low toxicity and high photostability, it is also great for cell imaging.

2.2.2.3 Hydrothermal/Solvothermal Method

Hydrothermal carbonisation (HTC) is a simple, inexpensive and green method. Normally carbon precursors are dissolved in an appropriate solvent and reacted in a hydrothermal reactor or an autoclave at high temperature.

Similar to the thermal method and microwave assisted method, the PL properties of the prepared CQDs are tuneable through modifying the conditions. These conditions include molar mass of carbon precursors, heating time,

temperature and also the nature of solvent (Anwar et al., 2019). CQDs prepared from this method often have uniform particle size and are high in quantum yield. For instance, Zhu et al. (2013) demonstrated a facile procedure where CQDs were produced at a high quantum yield of 80 %. It is almost equivalent to fluorescent dye and is by far the highest yield in the for fluorescent carbon-based materials. It was achieved through the hydrothermal process of ethylenediamine and citric acid. The synthesized CQDs can be used as a biosensor component as it is capable to detect iron (III) ions in living cells. Furthermore, Lu et al. (2019) reported that biomolecules that are abundant in nitrogen and carbon resource are able to finely adjust the structure of CQDs via hydrothermal condensation and indirectly tuning the fluorescence properties. The as-prepared CQDs are especially suitable for designing and synthesising electrocatalyst with tuneable electronic structures and doping composition.

On the other hand, to prepare GQDs through hydrothermal or solvothermal method, reduced GO sheets are typically used as the precursors, which will be treated with oxidizing agents. This step is necessary for the epoxy groups to be introduced on the carbon lattice at the cleavage sites. A facile hydrothermal method was demonstrated by Pan et al. (2010) where hydrothermal cutting technique was applied to cut graphene sheets into GQDs with nano-scale size and strong blue emission. The formation of structural models for the GQDs in alkali and acidic media is distinct. It was suggested that the blue luminescence might be originated from the fluctuating sites.

As for the synthesis of GOQDs, a one-pot hydrothermal method have been developed by Xu et al. (2019). Toner wastes was used as the precursor while H_2O_2 acted as the oxidant. The synthesis took relatively long which is around 4 hours but there is no strong acids or complicated purification procedures involved. The as prepared GOQDs exhibit blue fluorescence under UV lamp with a wavelength of 365 nm.

2.2.2.4 Template Method

Template method is also a relatively common method to synthesize CQDs. Generally, there are two stages in this synthetic method: (i) preparing CQDs

through calcination in appropriate mesoporous silicon spheres or template; and (ii) engraving to eliminate foundations and produce CQDs with nano-scale size.

Zong et al. (2011) demonstrated a simple approach where hydrophilic CQDs were synthesized with mesoporous silicon spheres as nanoreactors. The mesoporous spheres were first treated with the mixture of citric acid and complex salts. Afterwards, it is calcinated and the mesoporous supports were removed. The as-prepared CQDs possessed great luminescence properties and were photostable, monodisperse and have low toxicity. Furthermore, Yang et al. (2013) developed a new facile approach to synthesized a series of CQDs via the soft-hard template approach. Different organic molecules were used as the carbon precursor in this approach to obtain different sizes, compositions and crystalline degrees of CQDs. The synthesized CQDs are monodispersed and have PL properties. The stability of the as-prepared CQDs were outstanding and comparable to the CQDs that are synthesized at high temperatures over 900 °C (Liu et al., 2011). Table 2.3 and Table 2.4 summarizes different synthetic methods of carbon-based quantum dots and the yields from different methods respectively.

Table 2.3: Comparison Between Different Synthesis Methods (Singh et al., 2018; Chen et al., 2018)

Synthesis Methods		Advantages	Disadvantages
Top-down Methods	Arc Discharge Method	❖ Most realistic method	❖ Low quantum yield ❖ Strict condition.
	Laser Ablation Method	❖ Facile procedure ❖ Effective ❖ Different size of quantum dots can be attained	❖ Low quantum yield ❖ High amount of carbon material is needed ❖ Poor control over particle sizes
	Electrochemical Method	❖ Stable ❖ Mild condition ❖ High levels of stability ❖ Uniform quantum dots size	❖ Intricate procedure
Bottom-up Methods	Thermal Method	❖ Facile procedure ❖ The as-prepared CQDs have tuneable fluorescence property	❖ Low quantum yield

Table 2.3 (Continue)

Synthesis Methods	Advantages	Disadvantages
Microwave Assisted Method	<ul style="list-style-type: none"> ❖ Facile procedure ❖ Cost effective ❖ Environmentally friendly ❖ Short reaction time 	<ul style="list-style-type: none"> ❖ Poor control over particle sizes ❖ Expensive ❖ Volume is limited in industrial production
Hydrothermal/Solvothermal Method	<ul style="list-style-type: none"> ❖ Cost effective ❖ Facile procedure ❖ Environmentally friendly ❖ High quantum yield ❖ The as-prepared CQDs have tuneable fluorescence property 	<ul style="list-style-type: none"> ❖ Poor control over particle sizes
Template Method	<ul style="list-style-type: none"> ❖ Low toxicity ❖ Photostable 	<ul style="list-style-type: none"> ❖ Expensive ❖ Time consuming

Table 2.4: Quantum Yield of Carbon-based Quantum Dots from Different Synthesis Methods

Synthesis Method	Quantum Yield	References
Laser Ablation Method	CQDs – 4 – 10 %	(Sun et al., 2006)
	GQDs – 2 %	(Russo et al., 2016)
Electrochemical Method	CQDs – 8.9 %	(Yao, Hu and Li, 2014)
Thermal Method	CQDs – 0.1 – 3 %	(Singh et al., 2018)
	GQDs – 5.1 %	(Ma et al., 2015)
Microwave Assisted Method	GQDs – 14 %	(Zhang et al., 2016a)
	GQDs – 22.9 %	(Li et al., 2012b)
	CQDs – 18.9 %	(Guan et al., 2014)
Hydrothermal/Solvothermal Method	CQDs – 94 %	(Qu et al., 2014)
Template Method	CQDs – 32 %	(Lai et al., 2012)

2.3 Application of Carbon-based Quantum Dots

As carbon-based quantum dots possess unique properties, various researches have been performed on carbon-based quantum dots in order to utilize them to the fullest. In the past decade, carbon-based quantum dots have various applications in biomedicine delivery systems, analysing and detecting biomolecules, bioimaging, chemical sensors and others.

First of all, the most common application of carbon-based quantum dots is in the biomedical field. Due to the non-toxicity and biocompatibility of carbon-based quantum dots, it is especially suitable to be utilised for multimodal and fluorescent bioimaging (Wang and Hu, 2014; Tabish and Zhang, 2019). Besides, properties such as high solubility in water, high photostability, better cell permeability, and the flexibility of surface modification makes them potential biosensor carriers and be utilised in drug delivery system (Wang and Hu, 2014; Tabish and Zhang, 2019).

As the desirability of green process are increasing, the applications of carbon-based quantum dots have been developed in the catalysis field. It is widely known that UV light and visible light with short wavelength are harmful to natural compounds, which is highly unfavoured. In this matter, CQDs is a great choice to be utilised as photocatalysts in the natural synthetic process due to the exhibited capacity of outfitting the extended wavelength light (Singh et al., 2018). Besides, GQDs and GOQDs have been reported as a great support to synthesize metal NPs (Ran et al., 2013, 2014). For instance, metals such as copper (He et al., 2013), palladium (Yan, Li and Li, 2012), iron (Wu et al., 2014), and silver NPs (Ran et al., 2013, 2014), have been synthesized with GQDs or GOQDs as the stabilizer. Nevertheless, GQDs and GOQDs have only been reported as support to the stabilized gold NPs instead of direct stabilizers (Melo et al., 2018).

Moreover, carbon-based quantum dots have also gained attention from the optronic field. The stable light absorption and inexpensive carbon sources of carbon based quantum dots have shown its potential in dye-sensitized solar cells (DSCs) (Gao et al., 2020). The photoelectric conversion efficiency of DSCs has been improved by ~7 times due to the utilisation of CQDs in the dye or semiconductor (Wang and Hu, 2014). Recently, it was reported that CQD-based hybrids can be utilised as electrode materials for supercapacitors. CQDs-

based ionic liquid (CDIL) was used as a binder and conductive agent in the carbon electrode of the supercapacitors. The performance of the supercapacitor was improved as the wettability and conductivity of the electrode was improved by CDIL (Wei et al., 2013). As for GQDs, it was used in organic photovoltaic cells in the work of Li et al. (2011b) due to the outstanding absorption features such as large optical absorptivity and size-dependent band gap. Afterwards, carbon-based quantum dots are increasingly being used in solar cells. As yet, there has been a lot of studies on carbon-based quantum dots being used as co-sensitizers or sensitizers for DSCs (Gao et al., 2020).

In addition, carbon-based quantum dots were particularly suitable to be used as chemical detectors. The chemical sensing is done by examining the changes of the fluorescence strength from either external chemical or physical stimuli. According to Wang and Hu (2014), CQDs are able to detect deoxyribonucleic acid (DNA), iron (III) ions, mercury (II) ions, copper (II) ions, biothiol, glucose, phosphate, thrombin, and also nitrite. On the other hand, Ge et al. (2019) have shown the ability of GQDs as a sensor to detect iron (III) ions or protein that contains iron (III) ions. It is worth noting that in the study, GQDs can still perform well while facing complex samples, indicating its potential to be used practically.

Lately, the applications of carbon-based quantum dots have extended to the membrane filtration field. They are integrated into the filtration membrane as the size of the quantum dots is small and it is able to form chemical bonds with other compounds. The incorporation of carbon-based quantum dots into the membrane is able to improve the membrane performance or mitigate the inherent limitations of polymeric substrates (Zhao and Chung, 2018; Zhao et al., 2019b).

2.4 Nanofiltration and Reverse Osmosis

Nanofiltration (NF) is a type of membrane processes where its properties are between ultrafiltration (UF) and reverse osmosis (RO) (Bellona, 2014). The NF membranes were originally referred to as ‘loose RO’, ‘selective RO’, ‘open RO’, ‘intermediate RO/UF’ or ‘tight UF’ (Fane, Waite and Schaefer, 2004). These naming are based on the selectivity of the membranes. In several patents, NF membranes were described to have a better rejection of multivalent anion salts

than monovalent anion salts compared to RO membranes. At a fairly low transmembrane pressure, it is also capable to maintain a substantial water flux (Fibiger et al., 1989; Cadotte, 1981). Due to the characteristic variations of NF membranes in the industry, it is categorised into 2 major classes which are ‘loose’ and ‘tight’ to differentiate the membranes. Loose NF membranes rely on charge exclusion to limit the transport of ions and allow passage of low valance ions. In contrast, tight NF membranes are believed to rely on hindered diffusion in the membrane and also charge exclusion but to a lesser extent (Bellona, 2014).

On the other hand, RO is a pressure-driven membrane-based separation process which removes dissolved solids from a liquid (Wiles and Peirtsegaele, 2018). The flux rate of RO process is proportional to the applied pressure. In another words, theoretically, the higher the applied pressure, the higher the flux rate (Maddah et al., 2018). Although RO is the most widely used separation process for large scale fresh water production, it requires high electric energy (3-10 kWh/m³) to operate. RO membranes are normally dense and non-porous membranes which utilise the solution-diffusion model for separation. Figure 2.6 compares the nominal pore diameter of different membrane processes.

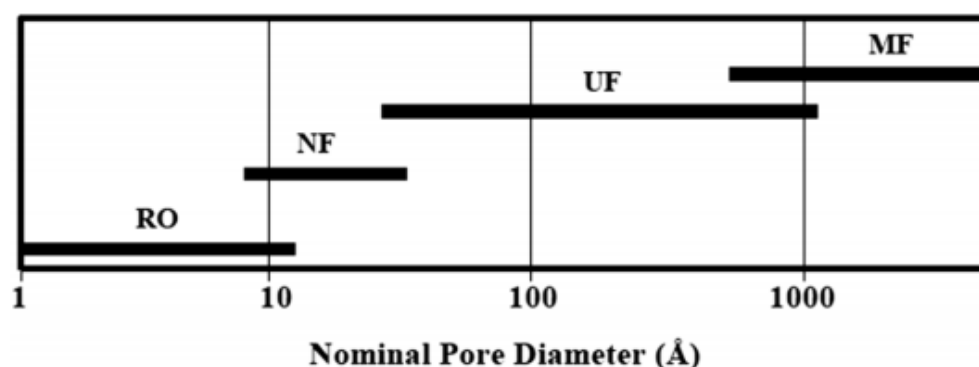


Figure 2.6: Comparison of Schematic Spectrum between Different Membrane Processes (Maddah et al., 2018)

The general comparison of the different membrane processes is presented in Table 2.5. In the industry, NF membranes are used in removal of salts in surface water, groundwater and saline. Besides, it is used in the elimination of disinfection by-products (DBPs) such as natural organic matter

(NOM) which can potentially react with disinfectants to form carcinogens. It is also widely used in lime softening and are more effective and RO membranes (Lee, Arnot and Mattia, 2011). Conversely, there are many applications of RO membranes in the industry while desalination being the most common application. In addition, it is used in peat water treatment to remove natural organic matter (NOM) and total dissolved solid (TDS). It can also be used as a concentration technique in food and beverage processing such as juice concentration and milk and whey concentration (Wenten and Khoiruddin, 2016).

Table 2.5: General Comparison between Membrane Processes (Shon et al., 2013; Abdel-Fatah, 2018)

Membrane Type	Operating Pressure (bar)	Pore Size (nm)	Typical Pure Water Flux ($Lm^{-2}h^{-1}$)	Retention Mechanism
Microfiltration (MF)	< 2	50 – 1000	500 – 10000	Sieving & Adsorption
Ultrafiltration (UF)	1 – 10	5 – 20	100 – 2000	Sieving & Preferential Adsorption
Nanofiltration (NF)	5 – 35	1 – 5	20 – 200	Sieving/ Diffusion/ Electrostatic Hydration
Reverse Osmosis (RO)	15 – 150	–	10 – 100	Diffusion

2.4.1 Retention Mechanisms of Nanofiltration

Both the size and charge effect play their role in the solute removal of NF membrane. Due to fact that NF membranes are porous, the pore size of the membrane becomes a vital factor in assessing the effect of the solute size. Besides, ionic groups such as SO_3H and $COOH$ are present on the structure of the polymer. The membrane becomes charged when it is in contact with the solution and rejects the charged components (Schaep et al., 1998).

Size effect plays an important role in NF process. It is essential to identify the membrane pore size in order to define the size effect. Normally gas adsorption-desorption or permoporometry is the go-to method to determine the

pore size of UF membrane. However, this method is not applicable on NF membranes as the pore size of NF membranes is too small. Advanced microscopic techniques such as atomic force microscopy (AFM) and field emission scanning electron microscopy (FESEM) are able to provide the image of the membrane surfaces. Nonetheless, information about the membrane pore structure cannot be obtained from these images. Thus, the pore size of the membranes is determined by filtration experiments in practice. Although any uncharged molecules can be used in the experiment, saccharides are preferred to for the identification of the membrane pore size. Spiegler-Kedem model is used to evaluate the membrane pore size. In order to obtain the membrane pore radii, σ , reflection coefficients are applied in the equation. This coefficient gives information of solute retention at infinitely high fluxes (Schaep et al., 1998). The equation is as follows,

$$R = \frac{\sigma(1-F)}{1-\sigma F} \quad \text{with} \quad F = \exp\left(-\frac{1-\sigma}{P}J\right) \quad (2.1)$$

$$\sigma = 1 - \left(1 + \frac{16r_s^2}{9r_p^2}\right) \left(1 - \frac{r_s}{r_p}\right)^2 \left(2 - \left(1 - \frac{r_s}{r_p}\right)^2\right) \quad (2.2)$$

where R (%) is the membrane solute rejection, J ($\text{L}\cdot\text{m}^{-2}\cdot\text{h}^{-1}$) is the flux, σ is the reflection coefficient, P ($\text{L}\cdot\text{m}^{-2}\cdot\text{h}^{-1}$) is the permeability, r_s (nm) is the solute radius, and r_p (nm) is the pore radius.

Beside size effect, the charged components also play a significant role in solute removal. In this case, charged ions, especially multivalent ions are removed by an additional repulsion force (Schaep et al., 1998). Multivalent ions have higher retention than monovalent ion. This phenomenon is caused by the charged surface of the membranes. According to Hoek, Tarabara and Van der Bruggen (2013), the membrane charge creates an unequal concentration of ion in the membrane. The ions that have an opposite charge from the membrane (counter-ion) have higher concentration in the membrane phase compared to the bulk solution and vice versa. At the interface of the membrane and bulk solution, a potential difference is created. This potential difference is referred to as Donnan potential. It will repel the co-ions to the membrane phase while counteracting the counter-ions to the solution phase. The counter-ion is rejected

due to the electroneutrality requirement. Hence, there is no net charge transfer through the membrane. The mechanism is called Donnan exclusion. However, as the concentration of the feed increases, the charge effect become less important. For a membrane with negative charge, a higher anion charge will have higher salt retention. In contrary, a higher cation charge will have lower salt retention (Schaep et al., 1998).

2.4.2 Retention Mechanisms of Reverse Osmosis

The retention mechanisms of RO can be described with the solution-diffusion model where the water flux is dependent on the pressure and concentration gradient across the membrane (Baker, 2012a). The concentration of the diffusing species at the surface of the membrane in equilibrium with the process fluid are determined by the composition, temperature, and pressure of the fluid at both side of the surface of the membranes. Diffusion of the permeants through the membrane will occur down a concentration gradient after they are dissolved in the membranes. Separation between different permeants is achieved because of the difference in the solubilities of the permeants in the membrane as well as the differences in the diffusing rates of the materials through the membrane (Baker, 2012a).

The effect of the driving forces on the water flux can be expressed with Equation 2.3 while the membrane rejection can be expressed with Equation 2.4

$$J_i = A(\Delta P - \Delta\pi) \quad (2.3)$$

$$R = \left[1 - \frac{\rho_i B}{A(\Delta P - \Delta\pi)} \right] \times 100\% \quad (2.4)$$

where J_i ($\text{g}\cdot\text{cm}^{-2}\cdot\text{s}^{-1}$) represents the flux, ΔP (Pa) is the pressure difference across the membrane, $\Delta\pi$ is the osmotic pressure differential across the membrane, ρ_i (g/cm^3) is the density of water, and B is the salt permeability constant.

From Equation 2.3, it can be interpreted that when the applied pressure is lower than the osmotic pressure, water tends to flow to the concentrated side from the dilute side by normal osmosis. When both of the parameters are equal, there is no flow across the membrane, and when the applied pressure is higher than the

osmotic pressure, water tends to flow from the concentrated side to the dilute side of the membrane.

2.5 Thin Film Composite Membranes

Thin film composite (TFC) membranes are the commonly used membrane in the industry. Normally TFC membranes are made up of 2 or more compositional layers, a thin selective layer on the top while, a porous sublayer at the bottom. These 2 layers are made with different materials and have different structures (Pinnau and Freeman, 1999). The top layer takes charge of the filtration process while the bottom layer supports the whole membrane in order to withstand high pressures. The top layer is typically made up of polyamide (PA) by interfacial polymerization (IP) technique (Khorshidi et al., 2016b). TFC membrane are highly desirable as the layers can be optimized separately according to the applications (Petersen, 1993).

Generally, conventional membranes face a common problem where choices have to be made between selectivity and permeability, i.e. high rejection of salt will lead to low water flux and vice versa. Hence, fabricating a membrane with high selectivity and water flux is highly desired. These researches include modifying the surface properties by grafting polymerization (Mohammad et al., 2015; Lee, Arnot and Mattia, 2011) and incorporating nanofillers to TFC membranes (Ng et al., 2013; Khorshidi et al., 2016a; Ahn et al., 2012). Even though previous researches have shown improvements in lab-scale, challenges such as to scale up the membranes in order to handle high volume of feed and fabricating cost still persists (Khorshidi et al., 2016b).

2.5.1 Thin Film Composite Membrane Fabrication

Interfacial polymerization (IP) is the most commonly used technique to fabricate thin film layer for NF and RO membranes. The thin film layer is fabricated by the copolymerization and reaction between two reactive monomers. The technique has gained attentions in the past decade because of the great enhancement of membrane performances and also the simplicity of the technique. The overall performance of the membrane such as salt retention, permeability and efficiency are determined by the thin film layer.

TFC membranes can be synthesized from different types of monomers. The performance of the membranes is determined by its structure and chemical properties. Hence, it is important to study the effect of using different active monomer on the membrane characteristics. Table 2.2 summarizes the information of the common and newly reported acyl chloride and amine monomers. Normally the PA layer of TFC membranes is formed through the reaction of amine monomers and acid chloride monomers. According to Lau et al. (2012), piperazine (PIP), p-phenylenediamine (PPD) and m-phenylenediamine (MPD) are the most commonly used monomers among the amine monomers. On the other hand, isophthaloyl chloride (IPC), 5-isocyanatoisophthaloyl chloride (ICIC) and trimesoyl chloride (TMC) are the most commonly used monomer among the acyl chloride monomer. Among these monomers, the TFC membrane synthesized from MPD and TMC by the interfacial polymerization is the most popular products in the market. Figure 2.7 shows the reaction pathway of MPD and TMC to synthesize a PA membrane with decent desalination characteristics. Namvar-Mahboub and Pakizeh (2013) reported a modified polyetherimide (PEI) membrane synthesized from MPD and TMC via IP technique. PEI membranes were modified with amino-functionalized silica nanoparticles by utilising a silane coupling agent (APDEMS). It was concluded that the thermal and mechanical stability of the PEI support were enhanced after the amino-functionalized silica was incorporated. Furthermore, Tsuru et al. (2013) demonstrated the fabrication of multi-layered PA membranes by two-step IP techniques assisted by spray with TMC and MPD as active monomers. Based on the study, the spray-assisted IP technique can enhance the water permeability of the membranes significantly.

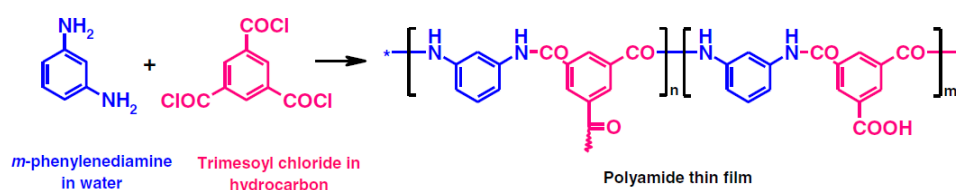


Figure 2.7: Interaction Between MPD and TMC to Form PA Selective Layer
(Lau et al., 2012)

Besides the monomer listed in Table 2.6, several new types of monomers such as tetraethylenepentamine (TEPA), triethylenetetramine (TETA) and diethylenetriamine (DETA) have been reported (Mohammad et al., 2015). Additionally, a new monomer, polyhexamethylene guanidine hydrochloride (PHGH) was reported by Li et al. (2014). It was reacted with TMC on polysulfone (PSf) UF membrane through IP to form NF membrane with good antibacterial property. The common problem of IP technique is the release of nanoparticles from the interfacial layer. The problem was avoided in this case as the medium of reaction was in aqueous phase.

Table 2.6: Different Monomers for TFC Membrane Synthesis (Lau et al., 2012)

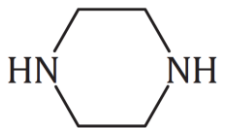
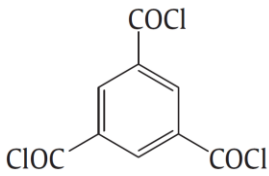
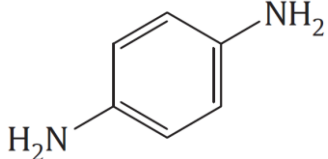
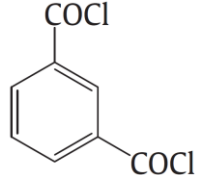
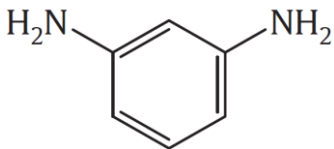
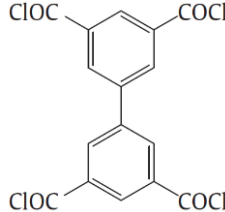
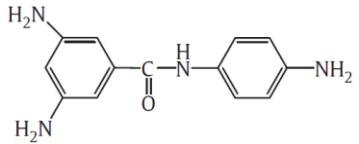
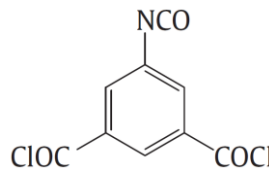
Amine Monomer	Chemical Structure	Molecular Weight	Acyl Chloride Monomer	Chemical Structure	Molecular Weight
Piperazine (PIP)		86.14	Trimesoyl chloride (TMC)		265.48
P-Phenylenediamine (PPD)		108.10	Isophthaloyl chloride (IPC)		203.02
M-Phenylenediamine (MPD)		108.10	mm-Biphenyl tetraacyl chloride (mm-BTEC)		404.03
3,5-diamino-N-(4-aminophenyl) benzamide (DABA)		242.27	5-isocyanatoisophthaloyl chloride (ICIC)		244.04

Table 2.6 (Continue)

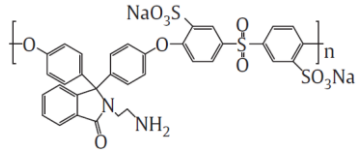
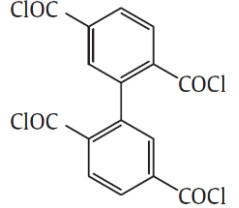
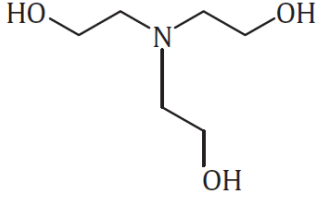
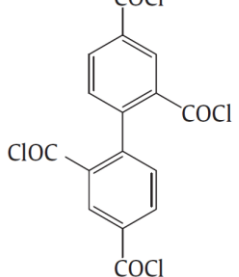
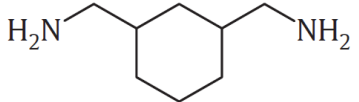
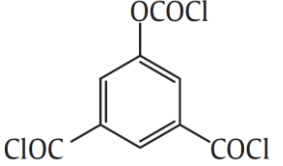
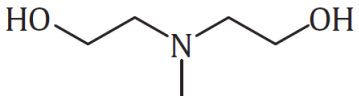
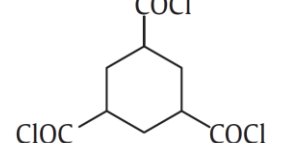
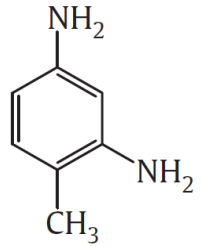
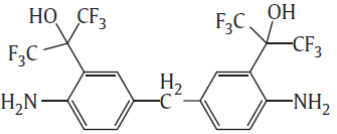
Amine Monomer	Chemical Structure	Molecular Weight	Acyl Chloride Monomer	Chemical Structure	Molecular Weight
Sulfonated cardo poly (arylene ether sulfone) (SPES-NH2)		774.71	op-Biphenyl tetraacyl chloride (op-BTEC)		404.03
Triethanolamine (TEOA)		149.19	om-Biphenyl tetraacyl chloride (om-BTEC)		404.03
1,3-cyclohexanebis (methylamine) (CHMA)		142.24	5-chloroformyloxy-isophthaloyl chloride (CFIC)		281.48
Methyl-diethanolamine (MDEOA)		119.16	Cyclohexane-1,3,5-tricarbonyl chloride (HTC)		271.53

Table 2.6 (Continue)

Amine Monomer	Chemical Structure	Molecular Weight	Acyl Chloride Monomer	Chemical Structure	Molecular Weight
m-phenylenediamine-4-methyl (MMPD)		122.17			
Hexafluoroalcohol-m-Phenylenediamine		530.31			

2.6 Thin Film Nanocomposite Membrane Modification

One of the ways to improve the performance in membrane filtration has been modifying existing membrane technology. Common method such as IP, NPs incorporation, UV treatment are used to achieve higher rejection tendency and selectivity, overcome membrane fouling, as well as increase water flux. The aforementioned techniques can be classified into IP and grafting polymerization. IP normally involves phase inversion to create the membrane support and followed by in situ IP to produce TFC membranes. Recently, NPs are often incorporated into the IP process to further improved the membrane properties. On the other hand, grafting polymerization includes layer-by layer (LbL) methods, electron beam (EB) irradiation, UV/photo-grafting, and plasma treatment (Mohammad et al., 2015).

2.6.1 Interfacial Polymerization (IP)

NPs are gaining more and more attention due to their great photoemission, microbial resistance and catalytic activity. As NPs are able to improve membrane performance through incorporation, the studies and researches on NPs incorporated membrane are increasing at an accelerated pace. The commonly incorporated NPs in NF membranes are silica, zinc oxide (ZnO), titanium dioxide (TiO₂) and silver (Mohammad et al., 2015).

Lee et al. (2007) reported silver (Ag) NPs immobilized PA membranes with improved anti-microbial properties. The membranes were prepared by in situ IP between TMC-Ag solutions and aqueous MPD. Based on the study, antibiofouling test were done upon the synthesized membrane and results showed that most of the bacteria were killed after the cultivation in the modified membrane. It showed the enhanced antifouling properties after the incorporation of silver NPs.

Besides, a study on boehmite NPs as a new nanofiller was reported by Vatanpour et al. (2012). Boehmite is an aluminium oxide hydroxide (γ -AlOOH) particle. It has an additional hydroxyl group on its exterior which helps in improving the surface properties and membrane hydrophilicity. It was found that the extra hydroxyl group of γ -AlOOH had significantly improved the antifouling properties and characteristic of the membranes compared to γ -Al₂O₃ (Vatanpour et al., 2012). On the other hand, Yin et al. (2012) reported the

utilization of MCM-41 silica NPs as a new nanofiller. The membranes were prepared through in situ IP of MPD in aqueous solution and TMC-NPs solution. As the loading of MCM-41 NPs increased, hydrophilicity, zeta potential and roughness of the membrane also increased. It is attributed to the porous characteristics of MCM-41 NPs.

Other than the incorporation of particular kind of NPs, the effects of the combination between two types of NPs were also studied. Based on the study performed by Daraei et al. (2012), polyaniline and iron(II, III) oxide (PANI/Fe₃O₄) NPs were utilised to produce membranes with enhanced copper (II) removal from water. The enhancement was attributed to the properties of PANI/Fe₃O₄ NPs which could improve the removal of heavy metal and organic matter. The incorporation of TiO₂/Al₂O₃ NPs to prepare hydrophilic composite membranes for photocatalysis and separation were also demonstrated by Mendret et al. (2013).

2.6.2 Grafting Polymerization

2.6.2.1 UV/Photo Grafting

UV-assisted grafting polymerization is a method where chemical bonds are formed between the active layer and membrane substrate while not having an effect on the bulk polymer. Thus, it has been commonly used for different surface modification works.

For UV grafting, Deng et al. (2011) have reported high flux membranes with positive charged which were prepared by the incorporation of methacryloxyethyl trimethyl ammonium chloride (DMC) onto PSf UF membranes by UV-induced grafting. The filtration performance is flexible and can be modified with different monomer concentration, irradiation distance and irradiation time. The synthesized membranes possessed high flux without sacrificing the salt rejection. It was reported that the membrane has a 94.8% rejection of magnesium chloride (MgCl₂). As the pressure increased, the salt rejection remains stable while the flux also increased.

Furthermore, Zhong et al. (2012) have fabricated positively charged membranes by UV-induced grafting of sulfonated polyphenylenesulfone (sPPSU). Two types of monomer have been used to modified the membrane which is 2-(methacryloyloxy)ethyl]trimethyl ammonium chloride (monomer A)

and diallyldimethyl ammonium chloride (monomer B). The pore size of the modified membrane has decreased from 10.86 to 1.2 nm for monomer A and 1.13 nm for monomer B. Besides, the molecular weight cut off (MWCO) of the sPPSU substrate decreased significantly after the modification (from 92972 Da to 1674 Da and 1627 Da). However, the membranes modified by monomer B have lower flux but higher salt rejection than monomer A due to the higher cross link density of monomer B. Figure 2.8 shows the comparison of the salts rejection between the membranes modified by different monomers.

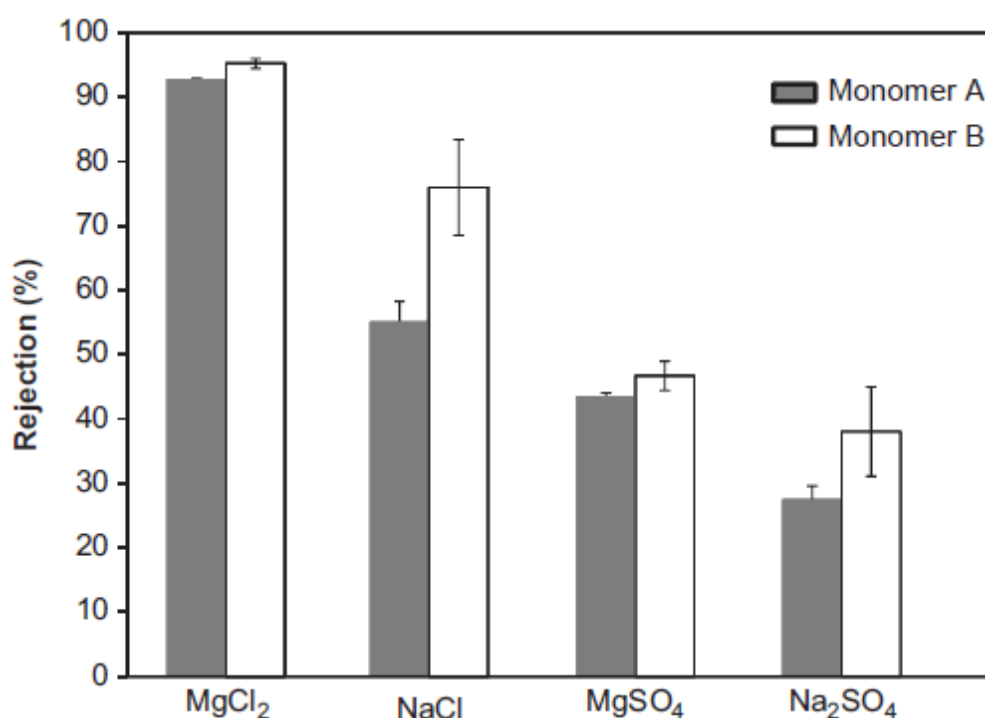


Figure 2.8: Rejection of Different Salts by the Different Modified Membranes (Zhong et al., 2012)

For photo grafting, Bernstein, Antón and Ulbricht (2013) have reported the conversion of polyethersulfone (PES) UF membranes into charged NF membranes by utilising hydrogel as selective layer via the UV-photo-induced grafting. The as-prepared NF membranes have high negative charges and barely changes with the pH due to the robust polyelectrolyte structure of the selective layer. Moreover, it was found that the membrane was highly hydrophilic through the measurement of the water contact angle. Besides, the influence of the polymerization conditions on the membrane performance was also studied.

According to Bernstein, Antón and Ulbricht (2013), the monomer concentration and the cross-linker could significantly affect the membrane performance. In this study, the monomer used was vinylsulfonic acid sodium salt (VSA). A NF membrane was obtained while the VSA concentration was higher than 25% while the cross-linker fraction was higher than 0.75 mol%. Further increase in the concentration of VSA leads to the improve in permeability but decline in salt retention. Besides, the irradiation time also governed the surface functionalization. NF membranes could be obtained after a few minutes of irradiation and further irradiation could improve the salt rejection but decrease the permeability. Due to the modification can be done easily on a large area UF membrane while preserving the membrane performance, it indicates that this modification procedure is able to be scaled up.

Similarly, Qiu, Nguyen and Ping (2007) demonstrated the modification of the membranes surface can be done via photo-grafted copolymer. The technique utilised both graft-copolymerization and UV irradiation of water-soluble monomers (allyl sulfonate and acrylate) on a cardo polyetherketone (PEK-C) membrane. The permeation flux was increased significantly without sacrificing on the salt rejection. The method is very attractive for industrial applications due to the facile procedure. The membrane characteristics are also controllable with factors such as the UV irradiation time, the distance of the membrane from the UV lamp and also the power of the UV lamp.

2.6.2.2 Electron Beam Irradiation

Electron beam (EB) irradiation is a great and simple technique to penetrate into polymer layer. This approach have gained attention from researchers as no special additives were needed to form active sites on the polymer (Mohammad et al., 2015).

Xu, Wei and Wang (2014) reported a highly negative charged membranes modified from a PSf UF membrane through the imbedding of 2-acrylamido-2-methylpropanesulfonic acid (AMPS) via EB radiation-induced technique. AMPS was grafted on both the inner and outer surface of the PSf UF membrane. The high grafting degree leads to the high negative charge density of the membrane. As a result of the increase of the negativity, the permeation

flux and pore size decrease which leads to better rejection of sodium sulphate (Na_2SO_4).

Furthermore, Linggawati, Mohammad and Ghazali (2009) demonstrated the modification of a semicrystalline polymer (nylon-66) that is able to be crosslinked via the EB irradiation. The surface and bulk morphology of the membrane was modified and it affects the membrane performance significantly. From the experiment, the membrane had high rejection of uncharged solutes but low rejection on salt solutions which indicates the formation of NF membranes. Additionally, another study were performed on nylon-66 by Linggawati, Mohammad and Leo (2012). In this work, γ -aminopropyltriethoxysilane (APTEOS) solution was added into nylon-66 and undergone EB irradiation before drying. Due to the addition of the APTEOS, more pores were formed in the membrane. In order to determine the optimum irradiation dose, the membrane was irradiated at 60 kGy, 70 kGy and 80 kGy. It was found that the increase in the irradiation dose has caused a dense layer to form in the membrane. Crosslinked silica was found in the membrane and it has achieved high degree of crystallinity. The nylon-66 membrane which was irradiated at 70 kGy was determined to be the most optimal membrane with great permeability, outstanding rejection of divalent ions and neutral solutes.

2.6.2.3 Plasma Treatment

Plasma treatment is a method that is able to increase the membrane surface hydrophilicity due the introduction of polar groups on the membrane surface. Besides, it is able to modify the chemical and physical properties of polymeric surface. However, the bulk properties are not affected.

Kim, Yu and Deng (2011) demonstrated the modification of the membrane surface through plasma treatment to enhance the anti-organic fouling properties of the membrane. The membranes were treated with ammonia (NH_3) plasma at low pressure and nitrogen-containing functional groups were introduced. Four types of membrane were treated in the experiment which were TFC-SR2, TFC-S, NF90 and NF270. As a result, the pure water flux, anti-fouling properties and salt rejection of all the membranes were enhanced significantly. The enhance water flux was attributed to the increased polar components and hydrophilic centre while the improved salt rejection of the

membrane was attributed to the plasma-induced surface crosslinking. Due to the improved hydrophilicity and negativity density of the membrane surface, the adsorption of organic foulants such as humic acid and bovine serum albumin (BSA) also decreases.

Similarly, Buonomenna et al. (2009) reported a low temperature plasma treatment to modify polymeric membranes surface. The plasma surface modification was done on a poly(ether ether ketone) (PEEKWC) membrane. Through the process, amino groups were introduced on the PEEKWC membrane by using argon gas or hydrogen gas as pre-treatment gases. Both modified and unmodified membrane were compared and similar results were obtained. The hydrophilicity of the modified membrane was improved after the plasma modification which leads to higher water permeation. Additionally, the plasma modified membrane discriminated between compounds that carry negative and positive charge without fouling and decreasing in flux.

Moreover, another recent work demonstrated the use of a two-step plasma method. Wang et al. (2012) reported a technique to prepare a negatively charged NF membrane via the grafting of AMPS on the PSf UF membrane via two-step plasma method. The PSf UF membrane was pre-treated by plasma and followed by the grafting of AMPS on the membrane via plasma-initiated grafting. It was found that the rejection performance of the membrane was governed by the pre-treatment and reaction time as well as the concentration of AMPS. As the pre-treatment time increases, the rejection of the sodium sulphate salt also increases. Nevertheless, the rejection performance decreases as the pre-treatment time exceed 30 s due to the membrane surface was damaged.

2.6.2.4 Layer-by Layer Assembly

Layer-by layer (LbL) technique is a facile process that is capable to prepare flat and thin structure. It can be done without polymerization or immobilization. Besides, it is capable to limit membrane fouling and the formation of biofilm on various type of membrane (Lasquellec et al., 2007).

In the study reported by Hadj Lajimi et al. (2011), cellulose acetate (CA) membranes was prepared through LbL technique. The surface was modified through the adsorption of alternate films of chitosan (CHI) and sodium alginate (ALG). From the experiment, an improved divalent salt rejection membrane

was obtained. It was concluded that the ratio of salt retention and permeation was optimum at 15 bilayers. It also gave better separation of monovalent and divalent salt. However, the performance of the membrane decreases when it was increased beyond 20 bilayers due to the decrease in hydrophilicity. The divalent salt rejection was dominated by charge density when the membrane was below 15 bilayers. Thus, the multilayer membrane has higher water flux and better divalent salt rejection. Beyond 20 bilayers, it was dominated by size exclusion which and have lower permeability of water and salts.

In addition, Ng et al. (2014) reported the fabrication of membrane with high performance stability and salt selectivity via LbL technique. The method is rapid in synthesis, facile, and most importantly effective in improving the salt rejection. It was found that the performance of the modified 5 polyelectrolyte bilayers on the membrane was on par with the other membrane with more than 50 bilayers. It indicates the potential of the polyelectrolyte membrane to be another way in fine tweaking the performance of membranes (Mohammad et al., 2015).

Moreover, the use of graphene oxide (GO) in membrane fabrication was shown in another work. Hu and Mi (2014) demonstrated a LbL method in the fabrication of membrane using negatively charged GO and positively charged poly(allylamine hydrochloride) (PAH) by electrostatic interactions. The as-prepared membrane possessed high sucrose rejection (~99%) and maintained a tight structure in low ionic strength solution. This indicates that the potential of the membranes to be applied in the water treatment process with low ionic strength. Table 2.7 and Table 2.8 summarizes different approaches used to fabricate TFN membranes.

Table 2.7: Interfacial Polymerization Technique Used in Preparing Polyamide Thin Film Nanocomposite (PA TFN) Membranes

Method	Type of Membrane/ Monomer	Type of Nanofiller	Enhanced Aspect Description	References
Interfacial Polymerization	MPD and TMC	Silver	Improved antibiofouling properties as colonies of microorganism were killed after they were cultivated on the membranes.	(Lee et al., 2007)
	PES	Boehmite (γ -AlOOH)	Enhanced reversible fouling resistance from 27.4 to 49.5 % while flux recovery ratio was increased from 58.2 to 84.5%.	(Vatanpour et al., 2012)
	MPD and TMC	MCM-41 silica	Improved water flux from 28.5 to 46.6 LMH while maintaining high salt rejection (NaCl – 97.9% and Na ₂ SO ₄ – 98.5).	(Yin et al., 2012)
	PES	PANI/Fe ₃ O ₄	High Cu (II) ions rejection (~85 %)	(Daraei et al., 2012)

Table 2.8: Grafting Polymerization Techniques Used in Preparing Polyamide Thin Film Nanocomposite (PA TFN) Membranes

Method	Type of Membrane/ Monomer	Type of Nanofiller	Enhanced Aspect Description	References
UV/Photo Grafting	PSf	DMC	High MgCl ₂ rejection 94.8 % with high flux of 20.3 LMH at low pressure (0.2 MPa)	(Deng et al., 2011)
	sPPSU	2-(Methacryloyloxy)ethyl]trimethyl ammonium chloride and diallyldimethyl ammonium chloride	Exhibit high MgCl ₂ rejection of 92.76 % and 95.20 % while maintaining high water permeability of 14 and 9 LMH/bar respectively	(Zhong et al., 2012)
	PES	VSA	Exhibit stable negative zeta potential across the entire pH range, indicating improved antifouling properties.	(Bernstein, Antón and Ulbricht, 2013)

Table 2.8 (Continue)

Method	Type of Membrane/ Monomer	Type of Nanofiller	Enhanced Aspect Description	References
UV/Photo Grafting	PEK-C	Allyl sulfonate and acrylate	Improved water flux of 9 LMH/bar while salt rejection and selectivity are kept constant	(Qiu, Nguyen and Ping, 2007)
Electron Beam Irradiation	PSf	AMPS	Enhanced Na ₂ SO ₄ rejection from 15 to 90 % and Cr (VI) rejection of 95.1 %	(Xu, Wei and Wang, 2014)
	Nylon-66	-	High vitamin B-12 and raffinose rejection (up to 88.4 %)	(Linggawati, Mohammad and Ghazali, 2009)
	Nylon-66	APTEOS	High vitamin B-12 and raffinose rejection (up to 92.6 %)	(Linggawati, Mohammad and Leo, 2012)

Table 2.8 (Continue)

Method	Type of Membrane/ Monomer	Type of Nanofiller	Enhanced Aspect Description	References
Plasma Treatment	NF270, NF90, TFC-S and TFC-SR2	-	Slight improvement on water flux from 0.9 to 1.0 LMH/psi	(Kim, Yu and Deng, 2011)
	PEEKWC	-	High rejection on dye (methylene blue – 100 % and methyl orange – 68 %)	(Buonomenna et al., 2009)
Layer-by Layer Assembly	CA	CHI and ALG	Improved antifouling properties as stable flux and rejection was obtained under long operation.	(Hadj Lajimi et al., 2011)
	PAH	GO	High sucrose rejection (~99%) and maintained a tight structure in low ionic strength solution.	(Hu and Mi, 2014)

CHAPTER 3

METHODOLOGY AND WORK PLAN

3.1 Research Methodology

A literature review is essential for research and academic fields since it provide an overview or evaluation of the previous works by relating them in one single work. Generally, there are three types of literature review: qualitative systematic review, quantitative systematic review, and narrative review (Green, Johnson and Adams, 2006). Herein, qualitative and quantitative systematic review are applied. Qualitative systematic review is where a thorough search of literatures was done based on a research question (Chambers, 1997). It helps the researcher to decide whether a research publication should be included or excluded from the final thesis (King, 2001). On the other hand, quantitative systematic review, which is also known as meta-analysis evaluates each publication critically and combines the results statistically (Slavin, 1995).

3.2 Work Plan

In general, the methodology of this study can be divided into three main sections: investigation, interpretation, and lastly presentation. Each of these sections can be further broken down into smaller tasks. The general flow is presented in Figure 3.1.

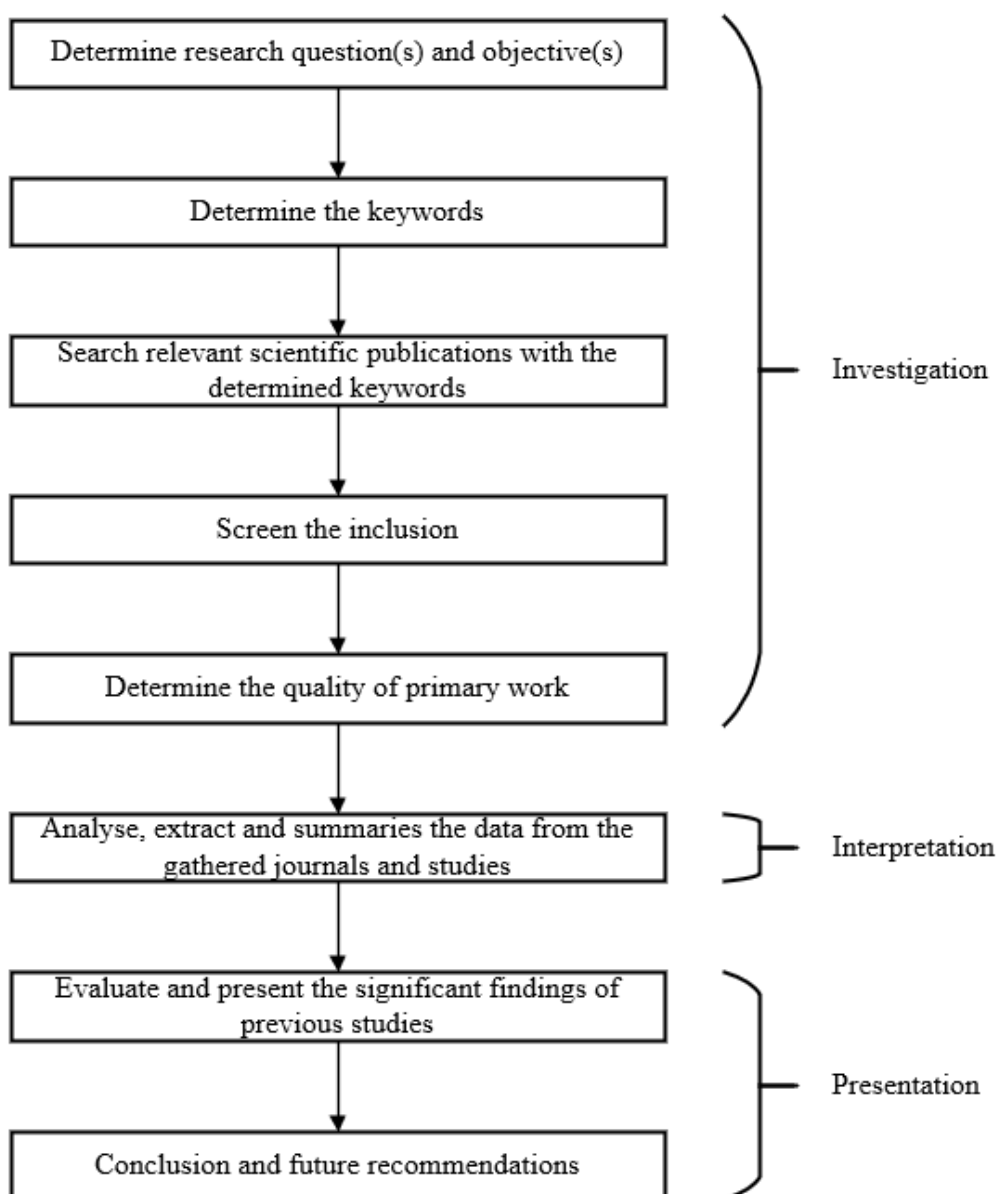


Figure 3.1: Illustration of the General Work Plan of This Study

3.2.1 Investigation Phase

First of all, it is vital to determine the research questions as it determines the impact of the study on the research community (Snyder, 2019). From the process, the formulation of the purpose, research interest as well as the scope are also addressed. These actions aid the identification of the approach used to conduct the review. This study aims to summarize and evaluate the effect of the incorporation of carbon-based quantum dots on the performance and characteristic of TFN membranes. Thus, an integrative review is not reliable and a systematic review approach is applied. In order to determine the research

questions and objectives, discussions were conducted with the supervisor to avoid divergence from the topic. It is the one of the keys to design a comprehensive review with well-defined direction to conduct the study. The determined research questions and objectives were presented in Chapter 1.

Subsequently, the keywords, inclusion and exclusion criteria can then be identified to smoothen the process of searching suitable publications to be analysed. This step will affect the quality of the research significantly (Snyder, 2019). For instance, the keywords include “thin film nanocomposite membranes”, “carbon quantum dots”, “graphene quantum dots”, “graphene oxide quantum dots”, and “interfacial polymerization”. Meanwhile, the journals with publication date within these 5 years will be included to make sure that the information and data collected are up to date. However, the search strategy might differ depending on the available information. Next, obtaining journals from a reputable source is also vital as it affects the trustworthiness of the work. Thus, the information and data presented in this study are acquired from reputable online journal websites. These websites include:

1. ScienceDirect
2. Wiley Online Library
3. ResearchGate
4. ACS Publications
5. Springer Link
6. Semantics Scholar
7. Royal Society of Chemistry
8. Hindawi
9. Elsevier

After a sufficient number of relevant journals are acquired with the aforementioned method, the journals were screened thoroughly to identify its relevancy and applicability based on the pre-defined inclusion and exclusion criteria. This process helps aim to minimize the mistakes or digressions while conducting the review. In order to manage the large number of journals, Mendeley Desktop was used to simplify the process of citing and referencing. The last process in the investigation phase is the determination of the primary work. It is important for a study as it provides detailed information of interest

together with new ideas and insight. Figure 3.2 shows the main page of Mendeley Desktop.

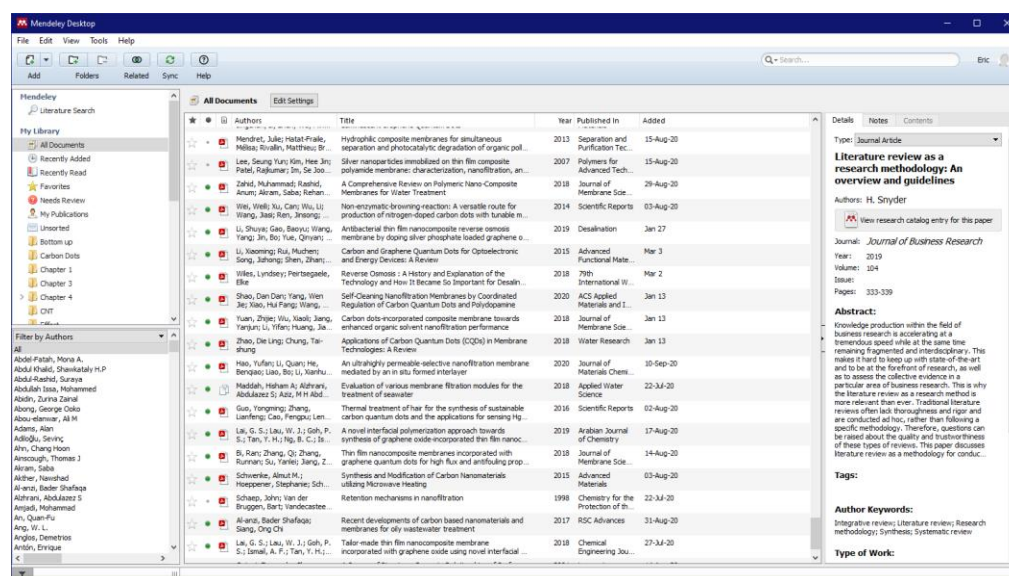


Figure 3.2: Main Page of Mendeley Desktop

3.2.2 Interpretation Phase

In the interpretation phase, the collected information and data were abstracted and analysed comparatively. In another words, the data were interpreted and related to form a comprehensible review based on the research questions and objectives. For example, interesting findings, similarities, and difference between previous studies were determined and presented in later phase. By conducting in-depth interpretation, the review is able to fill the gap in recent studies and offer a practical guide for future work. Generally, the gathered journals are categorized into two class, which is quantitative and qualitative. Table 3.1 presents the differences between qualitative research approach and qualitative approach and different data collected from each class.

Table 3.1: Differences between Qualitative and Quantitative Research Approaches (Apuke, 2017)

Criteria	Qualitative Research	Quantitative Research
Aim	<ul style="list-style-type: none"> - Identify types of carbon-based quantum dots incorporated into TFN membranes that would result in desired improvement in characteristics and performance. - Identify the methods to incorporate carbon-based quantum dots into TFN membranes. 	Identify the degree of improvements in the characteristics and performances after the incorporation of carbon-based quantum dots.
Group Studied	Large and randomly selected.	Small and not randomly selected.
Variables	<ul style="list-style-type: none"> - Incorporation methods - Type of carbon-based quantum dots 	Performance improvements
Type of Data Collected	<ul style="list-style-type: none"> - Words - Images 	<ul style="list-style-type: none"> - Number - Statistics
Results	<ul style="list-style-type: none"> - Types of carbon-based quantum dots - Function of the incorporation of carbon-based quantum dots - Effect of the incorporation of carbon-based quantum dots on the membranes. 	<ul style="list-style-type: none"> - Flux after the incorporation - Salt rejection after the incorporation - Zeta potential after the incorporation - Water contact angle after the incorporation

3.2.3 Presentation Phase

As per mentioned in Section 3.1, qualitative and quantitative systematic review are applied in this review to focus on the method to incorporate carbon-based quantum dots into TFN membrane and its effect on the membrane characteristic as well as the performance. By conducting the review with these approach, the conclusion is more generalizable as the review was produced from pooling of data from previous studies (Green, Johnson and Adams, 2006).

CHAPTER 4

RESULTS AND DISCUSSION

4.1 Incorporation of Carbon-based Quantum Dots Nanoparticles in Membrane

In recent years, many researchers have demonstrated the incorporation of CQDs, GQDs, and GOQDs in different types of membranes to modify the selective layer to improve membrane performance. Unlike nanosheets, carbon-based quantum dots can be easily integrated into the membranes due to their small sizes. It is popular due to their outstanding hydrophilicity, relatively inexpensive, chemically stable and has low toxicity (Singh et al., 2018). The most common ways to integrate the NPs in the membrane is through the IP process. Normally, these NPs are dispersed in the aqueous phase before it is brought into contact with the organic phase for the IP process (Zhao and Chung, 2018). It has been proven that the carbon-based NPs modified TFN membranes are able to deliver outstanding performance compared to the pristine ones even when the NPs are in a small amount. The resultant membranes show enhanced water permeability without compromising on the rejection of solute selectivity, improved surface hydrophilicity, and antifouling properties (Shirke et al., 2019). These properties and performances can be further enhanced through the proper tuning of the amount of carbon-based NPs as well as proper functionalization on the NPs. Figure 4.1 shows the incorporation of CQDs, GQDs and GOQDs into the membrane to form TFN membranes (Zhao and Chung, 2018). By modifying the selective layer, the material usage can be minimized while maximizing the performance as the carbon-based NPs only existed in the dense-selective layer.

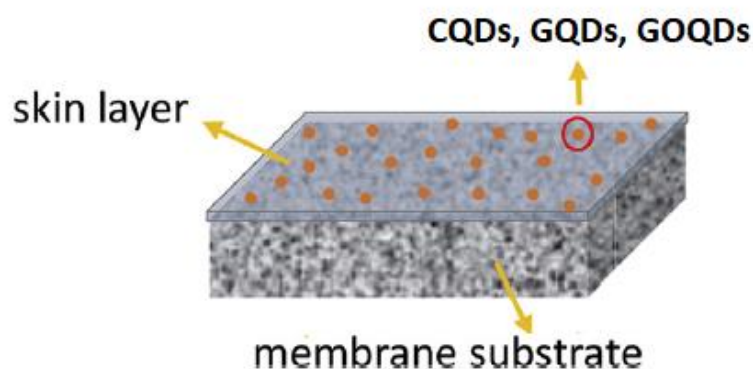


Figure 4.1: Typical Carbon-based Nanoparticles Incorporated Thin Film Nanocomposite Membrane (Zhao and Chung, 2018)

4.2 Carbon-based Quantum Dots Modified Thin Film Nanocomposite (TFN) Membranes

4.2.1 Preparation of Carbon-based Quantum Dots Nanofiltration Membrane

A number of studies had proven that CQDs were able to be incorporated into a number of different monomers and substrates which lead to a flux increment of a wide range, from 50% to 6.8 times. Yuan et al. (2018) fabricated TFN membranes comprising CQDs with sub-5 nm diameter in a PEI film by an interfacial polymerization reaction on a polyacrylonitrile (PAN) substrate for organic solvent recovery. The synthesized CQDs were first dispersed into water before added into the aqueous PEI solution. The mixture was then casted onto the PAN substrate and removed after 10 minutes. Afterwards, TMC organic solution was casted on the PEI saturated membrane for cross-linking reaction for another 2 minutes. Similar procedure was seen in the work of He, Zhao and Chung (2018), where the membrane with PES substrate was developed specifically for arsenic and selenium removal. Similar study was performed by Sun and Wu (2018) by using PSf as the substrate. In both studies, CQDs were dispersed in a PIP aqueous phase before being casted onto the porous substrate. During the IP, the carboxyl and hydroxyl groups of CQDs and the amine groups of PIP reacted with the acyl chloride groups of TMC to form a selective layer on the porous substrate. In a latest study, Guo et al. (2021) incorporated amino-rich CQDs (CQDs-NH₂) into the PA layer of a PES/PEI-TMC membrane. The CQDs-NH₂ was made by pyrolyzing PEI which is different from the

conventional method where citric acid was pyrolyzed instead. Figure 4.2 shows the mechanism of the reaction. In the reaction, CQDs-NH₂ solution was varied from 0 to 2.4 wt% and acted as the aqueous monomer solution and reacted with TMC organic solution.

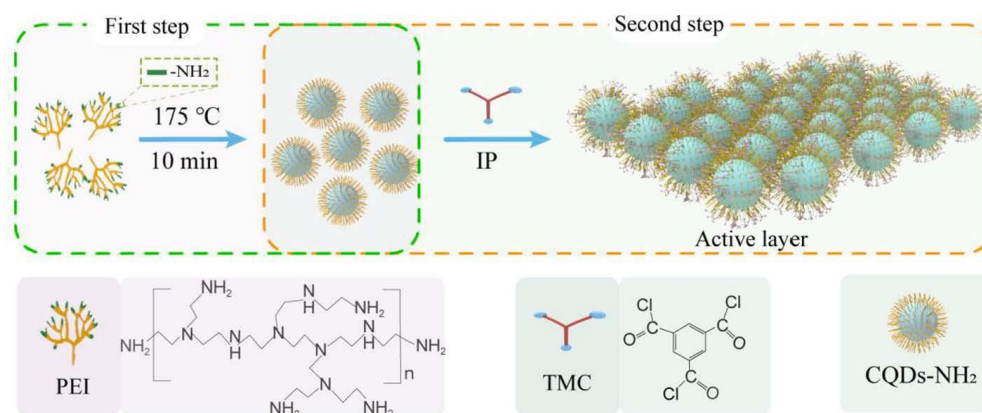


Figure 4.2: Schematic Diagram of the Methods to Fabricate the CQDs-NH₂-modified TFN Membranes (Guo et al., 2021)

Yang et al. (2020) took a different approach to incorporate CQDs on the porous substrate. The carboxyl groups of CQDs were first activated on the PES substrate by immersing the PES substrate in 2-chloro-1-methylpyridinium iodide (CMPI), NaOH, CQDs, and deionized water for 10 minutes. Then, the IP between PEI and TMC was conducted by first immersing the CQDs saturated substrate in PEI and TMC for 2 and 1 minutes respectively. Instead of dispersing the CQDs in the aqueous phase, the carboxyl groups-activated CQDs were directly casted onto the PES substrate before the IP between PEI and TMC. The resultant membrane was negatively charged which was ideal for the separation of amino acids and inorganic salts. Figure 4.3 shows the schematic diagram for the procedure to prepare the NF membrane.

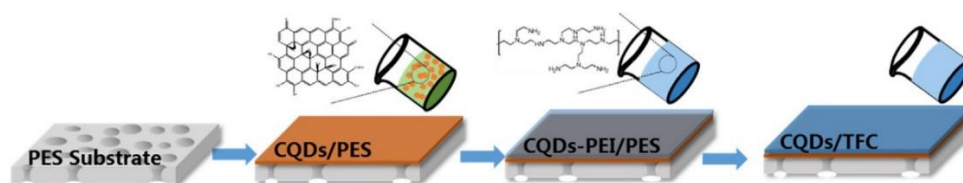


Figure 4.3: Schematic Diagram of the Preparation of TFN NF Membrane (Yang et al., 2020)

In a recent study conducted by Shao et al. (2020), the approach taken was similar to the study conducted by Yang et al., (2020). In the study, the CQDs was also activated with the same procedure and the membrane was further modified by treating it with polydopamine (PDA) solution for the self-polymerization in order to achieve a better antifouling property. Figure 4.4 shows the comparison between the PDA treated membrane and the pristine membrane. By coating a layer of PDA on the surface of the membrane, the negative charge density of the membrane was enhanced and led to less serious concentration polarization and eventually less fouling.

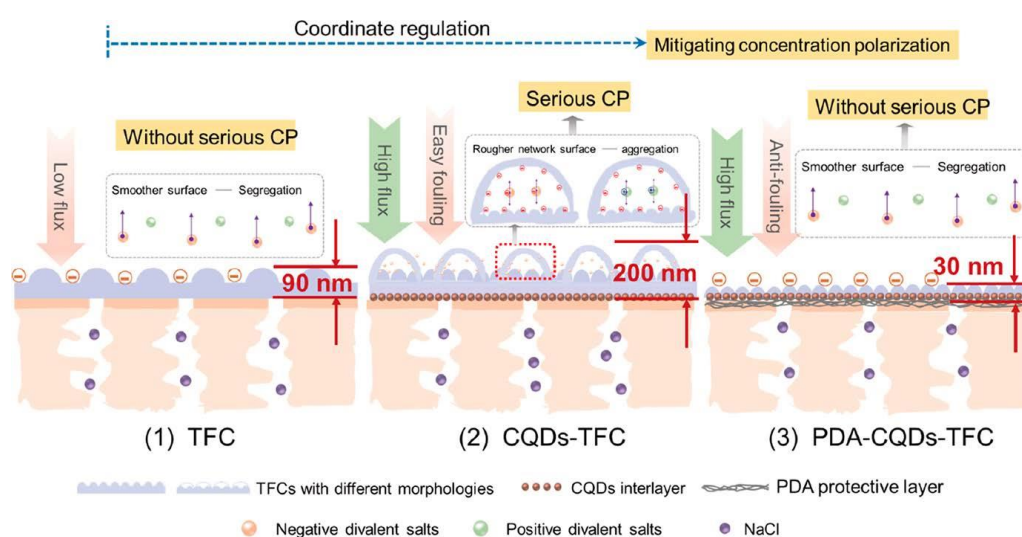


Figure 4.4: The Severity of Concentration Polarization on Different Membrane Surfaces (Shao et al., 2020)

On the other hand, GOQDs have also gained tremendous attention as it possesses both unique properties of graphene and also quantum dots (Zhang et al., 2017). For instance, it exhibits high mechanical strength, monatomic thickness, 2-dimensional structure and chemical inertness. All of these traits are able to further improve the performance of the membrane such as rejection and water permeability. When it comes to the fabrication process of GOQDs incorporated TFN membranes, there are more similarities than differences than the incorporation of CQDs. As illustrated in Figure 4.5, Zhang et al. (2017) uses PAN as the support while using less common monomers such as tannic acid (TA) and isophorone diisocyanate (IDPI) to form the selective layer. The other process was similar where the GOQDs with concentration ranging from 0 to 1

g/l with 0.25 g/L interval were dispersed in TA aqueous solution before the mixture was casted onto the surface of the support. The mixture was allowed to contact with the support for 20 minutes in order for the TA monomers and GOQDs to diffuse into the porous support. Upon removing the mixture, IPDI solution was casted onto the TA/GOQDs saturated surface for IP and leave for 10 minutes.

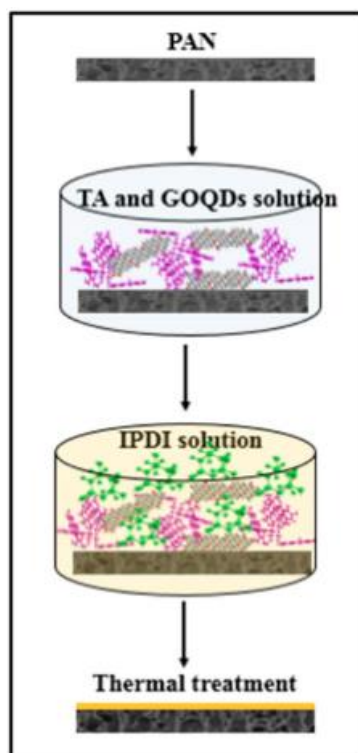


Figure 4.5: Illustration of the Preparation of GOQDs Incorporated TFN Membranes (Zhang et al., 2017)

In another work by Li et al. (2019b), the compatibility of GOQDs with other monomers such as MPD and 1,2,4,5-benzenetetracarboxylic acyl chloride (BTAC) was shown. The GOQDs were incorporated into in the MPD aqueous phase and tetra-acyl chloride was used as the organic monomer instead of TMC to form a selective layer of polyamic acid (PAA) through IP. As the membranes were subjected to further treatment, the contact time of the monomers with the substrate was relatively short which is 6 and 8 seconds for the organic phase and the aqueous phase respectively. This could prevent the formation of RO membranes as the membrane will undergo chemical cross-linking in 1,6-hexanediamine/isopropanol (HDA/IPA) solution for 1 hour after the IP process.

Afterwards, the membrane was activated using N, N-dimethylformamide (DMF) at 80 °C for 30 minutes to increase the permeability of ethanol in this particular application which is solvent resistant NF (SRNF).

In the case of GQDs, there are not much of a difference in the incorporation procedure compared to the incorporation of CQDs and GOQDs. In a study done by Bi et al. (2018), the PES substrate was immersed in the aqueous solution which contains PIP and GQDs for 10 minutes and dipped in the TMC organic solution for 2 minutes for the IP reaction. Figure 4.6 shows the general preparation of the GQDs incorporated TFN membranes.

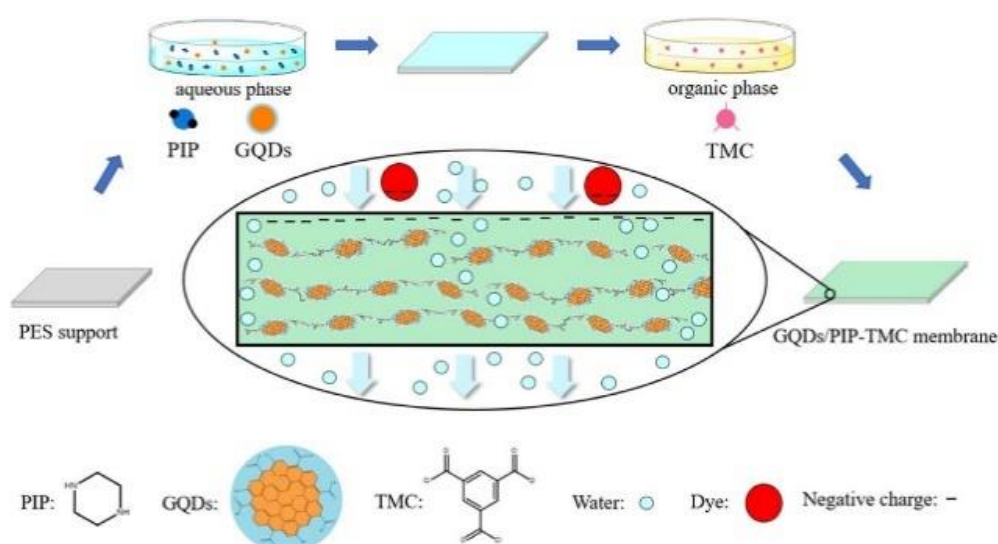


Figure 4.6: General Flow of the Preparation of the GQDs Incorporated TFN Membranes (Bi et al., 2018)

Besides, it is not uncommon that GQDs are used directly as the monomer for the IP process instead of being incorporated as NPs. In the studies of Bi et al. (2019), Lin et al. (2020), and Xue et al. (2020), the procedure, type of monomers and substrate were similar. Firstly, GQDs was dispersed in deionized water before the PES substrate was immersed in it for 15-30 minutes. The membranes were then drained with filter paper and immersed in the TMC organic phase for another 2-10 minutes for the IP reaction. The difference in the contact time have led to the performance difference which will be discussed in later section.

Next, functionalized GQDs also gained some attention recently which have expanded the application of GQDs significantly. For instance, amino-

functionalized GQDs (GQDs-NH₂) allows the GQDs to inherit the advantages of GQDs and also benefit from the amine groups (-NH₂). Similar to the functionalized CQDs in the work of Guo et al. (2021) which have been discussed earlier, the incorporation of GQDs-NH₂ introduced more amine groups and hydroxyl groups during IP and eventually lead to the improvement of properties such as chargeability and hydrophilicity (Xu et al., 2021). The incorporation of GQDs-NH₂ was also found in another work by Li et al. (2019c). In the study, GQDs-NH₂ with concentration ranging from 0 to 300 mg/L with 50 mg/L interval was dispersed in MPD aqueous solution by ultrasonication. The IP reaction was conducted by contacting the polyimide (PI) substrate with the mixture for 8 seconds followed by BTAC organic solution for another 6 seconds. Similar to the work of Li et al. (2019b), the resulting membrane was subjected to chemical crosslinking in HDA/IPA solution at 60 °C. DMF was also used to activate the membrane at 80 °C. Beside GQDs-NH₂, in a recent study done by Wu et al. (2021), L-aspartic acid functionalized GQDs (AGQDs) were incorporated in the TFN NF membranes. There are several advantages of AGQDs over the unfunctionalized GQDs. Firstly, the addition of L-aspartic acid grants the zwitterionic feature of AGQDs which will enhance the antifouling properties of the membrane. Secondly, AGQDs have better affinity and able to disperse better on the PSf substrate which will allow more AGQDs to participate in the IP reaction. Thus, the NPs are able to contribute more to the performance and structure of the TFN membranes (Wu et al., 2021). Figure 4.7 shows the preparation steps of the AGQDs incorporated TFN membranes.

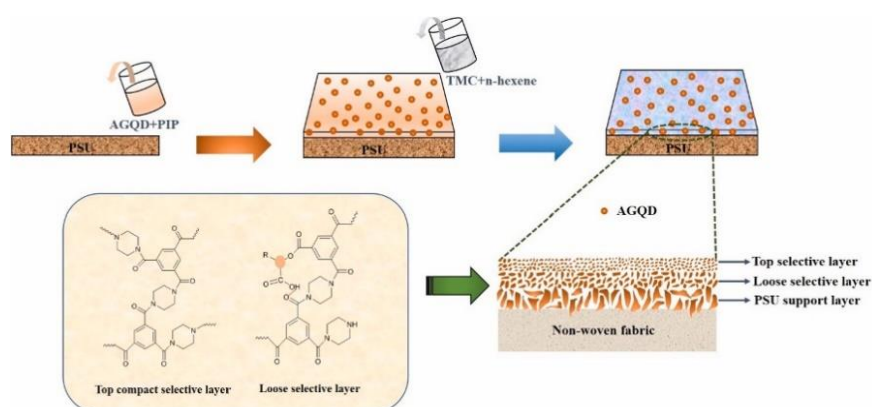


Figure 4.7: Preparation of L-aspartic Acid Functionalized GQDs incorporated TFN Membranes (Wu et al., 2021)

While comparing the approaches taken to conduct IP process from different journal, it can be categorized into two types: (1) rubber roller IP and (2) vacuum filtration-assisted IP. Conventional IP that requires rubber rolling to remove excess solution on the membranes could potentially cause an uneven distribution of NPs or loss of most of the NPs from the substrate surface (Lai et al., 2019). Vacuum filtration-assisted IP is able to overcome this limitation as the excess solution is removed by vacuum filtration. However, rubber roller IP is still adopted by most researchers mainly due to the simplicity of the process (Li et al., 2019b; Yang et al., 2020). Figure 4.8 shows the illustration of rubber roller IP and vacuum filtration-assisted IP. Similar to CQDs and GOQDs, GQDs are also compatible with different monomers such as MPD. Liang et al. (2020) demonstrated GQDs incorporated TFN membranes by using MPD and TMC as the monomers. The PEI substrate was immersed in the aqueous phase and organic phase for 2 and 1 minutes respectively. In summary, vacuum filtration-based IP is able to fabricate TFN membranes with better performance than the conventional rubber rolling IP as it is able to minimize the loss of carbon-based quantum dots during the fabrication at the cost of a more complex procedure.

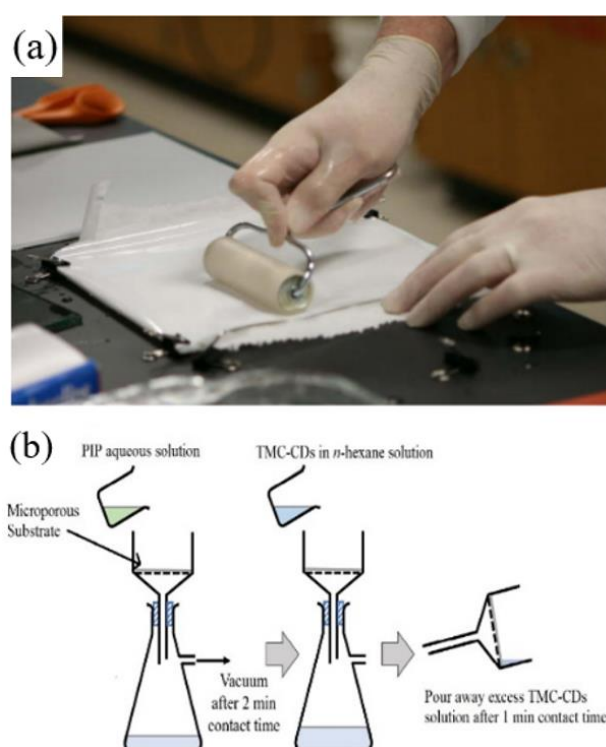


Figure 4.8: Illustration of (a) Rubber Rolling IP and (b) Vacuum Filtration-Assisted IP (Xie et al., 2012)

4.2.2 Preparation of Carbon-based Quantum Dots Reverse Osmosis Membrane

Generally, the fabrication process of RO membranes has more similarity than difference from the fabrication process of NF membranes. There is less recent paper reported on carbon based-quantum dots RO membranes compared to NF membranes as the RO technology have been widely researched and implemented for the past decades compared to the NF technology. Li, Li and Zhang (2017) demonstrated the incorporation of super hydrophilic CQDs with an average diameter of 6.8 nm into the selective layer of TFN membranes. Firstly, the PSf porous support was immersed in aqueous solution which contains MPD and CQDs with different concentration ranging from 0 to 0.08 wt%. The membrane was then removed from the solution and a rubber roller was used to remove the remaining excess solution. Afterwards, the membranes were immersed in TMC organic solution to form the PA selective layer. Although flat sheet membranes are being studied more extensively compared to hollow fibre (HF) membranes, HF membranes are the most widely used membranes in desalination due to its large surface area per unit module volume, no need of spacers, simplicity in module fabrication and has self-mechanical support (Gai, Zhao and Chung, 2019). Herein, Gai, Zhao and Chung (2019) used a Na⁺ functionalized CQDs (Na-CQDs) as NPs to fabricated TFN HF membranes. In their work, the support of the TFN HF membranes were prepared through a dry-jet wet spinning process through a spinning machine. A setup of spinning machine is shown in Figure 4.9 (Fried, 1997). The polymer solution which contains poly(ethylene glycol) (PEG) and N-methyl pyrrolidone (NMP) (1:1), PES and deionized (DI) water were fed into the middle channel of the dual layer spinneret while the DI water and NMP were fed into the inner and outer channel respectively. The prepared HF membranes were inner-selective. For the selective layer, MPD aqueous solution which contains Na-CQDs was introduced into the lumen of the support for 3 minutes before air was purged through the lumen for 5 minutes to remove the excess aqueous solution. Then, TMC organic solution was introduced into the lumen of the support for 5 minutes and another 1 minute for air purging.

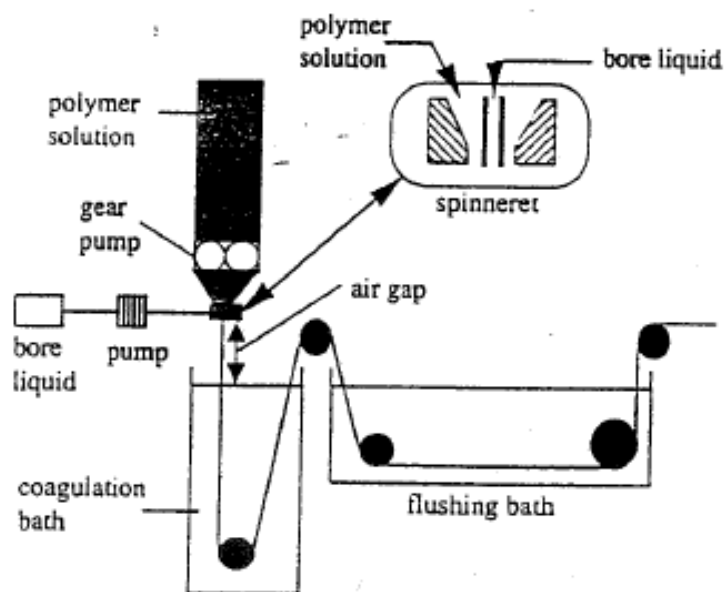


Figure 4.9: Illustration of a Spinning Machine (Fried, 1997)

On the other hand, the incorporation of GOQDs in TFN RO membranes also received a lot of attention over the past few years. For instance, Song et al. (2016) reported a GOQDs incorporated TFN RO membranes fabricated through vacuum filtration IP process with MPD and TMC as the monomers. The general procedure was illustrated in Figure 4.10. In this study, GOQDs with different mass (1, 2, 5, 10 mg) were added into the MPD aqueous solution. With the assistance of nitrogen pressure, the aqueous solution was filtered at 2 bar in a dead-end filtration cell to deposit the monomers and nanofillers on to the porous PSf support. TMC organic solution was used again in this study as the acyl chloride monomers to form the PA selective layer.

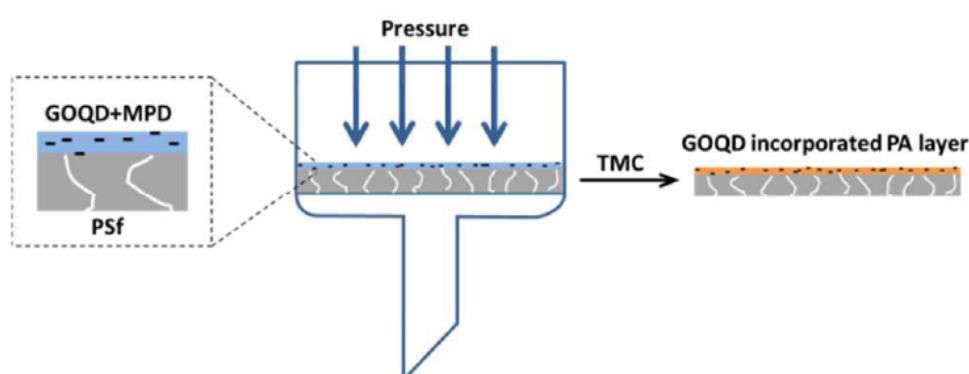


Figure 4.10: Schematic Diagram of the Fabrication of the TFN RO Membrane Through Vacuum Filtration IP Process (Song et al., 2016)

Recently, various functionalized GOQDs were also being put into application to fabricate TFN RO membranes with great performance. Nitrogen-doped GOQDs (N-GOQDs) have shown great potential in improving the performance of TFN membranes in the study done by Fathizadeh et al. (2019). In this work, PSf support was immersed in MPD solution containing N-GOQDs and TMC organic solution for 2 minutes and 1 minutes, respectively. The excess solution was removed by a rubber roller. In another work by Shen et al. (2020), heterostructured interface-functionalized of amine/sulfonic decoration on GOQD (N/S-d-GOQD) were synthesized and embedded into the PA selective layer of the TFN membrane. Firstly, a solution containing MPD, 10-camphorsulfonic acid (CSA), sodium dodecyl sulfate (SDS), triethyl amine (TEA), and N/S-d-GOQD was prepared. The solution was then poured onto the polyketone (PK) support and allowed to contact for 5 minutes. The excess solution was then removed before the TMC solution was brought into contact with the membrane for another 3 minutes for IP reaction. The reaction was illustrated in Figure 4.11.

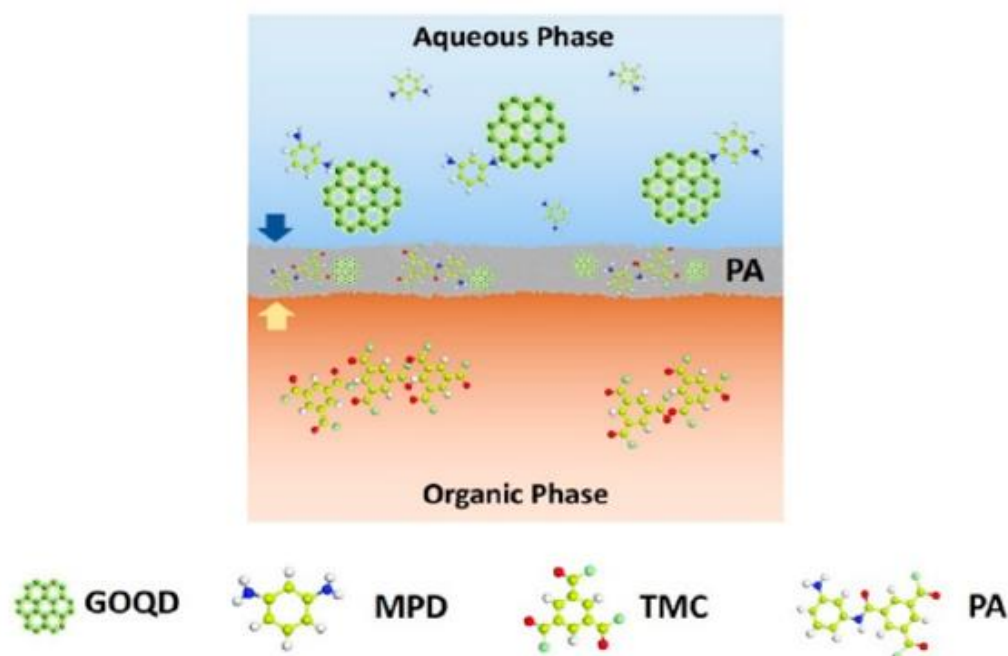


Figure 4.11: Illustration of IP Reaction Between MPD and TMC (Shen et al., 2020)

Other than functionalized GOQDs, Li et al. (2019a) made use of silver phosphate (AP) to synthesize GOQD/AP nanocomposite to overcome the limitation of AP such as uncontrollable morphology and poor stability. Due to the large number of negative charges that presented on GOQDs which have provided reaction sites of the silver ions, the morphology and nucleation of AP could be controlled effectively. On the other way round, the addition of AP to GOQDs could further improve the antibacterial property of GOQDs (Li et al., 2019a). Similarly, MPD and TMC were used as the monomers in this case. The PSf substrate was brought into contact with the solution that contains MPD and GOQDs/AP for 2 minutes before the TMC organic solution was deposited onto the surface for the IP reaction.

4.2.3 Others Methods

Apart the aforementioned methods for the fabrication of TFN membranes, some novel methods such as chemical grafting (Yi et al., 2020), covalent bonding (Zeng et al., 2016; Wu et al., 2020), physical coating (Zhao et al., 2019a), and ionic liquid method (Colburn et al., 2018) have also been implemented to fabricate carbon-based quantum dots membranes. Recently, ionic liquid was found to be effective at dissolving cellulose while heat was applied as the hydrogen bonding was disrupted (Colburn et al., 2018). In the work by Colburn et al. (2018), ionic liquid was used as a common solvent for GQDs and also cellulose to create unique properties for the membranes. It was found that the hydrogen bond networks help the bounding of GQDs into the cellulose domain causing the GQDs to be stable under shear stress and convective flow. During the phase inversion process, GQDs were driven to the interface between cellulose and water due to its hydrophilicity. The rearrangement allows the GQDs to improve the hydrophilicity of the membranes.

On the other hand, Zhao et al. (2019a) demonstrated a different way where GOQDs were physically coated onto the PA layer of TFC membranes. Unlike methods discussed in section 4.2.1 and 4.2.2, GOQDs were not involved in the IP process. With the assistance of pressure, the GOQDs aqueous solution was filtered with the TFC membranes where the water is allowed to pass through, leaving the GOQDs on the surface of the TFC membrane. The process was simple, inexpensive, and environmentally friendly.

Lately, chemical grafting of N-GOQDs onto the PA layer of the TFC membranes was demonstrated by Yi et al. (2020). The chemical grafting was done in 3 general steps: (1) the carboxyl groups present on the surface of the membrane was activated by 1-(3-dimethylaminopropyl)-3-ethylcarbodiimide hydrochloride (EDC) and N-hydroxysuccinimide (NHS), (2) Ethylenediamine (EDA) was grafted onto the surface of the membrane, and (3) The membrane was immersed into the N-GOQDs activated solution for 16 hours. Table 4.1 summarizes the comparison of different carbon-based quantum dots incorporation methods.

Table 4.1: Overall Comparison of the Incorporation Methods of Carbon-based Quantum Dots (Fang, Xu and Wu, 2013)

Method	Pore Size Adjustment	Functionalization	Cost-effectiveness	Fouling Remediation	“Green” Aspects	Versatility/Simplicity	Chemical Resistance
Chemical Grafting	+	+	+	+	-	+	+
Covalent Bonding	-	++	+	+	+	+	-
Interfacial Polymerization	+	++	+	++	+	++	++
Ionic Liquid	+	+	+	+	-	+	+
Physical Coating	-	++	+	+	+	+	-

* ++ represents excellent, + represents high, and – represents low

From above description, it can be observed that carbon-based quantum dots are able to be utilized in membrane fabrication via various methods. The structure and performance of the membranes are highly dependent on the fabrication methods which will be further discussed in the following sections.

4.3 Characterization of Carbon-based Quantum Dots Incorporated Thin Film Nanocomposite (TFN) Membranes

4.3.1 Surface Morphology Study

Based on previous studies, the introduction of carbon-based quantum dots will affect the morphology of the membranes in a certain number of ways. From the work of Yuan et al. (2018), it was observed that the unmodified membranes had no noticeable defects and the surface of the membrane was smooth and homogeneous. On the other hand, CQDs incorporated TFN membranes showed a relatively rough surface compared to the unmodified ones which is shown in Figure 4.12. For the cross-sectional image, which is shown in Figure 4.12d and Figure 4.12e, it was observed that CQDs were uniformly dispersed within the membrane matrix due to its great compatibility. No CQDs particles were observed even at high magnification. The thickness of the active layer was about 200 nm which is very similar to other thin film.

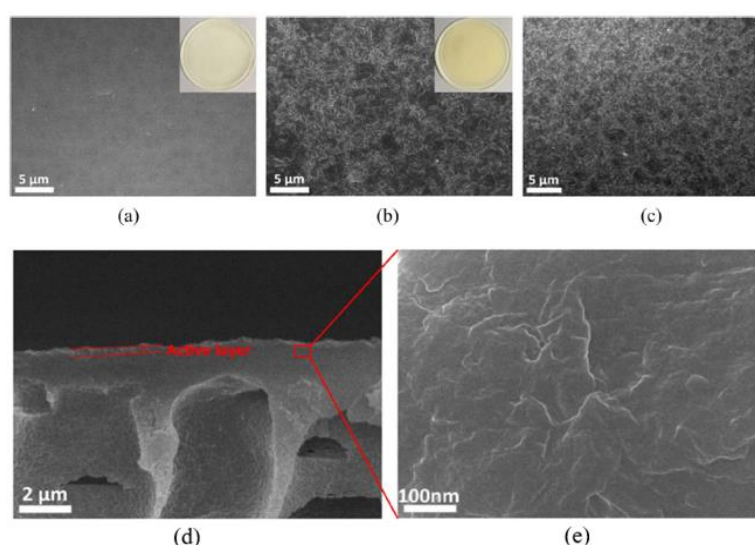


Figure 4.12: SEM Images of the Surface of Membranes with Different CQDs Loading: (a) 0 wt%, (b) 10 wt%, and (c) 30 wt%; the Cross-sectional Image of the Membranes With 10 wt% CQDs Loadings (d and e) (Yuan et al., 2018)

Likewise, as reported by He, Zhao and Chung (2018), the FESEM images shows a much rougher surface of the TFN membrane compared to the pristine TFC membrane. It can be adequately explained by the two roles played by CQDs. Firstly, at low loading, the interface between the organic and aqueous phase was enlarged by the hydrophilic CQDs as the organic phase was repelled by the hydrophilic functional groups. Secondly, the improvement of the diffusivity and solubility of PIP molecules by CQDs through hydrogen bonding had sped up the kinetics of the formation of the active layer and altered the microstructure of the active layer (Huang et al., 2008). Cross-sectional-wise, it was also found that the PA selective layer was 200 nm which is similar to the previous studies.

On the other hand, functionalized CQDs affects the morphology in a different way compared to normal CQDs. As reported by Sun and Wu (2018), the TFN-NCQD membrane was slightly smoother than the TFC membranes while the TFN-CCQD and TFN-SCQD membranes was significantly rougher than the pristine one which was presented in Table 4.2. In Table 4.2, parameters such as average roughness (R_a) and root mean square roughness (R_{rms}) were used for the comparison. Some of the contributing factors are the initial spot of PIP monomers and also the different diffusion rate (Xue et al., 2016; Zhu et al., 2017). For the preparation of the pristine TFC membranes, as the PIP monomers have small molecular weight, it can permeate through the interface between aqueous and organic phase easily which leads to a rough surface of PA layer. In contrary, the amino CQDs (NCQDs) modified membrane was fabricated, PIP monomers needed to overcome a greater resistance in order to diffuse across the interface. The diffusion resistance mainly came from the electrostatic repulsion between the cationic amine groups of NCQD and cationic PIP. Besides, the diffusion of PIP was further decreased by the steric hindrance of NCQDs which retards the formation of PA layer. All of these factors have led to a smoother surface on the TFN-NCQD membrane (Lai et al., 2016). However, completely opposite results were obtained for the fabrication of TFN-SCQD and TFN-CCQD membranes. A plausible explanation would be the increased adsorption of cationic PIP monomers due to the presence of anionic groups on carboxylic CQDs (CCQDs) and sulfonated CQDs (SCQDs). The same results for TFN-NCQD can also be seen in the study of Guo et al. (2021). As shown in Figure

4.13, the TFN-NCQD membranes exhibited a significantly smoother surface topography compared to the pristine TMC membrane which can also be explained with the explanation above.

Table 4.2: Surface Roughness of TFC and TFN Membranes Obtained from AFM

Membrane	PSf Substrate	TFC	TFN-NCQD	TFN-CCQD	TFN-SCQD
R_{rms}	6.5	37.9	33.1	40.0	50.8
R_a	5.2	29.7	26.6	31.1	38.6

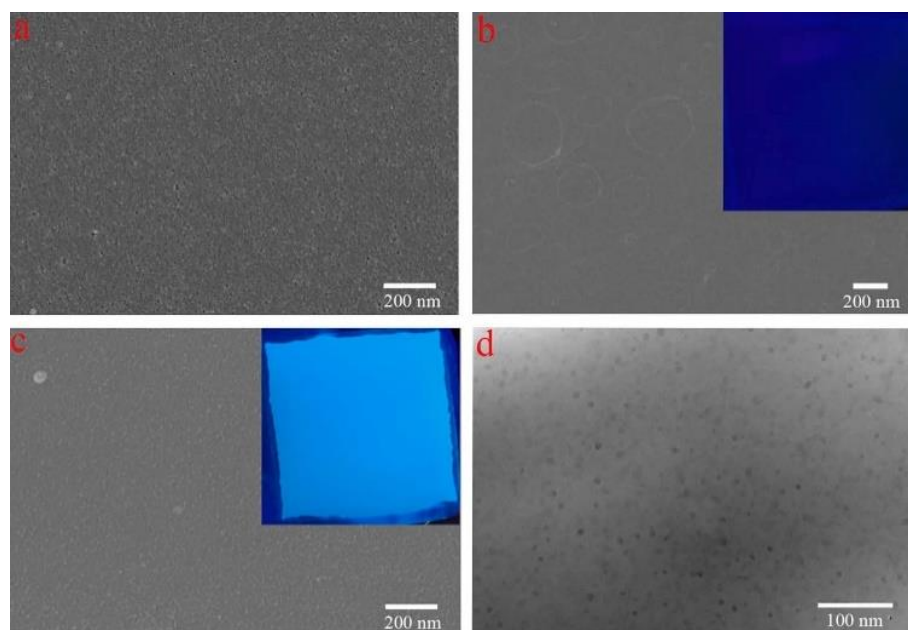


Figure 4.13: SEM Images of the Surface of (a) PES Substrate, (b) Unmodified TMC Membrane, (c) TFN-NCQD Membrane; (d) TEM Image of the Surface of TFN-NCQD (Guo et al., 2021)

In contrast to CQDs, for GOQDs incorporated TFN membranes, the results from the work of Zhang et al. (2017) shows that the modified membranes exhibit smoother surface compared to the unmodified ones which can be seen in Figure 4.14. It can be adequately explained by the steric hindrance of GOQDs and also by the excess aqueous monomers concentration which had led to the delayed IP reaction and caused a smoother surface to be formed (Bano et al.,

2015). The retarded IP reaction was further confirmed through the observation of the reduced thickness of the modified membranes.

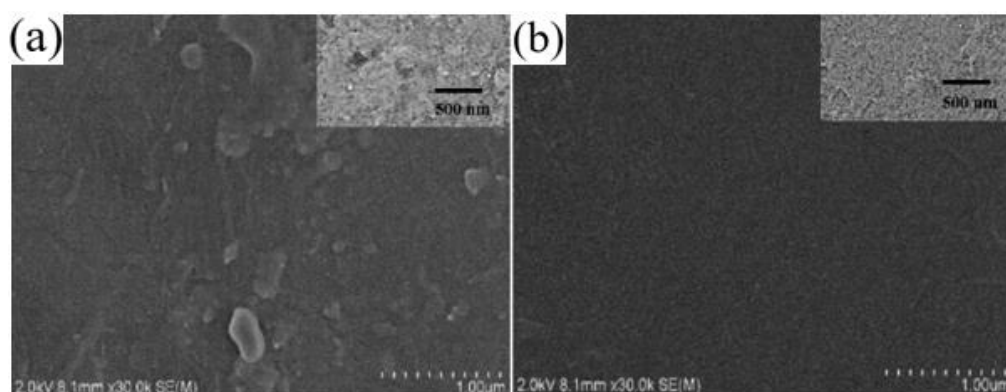


Figure 4.14: SEM Images of the Surface of (a) TFC and (b) GOQDs-TFN Membranes (Zhang et al., 2017)

Conversely, there are several studies where the SEM images are inconsistent with the previous images for GOQDs incorporated TFN membranes. Herein, Song et al. (2016) concluded that the surface of the fabricated GOQDs incorporated TFN membrane was significantly rougher than the TFC membrane. It may be attributed to the GOQDs which were forced out from the PA layer to form agglomerates. However, the incorporation of GOQDs had reduced the thickness of the PA layer which is consistent with previous paper. It is similar for GOQDs composite, Li et al. (2019a) reported that the surface of TFN membrane was noticeably rougher than TFC membrane which was caused by the formation of larger protuberance. It was found that the GOQD/AP reacted with MPD by dehydration condensation of amino and carboxyl groups which caused the retardation of the diffusion of MPD.

As for GQDs incorporated TFN membranes, Bi et al. (2018) reported that the modified membrane was relatively smoother than the pristine one due to the binding of GQDs with PIP and/or TMC which will decrease the crosslinking reaction rate. According to Huang et al. (2008), stronger intermolecular hydrogen bonding and slower crosslinking reaction rates will lead to the development of tinier nodular structure and eventually flatter membrane surface. Another possible explanation is the decreased diffusion rate of polymer due to the addition of GQDs which alter the microstructure of

membranes. In addition, in a similar work performed by Liang et al. (2020), the fabricated GQDs incorporated TFN membrane was also smoother than the TFC membrane, which was in accordance with the research work of Bi et al. (2018). It was also found that the incorporation of GQDs also led to a more uniform and denser membrane which was deduced from the decreased number and size of pores as shown in Figure 4.15.

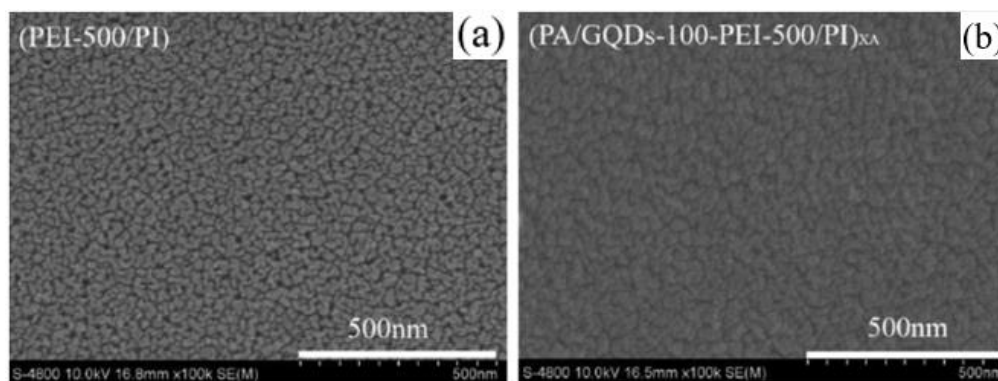


Figure 4.15: SEM Images of the Surface of (a) TFC Membrane and (b) GQDs Incorporated TFN Membranes (Liang et al., 2020)

As for functionalized GQDs, the results were similar to GQDs. However, it was the opposite when the functionalized GQDs loading was high. The surface roughness and pore size were increased after the incorporation of GQDs-NH₂ at high loading (Xu et al., 2021). It can be attributed to the enhanced electrostatic interaction between the amine groups of the functionalized GQDs and PEI. This can loosen the IP crosslinking net between the monomers (Lai et al., 2016). Besides, at high loading, the quantum dots cannot be distributed evenly in the PA matrix which will cause agglomeration of the quantum dots and leads to rougher membrane surface (Xu et al., 2021). For the incorporation of AGQDs, the membrane becomes smoother after the modification which is in accordance with the incorporation of GQDs-NH₂. However, it was worth noting that the membrane remains relatively smooth when the loading of AGQDs was increased. It is attributed to the excellent polymer affinity characteristic where it allows the excessive AGQDs to stay on the PSf support.

4.3.2 Functional Groups Characterization

The presence of functional groups on the surface of carbon-based quantum dots and the fabricated membranes was determined by conducting FTIR analysis (Singh et al., 2018). Generally, the quantum dots are made up of mainly carbon, oxygen and hydrogen. Due to the formation of carbon-based quantum dots by the partial oxidation of carbon precursors, functional groups such as carboxyl, hydroxyl, and ether are abundant on its surface. The existence of certain functional groups will decide the characteristics of the polymer membrane (Tadesse et al., 2020). FTIR is especially useful for the investigation of these oxygen-containing functional groups (Singh et al., 2018). However, some of the peaks are not well pronounced in the FTIR spectra occasionally as the amount are relatively small in the active layer. It is also common that the peaks of the quantum dots are masked by the peaks of the support and the active layer. Thus, X-ray photoelectron spectroscopy (XPS) was utilized to further study the chemical composition of the membrane surface as well as to verify the incorporation of the quantum dots (Sun and Wu, 2018).

In the case of CQDs, as shown in Figure 4.16a, comparing the spectra of TFN and TFC membranes with the PSf support, new peaks were observed at 1364 (nitrile groups), 1620 (carbonyl groups) and 3415 cm^{-1} (hydroxyl groups). Nevertheless, there are no significant differences between the spectra of TFN and TFC membranes. As per mentioned previously, it is due to the presence of CQDs in small amount in the PA layer which caused its characterization peaks to be covered by the support layer and the PA layer. In order to investigate the chemical composition of the membrane surface in a more detailed manner, it is necessary to use XPS for further characterization. From Figure 4.16b, there were clear peaks of O 1s, N 1s, and C 1s. These peaks mostly originate from the PA layer. Table 4.3 shows the calculated atomic concentrations of various element. It can be clearly seen that all of the TFN membranes possessed considerably higher oxygen contents than the TFC membrane. This phenomenon was attributed to the successful incorporation of CQDs which possess a lot of oxygen-rich functional groups. As for the C/N ratio, it can be used as an indicator to measure the degree of crosslinking. Beside TFN-NCQD, other TFN membranes such as TFN-CCQD and TFN-SCQD showed a higher C/N ratio after the incorporation of CQDs which indicates the decreased in the

degree of crosslinking. A plausible explanation is the retardation of the firm fixing of PA macromolecules around CCQD and SCQD caused by the carboxyl and sulfonyl groups (Ji et al., 2016). Consequently, spaces in the interface would be created and led to a looser PA structure which is in consistence with the SEM images. It is the opposite for TFN-NCQD where a lower C/N ratio was obtained which indicates the higher degree of crosslinking. It can be accounted for by the amidation reaction between the monomers on the NCQD surface which has led to the formation of a denser membrane (Xue et al., 2016).

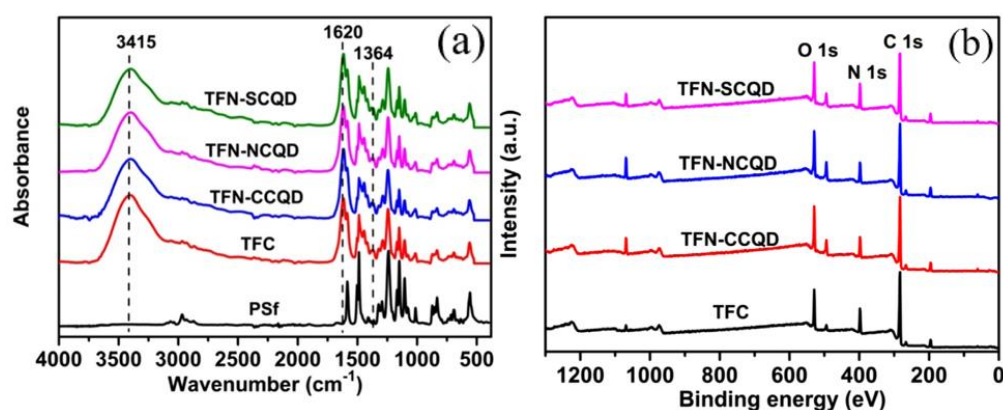


Figure 4.16: (a) FTIR and (b) XPS Spectra of the TFC and Functionalized CQDs Incorporated TFN Membranes (Sun and Wu, 2018)

Table 4.3: Chemical Composition of the TFN Membranes Determined from the XPS Spectra (Sun and Wu, 2018)

Membrane	Atomic Concentration				
	O (%)	N (%)	C (%)	S (%)	C/N
TFC	14.92	15.00	70.07	-	4.71
TFN-NCQD	15.28	15.69	69.03	-	4.40
TFN-SCQD	17.40	13.19	69.10	0.32	5.24
TFN-CCQD	17.30	13.40	69.30	-	4.95

In another work by He, Zhao and Chung (2018) where Na⁺ functionalized CQDs were embedded into the PA layer, a similar spectra was obtained. Sodium can hardly be seen in the spectra due to its low concentration in the active layer as shown in Figure 4.17. N/O ratio was used as the indicator for the degree of crosslinking instead C/N ratio in this study. From Table 4.4, it

can be seen that the N/O ratio decreases as the amount of Na-CQD increases. It indicates the decrease in the degree of crosslinking of the active layer. On the other hand, the O/C ratio was notably higher after the incorporation of Na-CQD. It can be adequately explained by the successful incorporation of Na-CQD as oxygen-rich functional groups are abundant on the Na-CQD surface.

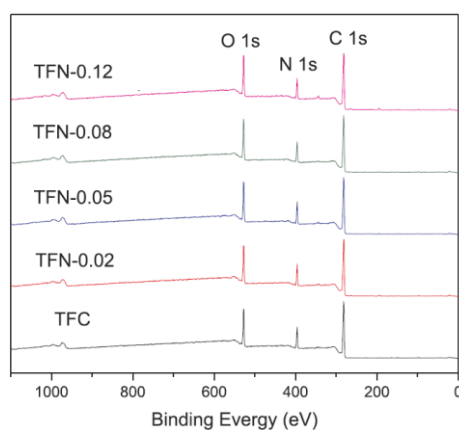


Figure 4.17: XPS Spectra of TFC and Na-CQDs Incorporated TFN Membranes (He, Zhao and Chung, 2018)

Table 4.4: XPS Analyses of the TFC and TFN Membranes

Membrane	Atomic Concentration					N/O	O/C
	O (%)	N (%)	C (%)	Na (%)			
TFC	13.73	12.25	74.02	0		0.892	0.185
TFN-0.02	18.26	12.91	68.81	0.02		0.707	0.265
TFN-0.05	19.10	12.76	68.04	0.05		0.668	0.280
TFN-0.08	19.22	12.78	68.07	0.08		0.665	0.282
TFN-0.12	19.76	12.48	67.68	0.10		0.632	0.292

In contrast, different results was obtained after the incorporation of GOQDs (Zhang et al., 2017). Figure 4.18a presents the FTIR spectra of the PAN support, pristine TFC membrane, and GOQDs incorporated TFN membranes. From the results, the incorporation of GOQDs has noticeable impact on the FTIR spectra. In the region between 1620 and 1640 cm^{-1} and at 1545 cm^{-1} which are attributed to the carbonyl groups and amide groups respectively, the intensity of the transmittance increased significantly after the addition of

GOQDs. It is due to the reaction between the carboxyl and hydroxyl groups of GOQDs and the isocyanate groups in the IDPI monomers. As for the XPS spectra shown in Figure 4.18b, it can be seen that it is similar to the CQDs incorporated TFN membrane where the elements on the membrane surface are mainly carbon, nitrogen, and oxygen. The N/O ratio also decreases when the loading increases which indicates the decrease in the degree of crosslinking which is in accordance with the SEM images.

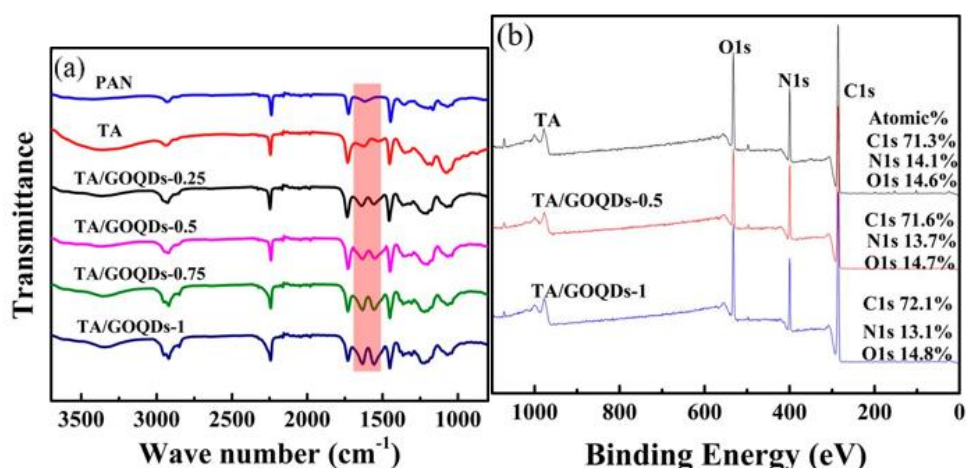


Figure 4.18: (a) FTIR and (b) XPS Spectra of TFC and GOQDs Incorporated TFN Membranes (Zhang et al., 2017)

On the other hand, as shown in Figure 4.19 the FTIR spectra of the GQDs incorporated TFN membranes are also identical to the GOQDs incorporated membranes where distinct peak around the region of 1600 cm^{-1} was detected after the introduction of GQDs into the TFN membranes. The peaks were found to be attributed to the amide I and amide II of the active layer (Li et al., 2019b). However, due to the amidation reaction, the intensity of the peaks around the region of 1720 and 1400 cm^{-1} decreased substantially.

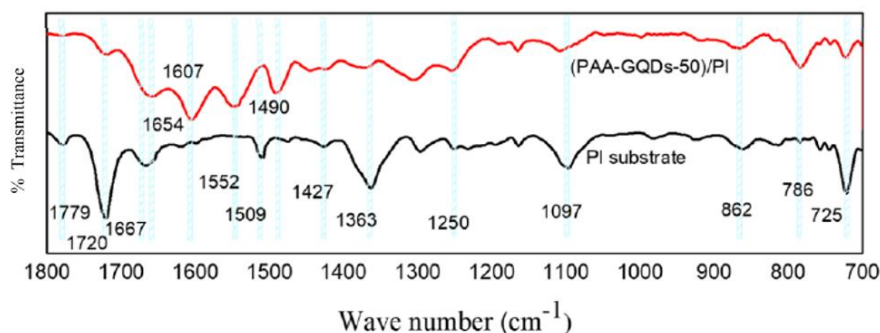


Figure 4.19: FTIR Spectra of the PI Substrate and the GQDs Incorporated TFN Membranes (Li et al., 2019b)

4.3.3 Water Contact Angle and Surface Charge

Other important factors that govern the performance of a membranes are the water contact angle and surface charges. It has been widely reported that the incorporation of carbon-based quantum dots will affect the water contact angle as well as the membrane surface charges. Both of these traits are closely related to the hydrophilicity and antifouling properties of the membranes. The increased hydrophilicity allows the formation of a water film to protect the membrane surface from foulants. On the other hand, the increased surface charge allows the membrane to repel the foulants that have similar charge with the membrane surface. Therefore, it is crucial to study and quantify these properties of membrane.

In a work by Yuan et al. (2018), the addition of CQDs further enhanced the membrane hydrophilicity as the contact angle decreased significantly. Figure 4.20 shows the contact angle results at different CQDs loading. It can be observed from Figure 4.20 that even when the loading of CQDs is relatively low, there are still significant impact on the contact angle. However, some of the results in the work of Yang et al. (2020) differs from the work of Yuan et al. (2018). As shown in Figure 4.21, the contact angle of the TFN membrane with 2% CQDs was much higher than the pristine TFC membrane. One of the contributing factor might be the preparation method used by Yang et al. (2020) where the excess CQDs solution was removed with a rubber roller compared to the filtration assisted method. Loss of NPs may occur during the rubber rolling process and cause the uneven distribution of CQDs on the TFN membranes. Nevertheless, the trend where the contact angle decreases with the increase of

CQDs loading remains the same. It is worth noting that the contact angles decreased faster after the incorporation of CQDs. This phenomenon can be appropriately explained by: (1) The CQDs layer are able to enhance the transport of water molecules across the PA layer due to the presence of abundant hydrophilic functional group and fast ions transport channel (Wang et al., 2017; Zhao and Chung, 2018). (2) The lowered degree of crosslinking after the incorporation of CQDs had facilitated the transport of water molecules due to a larger pore diameter.

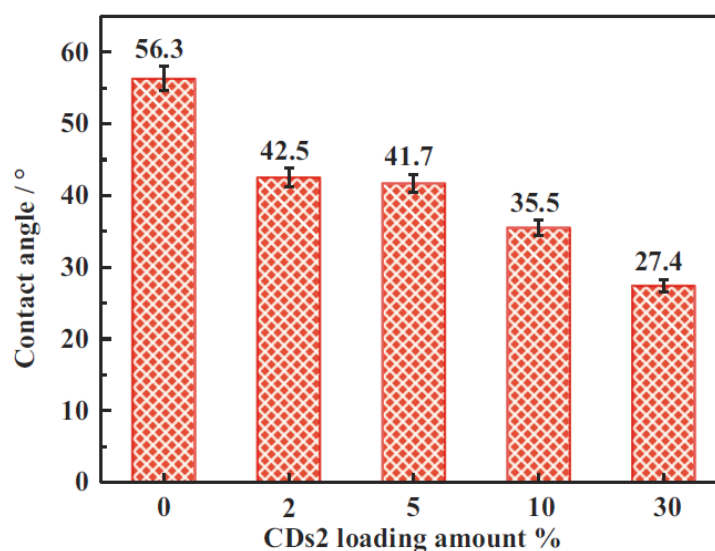


Figure 4.20: Water Contact Angles of TFN Membranes at Different CQDs Loading (Yuan et al., 2018)

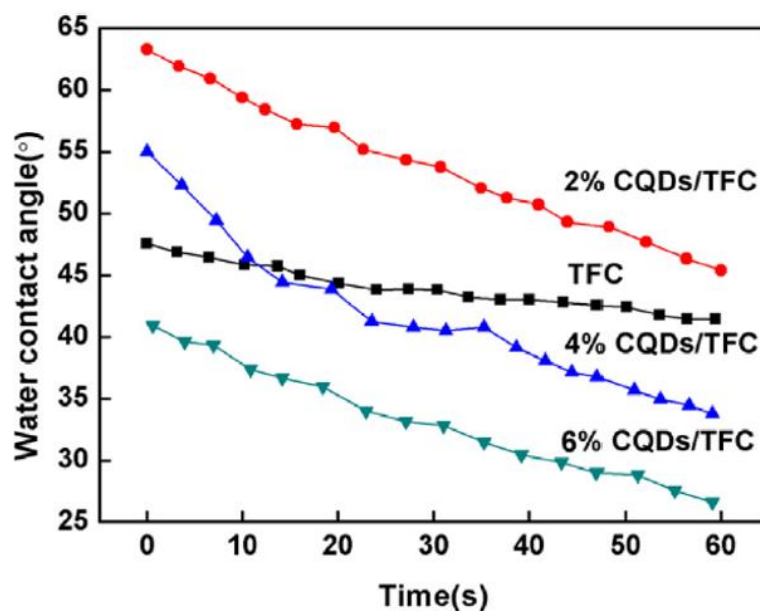


Figure 4.21: Water Contact Angles of TFN Membranes with Different CQDs Loadings (Yang et al., 2020)

For functionalized CQDs, the results were also similar even when the CQDs were differently functionalized. The water contact angles decreased significantly after the incorporation of different CQDs, namely CCQDs, NCQDs and SCQDs (Sun and Wu, 2018). On the other hand, comparable results was also obtained by Guo et al. (2021) after the incorporation of CQDs-NH₂. These phenomena can also be explained with the explanation for unmodified CQDs where the presence of abundant oxygen-rich functional groups on CQDs have led to the enhanced hydrophilicity.

Surface charge wise, the zeta potential analysis results showed that the CQDs incorporated membranes are negatively or positively charged in alkaline or acidic environment respectively which is shown in Figure 4.22, where CQDs/TFC is the CQDs incorporated TFC membranes, DK is the commercial Suez DK NF membranes, and DL is the commercial Suez DL NF membranes (Yang et al., 2020). Nonetheless, different results was observed in the work of Shao et al. (2020) as shown in Figure 4.23, where the CQDs incorporated TFN membranes are negatively charged over a wide range of pH value. It can be accounted to the lower degree of crosslinking and the abundant carboxyl groups present on the surface of the membranes (Shao et al., 2020). Besides, the PDA

precoating have enhanced the negative property while the isoelectric point is slightly higher.

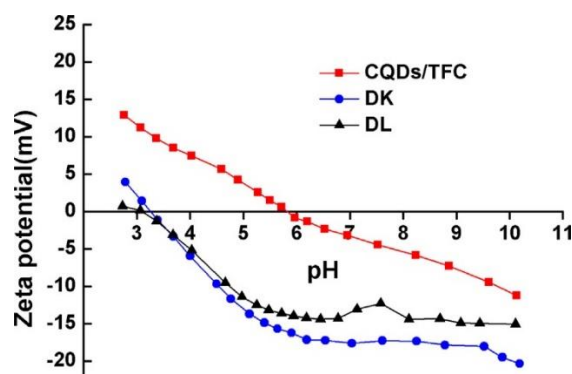


Figure 4.22: Zeta Potential Analysis Results for the TFN and the Commercial Membranes (Yang et al., 2020)

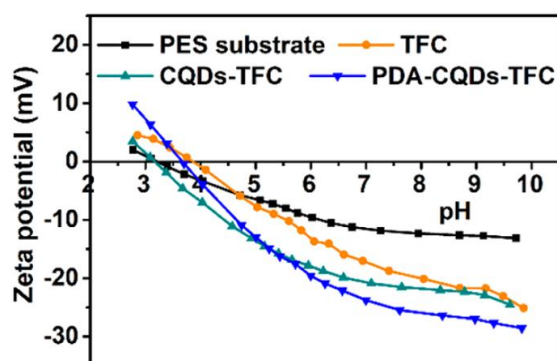


Figure 4.23: Zeta Potential Analysis Results of the Membranes at Different Stages (Shao et al., 2020)

As for GOQDs incorporated TFN membranes, similar trend to the CQDs was also obtained. In the work of Zhang et al. (2017), it can be seen in Figure 4.24 that although the trend is similar to CQDs, it is less significant compared to CQDs incorporated TFN membranes. This can be explained with the lower oxygen concentration on the GOQDs incorporated membrane surface compared to the CQDs incorporated ones, which can be seen in the XPS results discussed previously. In another work, the optimum GOQDs loading was found to be 2 mg as there is little gain on the hydrophilicity when the GOQDs loading exceed 2 mg (Song et al., 2016).

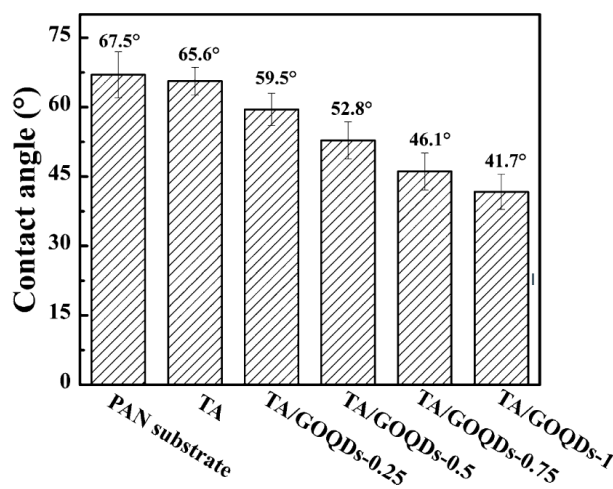


Figure 4.24: Water Contact Angle of TFC and GOQDs Incorporated TFN Membranes (Zhang et al., 2017)

For the surface charges of the GOQDs incorporated TFN membranes, the membranes were found to be negatively charged across different journals. Herein, Song et al. (2016) reported negatively charged TFN membranes with GOQDs loadings from 0 to 10 mg. The negative charge density is the highest at 10 mg of GOQDs loading which can be attributed to the numerous negatively charged oxygen-containing groups present on GOQDs. In another work by Li et al. (2019a), the negative charge density was even higher ranging from -30 to -40 mV. The pH value of the environment might explain this phenomenon.

Last but not least, GQDs incorporated membranes showed a greater improvement on hydrophilicity compared to GOQDs. Bi et al. (2018) reported that the water contact angle decreased continuously with increasing GQDs loading from 38° to 16° which is shown in Figure 4.25. The results are also in accordance with the results obtained in the study done by Liang et al. (2020) where the water contact angle decrease gradually while the GQDs loading increased from 20 to 150 mg/L. It can be attributed to the surface functionalization by the hydroxyl and carboxyl groups of GQDs which alter the microstructure of the surface (Yang et al., 2007). Besides, the introduction of GQDs was found to promote the formation of water channel structures and improved the wettability of the membrane surfaces.

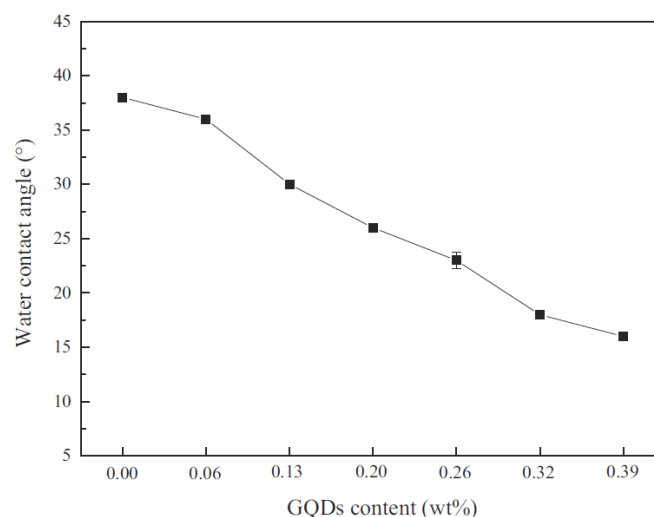


Figure 4.25: Water Contact Angle of TFN Membranes With Different GQDs Loadings (Bi et al., 2018)

In terms of surface charges, there are some interesting results reported. Figure 4.26 shows the surface charges of the TFN membranes incorporated with different amount of GQDs (Bi et al., 2018). In the work of Bi et al. (2018), all of the membranes with different GQDs loadings are negatively charged due to the presence of carboxyl groups on the surface of GQDs. However, it is worth noting that the negative charged density decreased with increasing GQDs loading. It can be adequately explained with the reaction between the active functional groups of GQDs, such as hydroxyl groups and acyl chloride groups of TMC during IP. As a result, the number of carboxyl groups present on the surface of the membrane decreased and led to a less electronegative membrane (Bano et al., 2015).

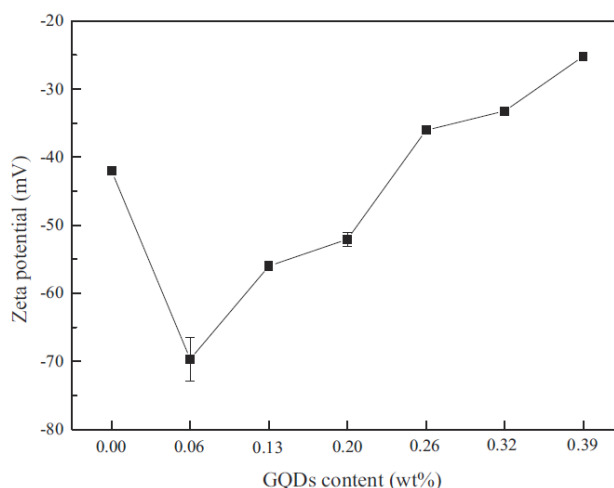


Figure 4.26: Zeta Potential Analysis Results of TFN Membranes Incorporated With Different GQDs Loadings (Bi et al., 2018)

Meanwhile, different results were obtained when functionalized GQDs were incorporated. In the work by Xu et al. (2021) which is shown in Figure 4.27, it was found that the electronegativity of the modified membranes was significantly lower than the pristine ones due to the presence of the amino groups on GQDs-NH₂. In contrast, the AGQDs incorporated TFN membranes tends to be more electrically neutral compared to the unmodified ones (Wu et al., 2021). Similar to unmodified GQDs, the abundant active groups on AGQDs tends to react with acyl chloride groups of TMC during IP and reducing the amount of carboxyl groups present on the surface of the membranes (Bano et al., 2015).

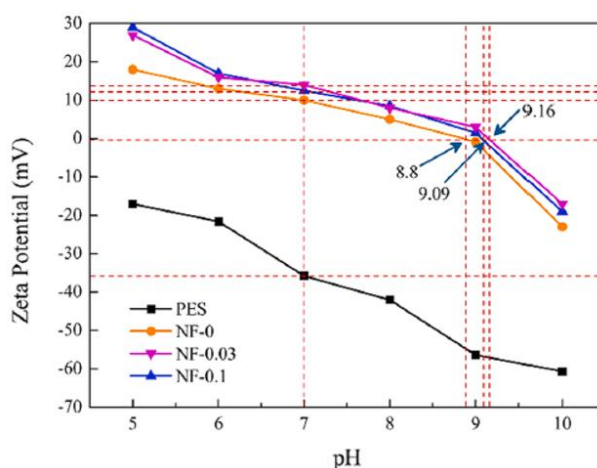


Figure 4.27: Zeta Potential Analysis Results of the Membranes at Different pH Values (Xu et al., 2021)

4.4 Effect on Performance

Based on various studies performed by the researchers, the incorporation of carbon-based quantum dots into the TFN membrane was known to have positive effects on the NF as well as RO performances such as salt rejection and water flux. Besides, the antifouling ability is also an equally important traits for membranes, especially for pressure-driven process such as NF and RO. In this matter, antifouling test was typically conducted to express the antifouling properties in terms of total fouling rate (R_t) and flux recovery rate (FRR).

4.4.1 Nanofiltration

As NF retention are governed by Donnan Exclusion, the surface charge of the membranes plays an important role. Due to the deprotonation of carboxyl groups of CQDs to COO^- , CQDs are often negatively charged over a wide range of pH. Thus, by embedding CQDs in the selective layer, the membranes have higher tendency to form hydrogen bonds with water and results in the improvement of surface hydrophilicity without comprising on the rejection. For instance, the pure water permeability (PWP) of the TFC membrane was increased from $5.2 \text{ L}\cdot\text{m}^{-2}\cdot\text{h}^{-1}\cdot\text{bar}^{-1}$ to $10.4 \text{ L}\cdot\text{m}^{-2}\cdot\text{h}^{-1}\cdot\text{bar}^{-1}$ (abbreviated as LMH bar^{-1}), which was 2 times of the pristine one (He, Zhao and Chung, 2018). Meanwhile, the rejection of SeO_3^{2-} and HAsO_4^{2-} was increased from 82.4% to 98.6% and 91.3% to 99.5% respectively. The increased in salt rejection can be explained with the narrowing of the pore size and pore size distribution after the addition of CQDs (He, Zhao and Chung, 2018). The increment in water flux can also be seen in the results of the work of Sun and Wu (2018). In this work, 3 types of functionalized CQDs, which are SCQDs, CCQDs and NCQDs were incorporated into the TFN membranes to study their effects on the performances of the TFN membranes. At an operating pressure of 0.6 MPa, the water flux of the unmodified membrane was $18 \text{ L}\cdot\text{m}^{-2}\cdot\text{h}^{-1}$ (abbreviated as LMH). The water flux was increased to 42.1 LMH after the incorporation of SCQDs which is the highest among the three functionalized CQDs. The incorporation of CCQDs and NCQDs also show great results which increased the water flux by a factor of 2. However, the retention of the membranes does not align with the trend of the previous paper. In terms of NaCl and MgCl_2 , the SCQDs-modified and CCQDs modified membranes show a noticeable decrement in the retention of the salts.

This is caused by the more negatively charged and looser PA layer. In contrast, the NCQDs modified membranes show a significant increase in the retention due to the higher crosslinking degree and lower negative charge density. As for the retention of Na_2SO_4 and MgSO_4 , all of the membranes including the TFC membrane show similar performance. As both of the salts contain SO_4^{2-} , a multivalent ion, the effect of steric hindrance and electrostatic repulsion governs the rejection and thus resulting in high rejection in all fabricated NF membranes. Figure 4.28 shows the pure water flux and rejection of different salts of the TFC and TFN membranes.

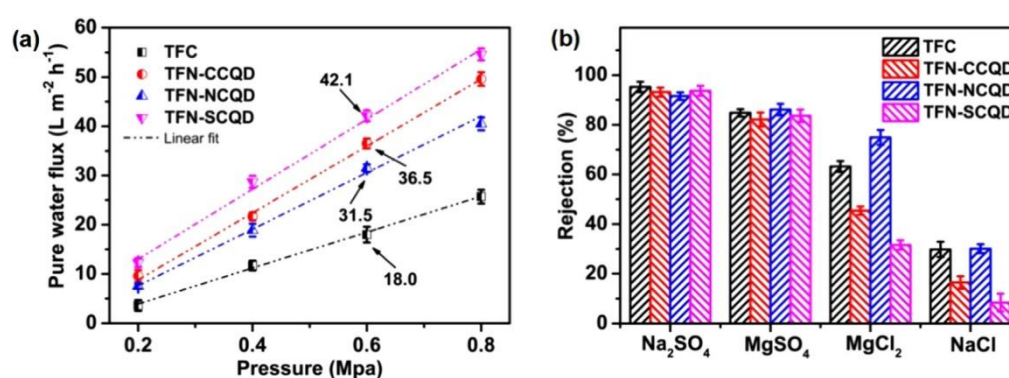


Figure 4.28: (a) Pure Water Flux and (b) Salt Rejection of the TFC and TFN Membranes at 0.6 MPa (Sun and Wu, 2018)

Beside the rejection of the common salt, the ability of CQDs incorporated TFN membranes to reject amino acids was also studied lately. In a recent work performed by Yang et al. (2020), the CQDs modified TFN membranes showed a PWP about 3 times of the unmodified TFC membranes and amino acid rejection of about twice of the pristine one. Nevertheless, the previous papers where the modified membranes were negatively charged over all pH, the modified TFN membranes were positively charged when the pH value is below 6. This can be useful in the rejection of amino acid due to the fact that amino acids are negatively or positively charged depending on the acidity or alkalinity of the environment. Compared to the unmodified membrane which are negatively charged, the addition of CQDs allows the membranes to perform better in this application.

As for GOQDs incorporated TFN membranes, Zhang et al. (2017) reported TFN membranes which can be operated under a relatively low pressure

of 0.2 MPa compared to the CQDs incorporated TFN membranes which normally have an operating pressure of 0.6 MPa according to previous studies. At 0.2 MPa, the TFN membrane was able to reach a water flux of 23.33 LMH, which is a 48% improvement compared the TFC membrane. Beside improvement on flux, as shown in Figure 4.29, there is also a noticeable boost on the salt rejection after the introduction of GOQDs. It can be clearly seen that the rejection on $MgCl_2$ was significantly lower than the CQDs incorporated TFN membranes which is around 40-70% (Sun and Wu, 2018). One of the reasons is the cross-lying structure of GOQD flake grid and led to a loose PA structure (Zhang et al., 2017).

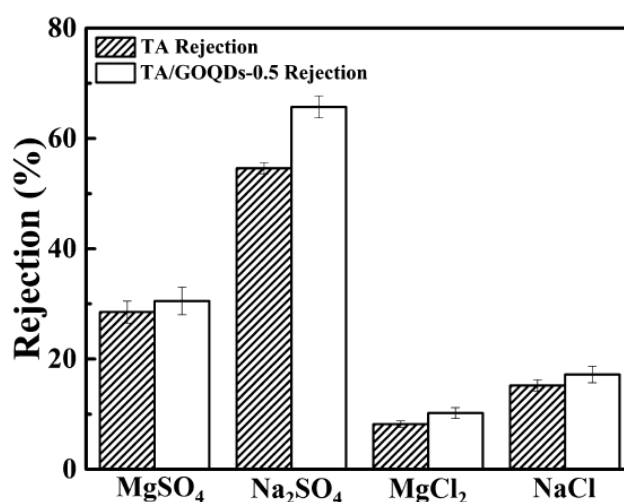


Figure 4.29: Salt Rejection of the Pristine TFC and GOQDs Incorporated TFN Membrane (Zhang et al., 2017)

Finally, similar to GOQDs, GQDs incorporated TFN membranes were also able to perform well under a relatively low pressure of 0.2 MPa. In the studies reported by Bi et al. (2018) there is a huge difference between the TFC and TFN membranes in terms of the water flux. As presented in Figure 4.30, up to 6.8 times improvements on the water flux were observed after the introduction of GQDs while maintaining the separation performance. It can be attributed to the largened water channels in the active layer caused by the addition of GQDs.

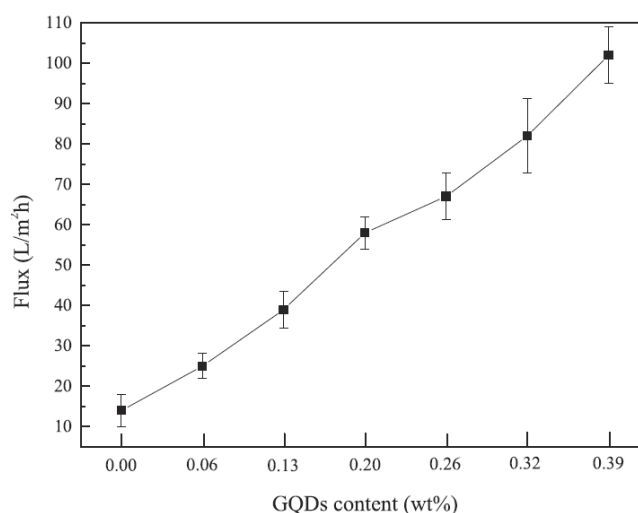


Figure 4.30: Water fluxes of the Membranes with Different GQDs Loadings (Bi et al., 2018)

In another study performed by Xu et al. (2021), GQDs-NH₂ was introduced into the PA layer. It was found that the water flux increased considerably even when the amount of GQDs-NH₂ was as little as 0.03 wt%. Figure 4.31 shows the salt rejection performance of the TFN membrane with 0.03 wt% loading. Compared to the GOQDs incorporated membrane reported by Zhang et al. (2017), the rejection of MgCl₂ was much higher in this work. The rejection for multivalent ions was relatively high while the rejections for monovalent ions were under 30%. Similar results can also be seen in several previous studies (Fang, Shi and Wang, 2014; Li et al., 2015b; Zhao and Wang, 2017).

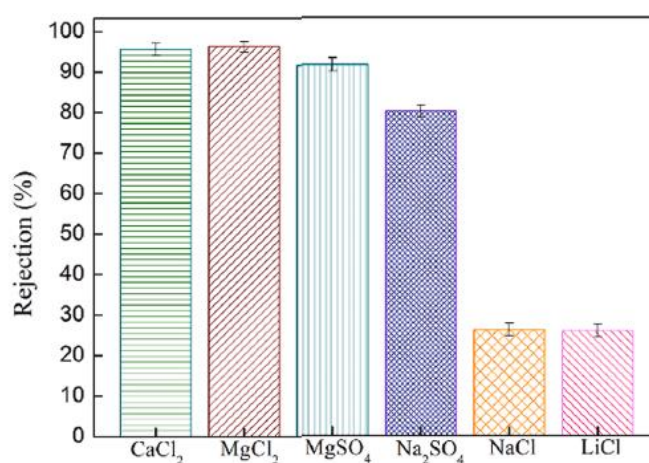


Figure 4.31: Salt Rejection of TFN Membranes Incorporated with GQDs-NH₂ (Xu et al., 2021)

4.4.2 Reverse Osmosis

TFN RO membranes were also reported to gain positive effect on the performance through the addition of carbon-based quantum dots. Generally, compared to TFN NF membranes, TFN RO membranes can achieve higher salt rejection but significantly lower water flux due to the smaller water channel. Herein, Li, Li and Zhang (2017) incorporated hydrophilic CQDs into the TFN RO membrane and obtained up to a 52.5% improvement on water flux (3.68 LMH to 5.72 LMH). Besides, a slight improvement on the NaCl rejection was also observed from 98.1% to 99% as shown in Figure 4.32a. Furthermore, it is worth noting that the deposition time of CQDs on the membranes have noticeable impact on the performance too. Figure 4.32b shows the effects of deposition time on water flux and NaCl rejection. The results indicated that the optimum deposition time is at 6 minutes where highest water flux and salt rejection were recorded. Nevertheless, further increasing the deposition time will decrease both water flux and rejection mainly due to the excess penetration of MPD monomers into the porous support. This could potentially narrow or block the membrane pores as PA was formed excessively and decrease the water flux (Li, Li and Zhang, 2017b).

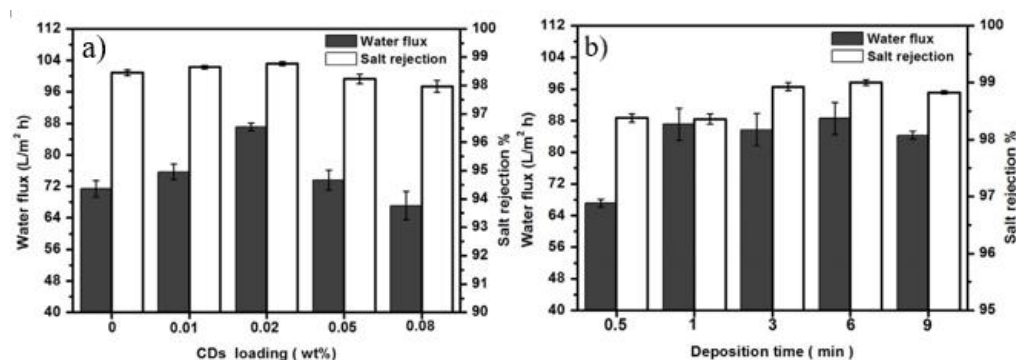


Figure 4.32: Effects of (a) CQDs Content and (b) Deposition Time on Water Flux and NaCl Salt at 2000 ppm and 225 psi (Li, Li and Zhang, 2017b)

However, the results from the study performed by Gai, Zhao and Chung, (2019) are not in accordance to previous study. As shown in Figure 4.33. the incorporation of unmodified CQDs into the PA layer has decreased the PWP with no gain on the salt permeability due to the decreased membrane roughness

which means the reduction of the effective surface area. In contrast, the incorporation of Na-CQDs provided notable enhancement on the PWP as well as on the salt permeability mainly due to the decreased membrane thickness, increased oxygen-containing functional groups and wider interstitial space between the PA chains (Gai, Zhao and Chung, 2019).

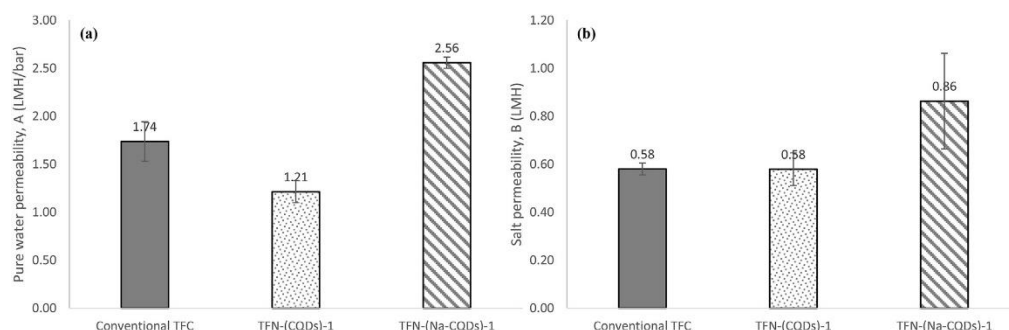


Figure 4.33: (a) Pure Water Permeability and (b) Salt Permeability of Different Membranes (Gai, Zhao and Chung, 2019)

As for GOQDs incorporated TFN RO membranes, the results were comparable to the CQDs modified TFN RO membranes, where obvious improvement on the water flux was observed with little improvement on the salt rejection. From Figure 4.34, it can be observed that there is hardly any difference in the water flux stability between the TFC and TFN membranes. However, the severe steric hindrance of GOQDs has led to the PA layer of the TFN membranes to be peeled off after the extensive RO test (Song et al., 2016). This indicates that the fabricated membranes are still susceptible to be used in large scale despite its outstanding performance. In addition, according to the antifouling test results shown in Figure 4.35, there is a great difference in the R_f and FRR between the TFC and TFN membranes. The TFN membranes are able to recover 10% more after the fouling and has lower R_f which indicates a higher water flux. These phenomena can be accounted to the improved surface hydrophilicity by GOQDs, where the desorption of the hydrophobic foulants from the membrane surface was promoted during the washing process and consequently lead to higher FRR. Similar test was also performed by Li et al. (2019a) and alike results were obtained. Table 4.5 and 4.6 summarize the separation performance of carbon-based quantum dots incorporated TFN NF and RO membranes respectively.

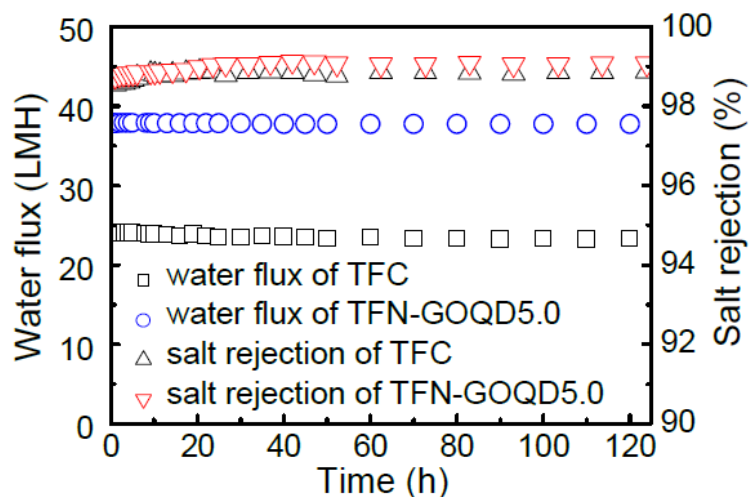


Figure 4.34: Water Flux and Salt Rejection of the Pristine TFC and GOQDs Incorporated TFN Membranes in Extensive RO Test (Song et al., 2016)

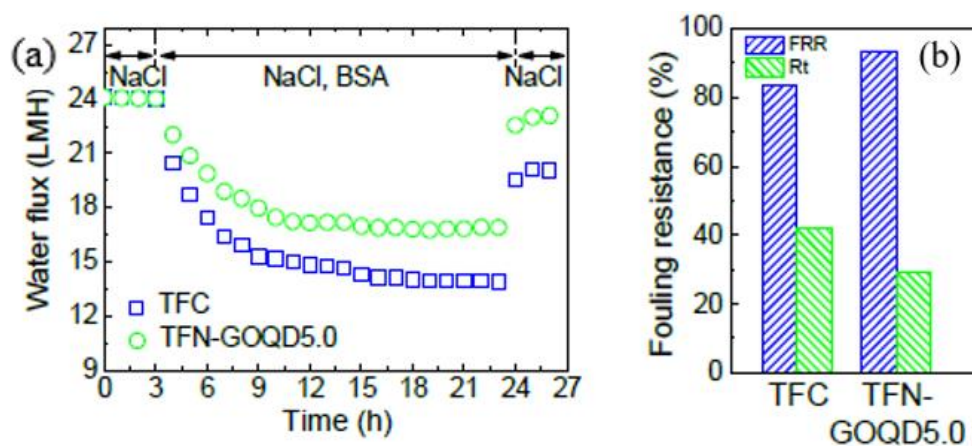


Figure 4.35: (a) Antifouling Behaviour and (b) Fouling Resistance of the TFC and TFN Membranes (Song et al., 2016)

Table 4.5: Separation Performance of Carbon-based Quantum Dots Incorporated TFN NF Membranes

Type of Substrate	Type of Membrane/ Monomer	Type of Nanofiller	Contact Angle (°)	Zeta Potential (mV)	Testing Conditions	Pure Water Permeability (PWP) (L/m ² h bar)	Rejection (%)	References
PES	PIP TMC	Na-CQDs	NA	-125	10 bar 1000 ppm pH 7	10.4	MgCl ₂ – 92 NaCl – 50 MgSO ₄ – 96 Na ₂ SO ₄ – 94	(He, Zhao and Chung, 2018)
PSf	PIP TMC	CCQDs	30	-16	6 bar 5 mmol/L	6.08	MgCl ₂ – 46 NaCl – 18 MgSO ₄ – 81 Na ₂ SO ₄ – 93	(Sun and Wu, 2018)
		SCQDs	31	-18		7.02	MgCl ₂ – 32 NaCl – 9 MgSO ₄ – 84 Na ₂ SO ₄ – 93	

Table 4.5 (Continue)

Type of Substrate	Type of Membrane/ Monomer	Type of Nanofiller	Contact Angle (°)	Zeta Potential (mV)	Testing Conditions	Pure Water Permeability (PWP) (L/m ² h bar)	Rejection (%)	References
PSf	PIP TMC	NCQDs	30	-7	6 bar 5 mmol/L	5.25	MgCl ₂ – 75 NaCl – 31 MgSO ₄ – 87 Na ₂ SO ₄ – 91	(Sun and Wu, 2018)
PES	PEI TMC	CQDs	64	-5	6 bar 300 ppm pH 3	9.7	MgCl ₂ – 98 Lysine – 93	(Yang et al., 2020)

Table 4.5 (Continue)

Type of Substrate	Type of Membrane/ Monomer	Type of Nanofiller	Contact Angle (°)	Zeta Potential (mV)	Testing Conditions	Pure Water Permeability (PWP) (L/m ² h bar)	Rejection (%)	References
PES	PIP TMC	-	31	-17.5	6 bar 1000 ppm pH 7	6.4	MgCl ₂ – 98 NaCl – 37 MgSO ₄ – 99 Na ₂ SO ₄ – 98	(Shao et al., 2020)
		CQDs	28	-20		16.5	MgCl ₂ – 92 NaCl – 24 MgSO ₄ – 94 Na ₂ SO ₄ – 91	

Table 4.5 (Continue)

Type of Substrate	Type of Membrane/ Monomer	Type of Nanofiller	Contact Angle (°)	Zeta Potential (mV)	Testing Conditions	Pure Water Permeability (PWP) (L/m ² h bar)	Rejection (%)	References
PES	PEI TMC	CQDs-NH ₂	36.8	16.98	2 bar 2000 ppm pH 6.3 25 °C	11.98	MgCl ₂ – 94.65 LiCl – 22.86	(Guo et al., 2021)
PAN	IDPI TA	GOQDs	52.8	-15.5	2 bar 1000 ppm pH 7	9	MgCl ₂ – 10 NaCl – 18 MgSO ₄ – 30.5 Na ₂ SO ₄ – 65	(Zhang et al., 2017)
PSf	PIP TMC	AGQDs	30	-20	5.5 bar 2000 ppm pH 7 25 °C	18.5	MgCl ₂ – 42 MgSO ₄ – 91 Na ₂ SO ₄ – 98.4 NaCl – 30	(Wu et al., 2021)

Table 4.5 (Continue)

Type of Substrate	Type of Membrane/ Monomer	Type of Nanofiller	Contact Angle (°)	Zeta Potential (mV)	Testing Conditions	Pure Water Permeability (PWP) (L/m ² h bar)	Rejection (%)	References
PES	PIP TMC	-	38	-42	2 bar 100 ppm pH 7	7.5	Na ₂ SO ₄ – 90 OG – 91 CR – 98	(Bi et al., 2018)
		GQDs	16	-25		51	Na ₂ SO ₄ – 40 OG – 80 CR – 96	
PES	PEI TMC	GQDs-NH ₂	23	14	3 bar pH 7	11.94	MgCl ₂ – 96 CaCl ₂ – 95 MgSO ₄ – 91 Na ₂ SO ₄ – 80 NaCl – 26 LiCl – 26	(Xu et al., 2021)

Table 4.6: Separation Performance of Carbon-based Quantum Dots Incorporated TFN RO Membranes

Type of Substrate	Type of Membrane/ Monomer	Type of Nanofiller	Contact Angle (°)	Zeta Potential (mV)	Testing Conditions	Pure Water Permeability (PWP) (L/m ² h bar)	Rejection (%)	References
PSf	MPD TMC	CQDs	74	NA	15.5 bar 2000 ppm 25 °C	5.72	NaCl – 99	(Li, Li and Zhang, 2017b)
PES	MPD TMC	-	NA	NA	15 bar 2000 ppm	2.93	NaCl – 98.7	(Gai, Zhao and Chung, 2019)
		CQDs	NA	NA		1.98	NaCl – 97.8	
		Na-CQDs	NA	NA		4.27	NaCl – 98.6	

Table 4.6 (Continue)

Type of Substrate	Type of Membrane/ Monomer	Type of Nanofiller	Contact Angle (°)	Zeta Potential (mV)	Testing Conditions	Pure Water Permeability (PWP) (L/m ² h bar)	Rejection (%)	References
PSf	MPD TMC	GOQDs	48	-14	16 bar 2000 ppm	2.34	NaCl – 98.8	(Song et al., 2016)
PSf	MPD TMC	GOQD/AP	67	-42	16 bar 2000 ppm	2.48	NaCl – 98.4	(Li et al., 2019a)
PSf	MPD TMC	N-GOQDs	NA	NA	15 bar 2000 ppm	1.66	NaCl – 93	(Fathizadeh et al., 2019)
PK	MPD TMC	N/S-d- GOQDs	NA	NA	15 bar 2000 ppm 25 °C	5.89	NaCl – 97.1	(Shen et al., 2020)

CHAPTER 5

CONCLUSIONS AND RECOMMENDATIONS

5.1 Conclusions

Overall, all the objectives of this study were achieved. This study has evaluated and compiled the significant findings on the carbon-based quantum dots incorporated TFN membranes and the possible mechanism behind from previous works. The review mainly focuses on the incorporation method, membrane characteristics, and performance. The carbon-based quantum dots have demonstrated great potential in NF and RO membrane technology. In most of the previous studies reviewed, carbon-based quantum dots incorporated TFN membranes have shown a tremendous jump in performance compared to the pristine TFC membranes. It was found that the fabrication method of carbon-based quantum dots incorporated TFN membranes is very similar across different journals. The carbon-based quantum dots were mixed with aqueous phase monomers or organic phase monomers depending on the size of the quantum dots. The studies showed good compatibility of the quantum dots with a wide variety of amine and acyl chloride monomers.

In addition, carbon-based quantum dots had significant effects on the membrane characteristics. The surface roughness was inconsistent across the reviewed journals mainly due to the difference of the size of the quantum dot. Besides, oxygen-containing functional groups were observed after the introduction of carbon-based quantum dots which indicates the improved hydrophilicity as it allows the membrane to form more hydrogen bond with water.

The membrane performance was improved significantly with a little amount of carbon-based quantum dots. It was noticed that functionalized carbon-based quantum dots were more effective than pristine carbon-based quantum dots in terms of improving membrane performance such as water flux and salt rejection. Furthermore, the addition of carbon-based quantum dots into the PA matrix also helps to overcome the conventional limitation of filtration membrane, which is membrane fouling. It can be attributed to the increased hydrophilicity which can form a water film to protect the membrane surface from foulants. Moreover, the increased surface charge also plays an important

role as it allows the membrane to repel the foulants that have similar charge with the membrane surface. All in all, carbon-based quantum dots have shown excellent results in enhancing the membrane characteristics and performance.

5.2 Recommendations for Future Work

Although the carbon-based quantum dots have shown impressive results, continuous research is required to overcome the limitations. Firstly, the concentration of carbon-based quantum dots should be optimized according to different membrane materials and monomers as the concentration have a huge impact on the membrane performance. On one hand, at high concentration of carbon-based quantum dots, agglomerates may form which will increase the membrane surface roughness and lead to serious fouling. On the other hand, low concentration of carbon-based quantum dots may not improve the membrane performance as significant. Thus, further analysis should be carried out to optimize the concentration of carbon-based quantum dots in order to maximize the membrane performance.

Secondly, most of the synthesis of carbon-based quantum dots are synthesized from chemical which is neither sustainable in long term nor feasible in large scale fabrication. Hence, the synthesis of carbon-based quantum dots from sustainable resource should be further investigated to enable to application of carbon-based quantum dots incorporated TFN membranes in real world.

Additionally, a commonly encountered problem for NPs embedded membranes is the leaching of NPs from membranes. Thus, further identification on the practical means to form chemical bonds between carbon-based quantum dots and the polymeric membranes should be done to ensure the stability of carbon-based quantum dots in the membrane matrix.

Last but not least, all of the previous studies included in this review are only limited to lab-scale and the large-scale fabrication of the TFN membranes have not been investigated expansively. Therefore, continuous research on the membranes at pilot-scale are required to enable the application of carbon-based quantum dots in the industry.

REFERENCES

- Abdel-Fatah, M.A., 2018. Nanofiltration systems and applications in wastewater treatment: Review article. *Ain Shams Engineering Journal*, 9(4), pp.3077–3092.
- Ahn, C.H., Baek, Y., Lee, C., Kim, S.O., Kim, S., Lee, S., Kim, S.H., Bae, S.S., Park, J. and Yoon, J., 2012. Carbon nanotube-based membranes: Fabrication and application to desalination. *Journal of Industrial and Engineering Chemistry*, 18(5), pp.1551–1559.
- Al-anzi, B.S. and Siang, O.C., 2017. Recent developments of carbon based nanomaterials and membranes for oily wastewater treatment. *RSC Advances*, 7(34), pp.20981–20994.
- Amjadi, M., Manzoori, J.L. and Hallaj, T., 2014. Chemiluminescence of graphene quantum dots and its application to the determination of uric acid. *Journal of Luminescence*, 153, pp.73–78.
- Anwar, S., Ding, H., Xu, M., Hu, X., Li, Z., Wang, J., Liu, L., Jiang, L., Wang, D., Dong, C., Yan, M., Wang, Q. and Bi, H., 2019. Recent Advances in Synthesis , Optical Properties , and Biomedical Applications of Carbon Dots. *ACS Applied Bio Materials*, 2, pp.2317–2338.
- Apuke, O., 2017. Quantitative Research Methods : A Synopsis Approach. *Arabian Journal of Business and Management Review (kuwait Chapter)*., 6, pp.40–47.
- Arora, N. and Sharma, N.N., 2014. Diamond & Related Materials Arc discharge synthesis of carbon nanotubes : Comprehensive review. *Diamond & Related Materials*, 50, pp.135–150.
- Bai, L., Bossa, N., Qu, F., Winglee, J., Li, G., Sun, K., Liang, H. and Wiesner, M.R., 2017. Comparison of Hydrophilicity and Mechanical Properties of Nanocomposite Membranes with Cellulose Nanocrystals and Carbon Nanotubes. *Environmental Science & Technology*, 51(1), pp.253–262.
- Baker, R.W., 2012a. *Membrane Transport Theory*. Wiley Online Books. *Membrane Technology and Applications*, pp.15-96.
- Baker, R.W., 2012b. *Overview of Membrane Science and Technology*. Wiley Online Books. *Membrane Technology and Applications*, pp.1-14.
- Bano, S., Mahmood, A., Kim, S.J. and Lee, K.H., 2015. Graphene Oxide Modified Polyamide Nanofiltration Membrane with Improved Flux and Antifouling Properties. *J. Mater. Chem. A*, 3(5), p.2065.

Bellona, C., 2014. *Nanofiltration – Theory and Application*. Wiley Online Books. *Desalination*, pp.205-253.

Bernstein, R., Antón, E. and Ulbricht, M., 2013. Tuning the nanofiltration performance of thin film strong polyelectrolyte hydrogel composite membranes by photo-grafting conditions. *Journal of Membrane Science*, 427, pp.129–138.

Bi, R., Zhang, Q., Zhang, R., Su, Y. and Jiang, Z., 2018. Thin film nanocomposite membranes incorporated with graphene quantum dots for high flux and antifouling property. *Journal of Membrane Science*, 553, pp.17–24.

Bi, R., Zhang, R., Shen, J., Liu, Y., He, M. and You, X., 2019. Graphene quantum dots engineered nanofiltration membrane for ultrafast molecular separation. *Journal of Membrane Science*, 572(92), pp.504–511.

Bourlinos, A.B., Stassinopoulos, A., Anglos, D., Zboril, R., Karakassides, M. and Giannelis, E.P., 2008. Surface functionalized carbogenic quantum dots. *Small*, 4(4), pp.455–458.

Van der Bruggen, B., Mänttari, M. and Nyström, M., 2008. Drawbacks of applying nanofiltration and how to avoid them: A review. *Separation and Purification Technology*, 63(2), pp.251–263.

Buonomenna, M.G., Lopez, L.C., Davoli, M., Favia, P., d’Agostino, R. and Drioli, E., 2009. Polymeric membranes modified via plasma for nanofiltration of aqueous solution containing organic compounds. *Microporous and Mesoporous Materials*, 120(1–2), pp.147–153.

Cadotte, J., 1981. *Reverse osmosis membrane*. 4259183.

Cao, L.I., Meziani, M.J. and Sahu, S., 2013. Photoluminescence Properties of Graphene versus Other Carbon Nanomaterials. *Accounts of Chemical Research*, 46(1), pp.171–180.

Chambers, L., 1997. Evidence-Based Healthcare: How to Make Health Policy and Management Decisions. *Canadian Medical Association Journal*, 157.

Chang, H. and Wu, H., 2013. Graphene-Based Nanomaterials: Synthesis, Properties, and Optical and Optoelectronic Applications. *Advanced Functional Materials*, 23(16), pp.1984–1997.

Chen, W., Lv, G., Hu, W., Li, D., Chen, S. and Dai, Z., 2018. Synthesis and applications of graphene quantum dots: a review. *Nanotechnology Reviews*, 7(2), pp.157–185.

Colburn, A., Wanninayake, N., Kim, D.Y. and Bhattacharyya, D., 2018. Cellulose-graphene quantum dot composite membranes using ionic liquid. *Journal of Membrane Science*, 556(February), pp.293–302.

Cong, S. and Zhao, Z., 2018. Carbon Quantum Dots: A Component of Efficient Visible Light Photocatalysts. *Visible-Light Photocatalysis of Carbon-Based Materials*, pp.47–66.

Daraei, P., Madaeni, S.S., Ghaemi, N., Salehi, E., Khadivi, M.A., Moradian, R. and Astinchap, B., 2012. Novel polyethersulfone nanocomposite membrane prepared by PANI/Fe₃O₄ nanoparticles with enhanced performance for Cu(II) removal from water. *Journal of Membrane Science*, 415–416, pp.250–259.

Deng, H., Xu, Y., Chen, Q., Wei, X. and Zhu, B., 2011. High flux positively charged nanofiltration membranes prepared by UV-initiated graft polymerization of methacrylateoethyl trimethyl ammonium chloride (DMC) onto polysulfone membranes. *Journal of Membrane Science*, 366(1–2), pp.363–372.

Deng, J., Lu, Q., Li, H., Zhang, Y. and Yao, S., 2015. Large scale preparation of graphene quantum dots from graphite oxide in pure water via one-step electrochemical tailoring. *RSC Advances*, 5(38), pp.29704–29707.

Deng, J., Lu, Q., Mi, N., Li, H., Liu, M., Xu, M., Tan, L. and Xie, Q., 2014. Electrochemical Synthesis of Carbon Nanodots Directly from Alcohols. pp.4993–4999.

Fane, A., Waite, T. and Schaefer, A., 2004. *Nanofiltration*. 1st ed. Oxford, UK: Elsevier Advanced Technology, pp.1-560.

Fang, W., Shi, L. and Wang, R., 2014. Mixed polyamide-based composite nanofiltration hollow fiber membranes with improved low-pressure water softening capability. *Journal of Membrane Science*, 468, pp.52–61.

Fang, Y., Xu, Z.-K. and Wu, J., 2013. *Surface Modification of Membranes*. Major Reference Works. *Encyclopedia of Membrane Science and Technology*, pp.1-15.

Fathizadeh, M., Tien, H.N., Khivantsev, K., Song, Z., Zhou, F. and Yu, M., 2019. Polyamide/nitrogen-doped graphene oxide quantum dots (N-GOQD) thin film nanocomposite reverse osmosis membranes for high flux desalination. *Desalination*, 451(June 2017), pp.125–132.

Fibiger, R., Koo, J.Y., Forgach, D., Peterson, R., Schmidt, D., Wessling, R. and Stocker, T., 1989. *Novel polyamide reverse osmosis membranes*. 4859384.

Fried, J.R., 1997. Basic Principles of Membrane Technology. *Journal of the American Chemical Society*, 119(36), p.8582.

Gai, W., Zhao, D.L. and Chung, T.S., 2019. Thin film nanocomposite hollow fiber membranes comprising Na⁺-functionalized carbon quantum dots for brackish water desalination. *Water Research*, 154, pp.54–61.

Gao, N., Huang, L., Li, T., Song, J., Hu, H., Liu, Y. and Ramakrishna, S., 2020. Application of carbon dots in dye-sensitized solar cells: A review. *Journal of Applied Polymer Science*, 137(10), p.48443.

Ge, S., He, J., Ma, C., Liu, J., Xi, F. and Dong, X., 2019. One-step synthesis of boron-doped graphene quantum dots for fluorescent sensors and biosensor. *Talanta*, 199, pp.581–589.

Green, B.N., Johnson, C.D. and Adams, A., 2006. Writing narrative literature reviews for peer-reviewed journals: secrets of the trade. *Journal of chiropractic medicine*, 5(3), pp.101–117.

Guan, W., Gu, W., Ye, L., Guo, C., Su, S., Xu, P. and Xue, M., 2014. Microwave-assisted polyol synthesis of carbon nitride dots from folic acid for cell imaging. *International Journal of Nanomedicine*, 9(1), pp.5071–5078.

Guo, C., Qian, X., Tian, F., Li, N., Wang, W. and Xu, Z., 2021. Amino-rich carbon quantum dots ultrathin nanofiltration membranes by double “one-step” methods: Breaking through trade-off among separation, permeation and stability. *Chemical Engineering Journal*, 404, p.127144.

Guo, Y., Zhang, L., Cao, F. and Leng, Y., 2016. Thermal treatment of hair for the synthesis of sustainable carbon quantum dots and the applications for sensing Hg²⁺. *Scientific Reports*, 6(October), pp.1–7.

Hadj Lajimi, R., Ferjani, E., Roudesli, M.S. and Deratani, A., 2011. Effect of LbL surface modification on characteristics and performances of cellulose acetate nanofiltration membranes. *Desalination*, 266(1), pp.78–86.

Hao, Y., Li, Q., He, B., Liao, B., Li, X., Hu, M., Ji, Y., Cui, Z., Younas, M. and Li, J., 2020. An ultrahighly permeable-selective nanofiltration membrane mediated by an in situ formed interlayer. *Journal of Materials Chemistry A*, 8(10), pp.5275–5283.

He, G., Song, Y., Liu, K., Walter, A., Chen, S. and Chen, S., 2013. Oxygen Reduction Catalyzed by Platinum Nanoparticles Supported on Graphene Quantum Dots. *ACS Catalysis*, 3(5), pp.831–838.

He, P., Sun, J., Tian, S., Yang, S., Ding, S., Ding, G., Xie, X. and Jiang, M., 2015. Processable Aqueous Dispersions of Graphene Stabilized by Graphene Quantum Dots. *Chemistry of Materials*, 27(1), pp.218–226.

He, Y., Zhao, D.L. and Chung, T.-S., 2018. Na⁺ functionalized carbon quantum dot incorporated thin-film nanocomposite membranes for selenium and arsenic removal. *Journal of Membrane Science*, 564, pp.483–491.

Hou, Y., Lu, Q., Deng, J., Li, H. and Zhang, Y., 2015. Analytica Chimica Acta One-pot electrochemical synthesis of functionalized fluorescent carbon dots and their selective sensing for mercury ion. *Analytica Chimica Acta*, pp.1–6.

Hu, M. and Mi, B., 2014. Layer-by-layer assembly of graphene oxide membranes via electrostatic interaction. *Journal of Membrane Science*, 469, pp.80–87.

Hu, S., Niu, K., Sun, J., Yang, J., Zhao, N. and Du, X., 2009. One-step synthesis of fluorescent carbon nanoparticles by laser irradiation †. *Journal of Materials Chemistry*, 19, pp.484–488.

Huang, S.H., Hsu, C.J., Liaw, D.J., Hu, C.C., Lee, K.R. and Lai, J.Y., 2008. Effect of chemical structures of amines on physicochemical properties of active layers and dehydration of isopropanol through interfacially polymerized thin-film composite membranes. *Journal of Membrane Science*, 307(1), pp.73–81.

Jeong, B., Hoek, E.M. V, Yan, Y., Subramani, A., Huang, X., Hurwitz, G., Ghosh, A.K. and Jawor, A., 2007. Interfacial polymerization of thin film nanocomposites : A new concept for reverse osmosis membranes. *Journal of Membrane Science*, 294(1–2), pp.1–7.

Ji, Y.-L., An, Q.-F., Guo, Y.-S., Hung, W.-S., Lee, K.-R. and Gao, C.-J., 2016. Bio-inspired fabrication of high perm-selectivity and anti-fouling membranes based on zwitterionic polyelectrolyte nanoparticles. *Journal of Materials Chemistry A*, 4(11), pp.4224–4231.

Jiang, K., Wang, Y., Gao, X., Cai, C. and Lin, H., 2018. Facile, Quick, and Gram-Scale Synthesis of Ultralong-Lifetime Room-Temperature-Phosphorescent Carbon Dots by Microwave Irradiation. *Angewandte Chemie - International Edition*, 57(21), pp.6216–6220.

Kang, S., Ryu, J.H., Lee, B., Jung, K.H., Shim, K.B., Han, H. and Kim, K.M., 2019. Laser wavelength modulated pulsed laser ablation for selective and efficient production of graphene quantum dots. *RSC Advances*, 9(24), pp.13658–13663.

Khorshidi, B., Hajinasiri, J., Ma, G., Bhattacharjee, S. and Sadrzadeh, M., 2016a. Thermally resistant and electrically conductive PES/ITO nanocomposite membrane. *Journal of Membrane Science*, 500, pp.151–160.

Khorshidi, B., Thundat, T., Fleck, B.A. and Sadrzadeh, M., 2016b. A novel approach toward fabrication of high performance thin film composite polyamide membranes. *Scientific Reports*, 6(February), pp.1–10.

Kim, E.S., Yu, Q. and Deng, B., 2011. Plasma surface modification of nanofiltration (NF) thin-film composite (TFC) membranes to improve anti organic fouling. *Applied Surface Science*, 257(23), pp.9863–9871.

King, D., 2001. Evidence-Based Medicine: A Framework for Clinical Practice. *Evidence Based Medicine*, 6(4), pp.103 LP – 103.

Kolbasov, A., Sinha-Ray, S., Yarin, A.L. and Pourdeyhimi, B., 2017. Heavy metal adsorption on solution-blown biopolymer nanofiber membranes. *Journal of Membrane Science*, 530, pp.250–263.

Lai, C.W., Hsiao, Y.H., Peng, Y.K. and Chou, P.T., 2012. Facile synthesis of highly emissive carbon dots from pyrolysis of glycerol; Gram scale production of carbon dots/mSiO₂ for cell imaging and drug release. *Journal of Materials Chemistry*, 22(29), pp.14403–14409.

Lai, G.S., Lau, W.J., Goh, P.S., Ismail, A.F., Tan, Y.H., Chong, C.Y., Krause-Rehberg, R. and Awad, S., 2018. Tailor-made thin film nanocomposite membrane incorporated with graphene oxide using novel interfacial polymerization technique for enhanced water separation. *Chemical Engineering Journal*, 344(March), pp.524–534.

Lai, G.S., Lau, W.J., Goh, P.S., Tan, Y.H., Ng, B.C. and Ismail, A.F., 2019. A novel interfacial polymerization approach towards synthesis of graphene oxide-incorporated thin film nanocomposite membrane with improved surface properties. *Arabian Journal of Chemistry*, 12, pp.75–87.

Lai, G.S., Lau, W.J., Gray, S.R., Matsuura, T., Gohari, R.J., Subramanian, M.N., Lai, S.O., Ong, C.S., Ismail, A.F., Emazadah, D. and Ghanbari, M., 2016. A practical approach to synthesize polyamide thin film nanocomposite (TFN) membranes with improved separation properties for water/wastewater treatment. *Journal of Materials Chemistry A*, 4(11), pp.4134–4144.

Lasquelles, V., Marcq, J., Sbai, M., Filmon, R., Nguyen, T.Q., Nardi, F. and Maxime, P., 2007. Nouvelle stratégie antibiofilm par dépôt LBL d'un polyélectrolyte cationique sur la membrane de dialyse anionique AN69. *Revue des sciences de l'eau*, 20, p.175.

Lau, W.J., Ismail, A.F., Misdan, N. and Kassim, M.A., 2012. A recent progress in thin film composite membrane: A review. *Desalination*, 287(April 2019), pp.190–199.

Lee, K.P., Arnot, T.C. and Mattia, D., 2011. A review of reverse osmosis membrane materials for desalination-Development to date and future potential. *Journal of Membrane Science*, 370(1–2), pp.1–22.

Lee, S.Y., Kim, H.J., Patel, R., Im, S.J., Kim, J.H. and Min, B.R., 2007. Silver nanoparticles immobilized on thin film composite polyamide membrane: characterization, nanofiltration, antifouling properties. *Polymers for Advanced Technologies*, 18(7), pp.562–568.

Li, H., He, X., Kang, Z., Huang, H., Liu, Y., Liu, J., Lian, S., Tsang, C.H.A., Yang, X. and Lee, S., 2010. Zuschriften Water-Soluble Fluorescent Carbon Quantum Dots and Photocatalyst Design **. *Angew. Chem*, 122, pp.4532–4536.

Li, H., Kang, Z., Liu, Y. and Lee, S.T., 2012a. Carbon nanodots: Synthesis, properties and applications. *Journal of Materials Chemistry*, 22(46), pp.24230–24253.

Li, L.-L., Ji, J., Fei, R., Wang, C.-Z., Lu, Q., Zhang, J.-R., Jiang, L.-P. and Zhu, J.-J., 2012b. A Facile Microwave Avenue to Electrochemiluminescent Two-Color Graphene Quantum Dots. *Advanced Functional Materials*, 22(14), pp.2971–2979.

Li, L., Wu, G., Yang, G., Peng, J., Zhao, J. and Zhu, J.-J., 2013. Focusing on luminescent graphene quantum dots: current status and future perspectives. *Nanoscale*, 5(10), pp.4015–4039.

Li, S., Gao, B., Wang, Y., Jin, B., Yue, Q. and Wang, Z., 2019a. Antibacterial thin film nanocomposite reverse osmosis membrane by doping silver phosphate loaded graphene oxide quantum dots in polyamide layer. *Desalination*, 464(March), pp.94–104.

Li, S., Li, C., Song, X., Su, B., Mandal, B., Prasad, B., Gao, X. and Gao, C., 2019b. Graphene Quantum Dots-Doped Thin Film Nanocomposite Polyimide Membranes with Enhanced Solvent Resistance for Solvent-Resistant Nanofiltration. *ACS Applied Materials and Interfaces*, 11, pp.6527–6540.

Li, S., Li, C., Su, B., Hu, M.Z., Gao, X. and Gao, C., 2019c. Amino-functionalized graphene quantum dots (aGQDs)-embedded thin film nanocomposites for solvent resistant nanofiltration (SRNF) membranes based on covalence interactions. *Journal of Membrane Science*, 588(May), p.117212.

Li, X., Cao, Y., Yu, H., Kang, G., Jie, X., Liu, Z. and Yuan, Q., 2014. A novel composite nanofiltration membrane prepared with PHGH and TMC by interfacial polymerization. *Journal of Membrane Science*, 466, pp.82–91.

Li, X., Rui, M., Song, J., Shen, Z. and Zeng, H., 2015a. Carbon and Graphene Quantum Dots for Optoelectronic and Energy Devices: A Review. *Advanced Functional Materials*, 25(31), pp.4929–4947.

Li, X., Wang, H., Shimizu, Y., Pyatenko, A., Kawaguchi, K. and Koshizaki, N., 2011a. Preparation of carbon quantum dots with tunable photoluminescence by rapid laser passivation in ordinary organic solvents. pp.932–934.

Li, X., Zhang, C., Zhang, S., Li, J., He, B. and Cui, Z., 2015b. Preparation and characterization of positively charged polyamide composite nanofiltration hollow fiber membrane for lithium and magnesium separation. *Desalination*, 369, pp.26–36.

Li, Y., Hu, Y., Zhao, Y., Shi, G., Deng, L., Hou, Y. and Qu, L., 2011b. An Electrochemical Avenue to Green-Luminescent Graphene Quantum Dots as Potential Electron-Acceptors for Photovoltaics. *Advanced Materials*, 23(6), pp.776–780.

Li, Y., Li, S. and Zhang, K., 2017a. Influence of hydrophilic carbon dots on polyamide thin film nanocomposite reverse osmosis membranes. *Journal of Membrane Science*, 537(May), pp.42–53.

Li, Y., Li, S. and Zhang, K., 2017b. Influence of hydrophilic carbon dots on polyamide thin film nanocomposite reverse osmosis membranes. *Journal of Membrane Science*, 537(April), pp.42–53.

Liang, Y., Li, C., Li, S., Su, B., Hu, M.Z. and Gao, X., 2020. Graphene quantum dots (GQDs) -polyethyleneimine as interlayer for the fabrication of high performance organic solvent nano filtration (OSN) membranes. *Chemical Engineering Journal*, 380(June 2019), p.122462.

Lin, Y., Shen, Q., Kawabata, Y., Segawa, J., Cao, X., Guan, K., Istirokhatun, T., Yoshioka, T. and Matsuyama, H., 2020. Graphene quantum dots (GQDs) - assembled membranes with intrinsic functionalized nanochannels for high-performance nanofiltration. *Chemical Engineering Journal*, (September), p.127602.

Linggawati, A., Mohammad, A.W. and Ghazali, Z., 2009. Effect of electron beam irradiation on morphology and sieving characteristics of nylon-66 membranes. *European Polymer Journal*, 45(10), pp.2797–2804.

- Linggawati, A., Mohammad, A.W. and Leo, C.P., 2012. Effects of APTEOS content and electron beam irradiation on physical and separation properties of hybrid nylon-66 membranes. *Materials Chemistry and Physics*, 133(1), pp.110–117.
- Liu, R., Wu, D., Feng, X. and Müllen, K., 2011. Bottom-up fabrication of photoluminescent graphene quantum dots with uniform morphology. *Journal of the American Chemical Society*, 133(39), pp.15221–15223.
- Lu, Q., Wu, C., Liu, D., Wang, H., Su, W., Li, H., Zhang, Y. and Yao, S., 2017. A facile and simple method for synthesis of graphene oxide quantum dots from black carbon. *Green Chemistry*, 19(4), pp.900–904.
- Lu, S., Sui, L., Wu, M., Zhu, S., Yong, X. and Yang, B., 2019. Graphitic Nitrogen and High-Crystalline Triggered Strong Photoluminescence and Room-Temperature Ferromagnetism in Carbonized Polymer Dots. *Advanced Science*, 6(2), p.1801192.
- Ma, C.-B., Zhu, Z.-T., Wang, H.-X., Huang, X., Zhang, X., Qi, X., Zhang, H.-L., Zhu, Y., Deng, X., Peng, Y., Han, Y. and Zhang, H., 2015. A general solid-state synthesis of chemically-doped fluorescent graphene quantum dots for bioimaging and optoelectronic applications. *Nanoscale*, 7(22), pp.10162–10169.
- Maddah, H.A., Alzhrani, A.S., Aziz, M.H.A. and Zoromba, M., 2018. Evaluation of various membrane filtration modules for the treatment of seawater. *Applied Water Science*, 8(6), pp.1–13.
- Melo, J.P., Ríos, P.L., Povea, P., Morales-Verdejo, C. and Camarada, M.B., 2018. Graphene Oxide Quantum Dots as the Support for the Synthesis of Gold Nanoparticles and Their Applications as New Catalysts for the Decomposition of Composite Solid Propellants. *ACS Omega*, 3(7), pp.7278–7287.
- Mendret, J., Hatat-Fraile, M., Rivallin, M. and Brosillon, S., 2013. Hydrophilic composite membranes for simultaneous separation and photocatalytic degradation of organic pollutants. *Separation and Purification Technology*, 111, pp.9–19.
- Mohammad, A.W., Teow, Y.H., Ang, W.L., Chung, Y.T., Oatley-Radcliffe, D.L. and Hilal, N., 2015. Nanofiltration membranes review: Recent advances and future prospects. *Desalination*, 356, pp.226–254.
- Namasivayam, M. and Shapter, J., 2017. Factors affecting carbon nanotube fillers towards enhancement of thermal conductivity in polymer nanocomposites: A review. *Journal of Composite Materials*, 51(26), pp.3657–3668.

Namvar-Mahboub, M. and Pakizeh, M., 2013. Development of a novel thin film composite membrane by interfacial polymerization on polyetherimide/modified SiO₂ support for organic solvent nanofiltration. *Separation and Purification Technology*, 119, pp.35–45.

Ng, L.Y., Mohammad, A.W., Leo, C.P. and Hilal, N., 2013. Polymeric membranes incorporated with metal/metal oxide nanoparticles: A comprehensive review. *Desalination*, 308, pp.15–33.

Ng, L.Y., Mohammad, A.W., Ng, C.Y., Leo, C.P. and Rohani, R., 2014. Development of nanofiltration membrane with high salt selectivity and performance stability using polyelectrolyte multilayers. *Desalination*, 351, pp.19–26.

Nurunnabi, M., Khatun, Z., Huh, K.M., Park, S.Y., Lee, D.Y., Cho, K.J. and Lee, Y., 2013. In Vivo Biodistribution and Toxicology of Carboxylated Graphene Quantum Dots. *ACS Nano*, 7(8), pp.6858–6867.

Ostarcevic, E.R., Jacangelo, J., Gray, S.R. and Cran, M.J., 2018. Current and Emerging Techniques for High-Pressure Membrane Integrity Testing. *Membranes*, 8(60), pp.1–27.

Pan, D., Zhang, J., Li, Z. and Wu, M., 2010. Hydrothermal Route for Cutting Graphene Sheets into Blue-Luminescent Graphene Quantum Dots. *Advanced Materials*, 22(6), pp.734–738.

Petersen, R.J., 1993. Composite reverse osmosis and nanofiltration membranes. *Journal of Membrane Science*, 83(1), pp.81–150.

Pinnau, I. and Freeman, B., 1999. *Membrane Formation and Modification*. American Chemical Society.

Qiu, C., Nguyen, Q.T. and Ping, Z., 2007. Surface modification of cardo polyetherketone ultrafiltration membrane by photo-grafted copolymers to obtain nanofiltration membranes. *Journal of Membrane Science*, 295(1–2), pp.88–94.

Qu, D., Zheng, M., Zhang, L., Zhao, H., Xie, Z., Jing, X., Haddad, R.E., Fan, H. and Sun, Z., 2014. Formation mechanism and optimization of highly luminescent N-doped graphene quantum dots. *Scientific Reports*, 4, pp.1–9.

Rai, S., Singh, B.K., Bhartiya, P., Singh, A., Kumar, H., Dutta, P.K. and Mehrotra, G.K., 2017. Lignin derived reduced fluorescence carbon dots with theranostic approaches: Nano-drug-carrier and bioimaging. *Journal of Luminescence*, 190, pp.492–503.

- Rajaeian, B., Rahimpour, A., Tade, M.O. and Liu, S., 2013. Fabrication and characterization of polyamide thin film nanocomposite (TFN) nanofiltration membrane impregnated with TiO₂ nanoparticles. *Desalination*, 313, pp.176–188.
- Ran, C., Wang, M., Gao, W., Yang, Z., Shao, J., Deng, J. and Song, X., 2014. A general route to enhance the fluorescence of graphene quantum dots by Ag nanoparticles. *RSC Advances*, 4(42), pp.21772–21776.
- Ran, X., Sun, H., Pu, F., Ren, J. and Qu, X., 2013. Ag Nanoparticle-decorated graphene quantum dots for label-free, rapid and sensitive detection of Ag⁺ and biothiols. *Chemical Communications*, 49(11), pp.1079–1081.
- Roy, P., Chen, P., Periasamy, A.P., Chen, Y. and Chang, H., 2015. Photoluminescent carbon nanodots : synthesis , physicochemical properties and analytical applications. *Biochemical Pharmacology*, 00(00), pp.1–12.
- Russo, P., Liang, R., Jabari, E., Marzbanrad, E., Toyserkani, E. and Zhou, Y.N., 2016. Single-step synthesis of graphene quantum dots by femtosecond laser ablation of graphene oxide dispersions. *Nanoscale*, 8(16), pp.8863–8877.
- Sarno, M., Tamburrano, A., Arurault, L., Fontorbes, S., Pantani, R., Datas, L., Ciambelli, P. and Sarto, M.S., 2013. Electrical conductivity of carbon nanotubes grown inside a mesoporous anodic aluminium oxide membrane. *Carbon*, 55, pp.10–22.
- Schaep, J., Van der Bruggen, B., Vandecasteele, C. and Wilms, D., 1998. Retention mechanisms in nanofiltration. *Chemistry for the Protection of the Environment*, 3, pp.117–125.
- Schwenke, A.M., Hoepfner, S. and Schubert, U.S., 2015. Synthesis and Modification of Carbon Nanomaterials utilizing Microwave Heating. *Advanced Materials*, 27(28), pp.4113–4141.
- Shao, D.D., Yang, W.J., Xiao, H.F., Wang, Z.Y., Zhou, C., Cao, X.L. and Sun, S.P., 2020. Self-Cleaning Nanofiltration Membranes by Coordinated Regulation of Carbon Quantum Dots and Polydopamine. *ACS Applied Materials and Interfaces*, 12(1), pp.580–590.
- Shen, J., Zhu, Y., Chen, C., Yang, X. and Li, C., 2011. Facile preparation and upconversion luminescence of graphene quantum dots. *Chemical Communications*, 47(9), pp.2580–2582.

Shen, Q., Lin, Y., Kawabata, Y., Jia, Y., Zhang, P., Akther, N., Guan, K., Yoshioka, T., Shon, H. and Matsuyama, H., 2020. Engineering Heterostructured Thin-Film Nanocomposite Membrane with Functionalized Graphene Oxide Quantum Dots (GOQD) for Highly Efficient Reverse Osmosis. *ACS Applied Materials and Interfaces*, 12(34), pp.38662–38673.

Shen, Z., Zhang, C., Yu, X., Li, J., Wang, Z., Zhang, Z. and Liu, B., 2018. Microwave-assisted synthesis of cyclen functional carbon dots to construct a ratiometric fluorescent probe for tetracycline detection. *Journal of Materials Chemistry C*, 6(36), pp.9636–9641.

Shirke, Y.M., Abou-elanwar, A.M., Choi, W., Lee, H., Hong, S., Lee, H. and Jeon, J.-D., 2019. Influence of nitrogen/phosphorus-doped carbon dots on polyamide thin film membranes for water vapor/N₂ mixture gas separation. *RSC Advances*, 9, pp.32121–32129.

Shon, H., Phuntsho, S., Chaudhary, D., Vigneswaran, S. and Cho, J., 2013. Nanofiltration for water and wastewater treatment – a mini review. *Drinking Water Engineering and Science*, 6, pp.47–53.

Singh, I., Arora, R., Dhiman, H. and Pahwa, R., 2018. Carbon quantum dots: Synthesis, characterization and biomedical applications. *Turkish Journal of Pharmaceutical Sciences*, 15(2), pp.219–230.

Slavin, R.E., 1995. Best evidence synthesis: An intelligent alternative to meta-analysis. *Journal of Clinical Epidemiology*, 48(1), pp.9–18.

Snyder, H., 2019. Literature review as a research methodology: An overview and guidelines. *Journal of Business Research*, 104, pp.333–339.

Song, X., Zhou, Q., Zhang, T., Xu, H. and Wang, Z., 2016. Pressure-assisted Preparation of Graphene Oxide Quantum Dot Incorporated Reverse Osmosis Membranes: Antifouling and Chlorine Resistance Potentials. *J. Mater. Chem. A*, 4(43), p.16896.

Sun, H. and Wu, P., 2018. Tuning the functional groups of carbon quantum dots in thin film nanocomposite membranes for nanofiltration. *Journal of Membrane Science*, 564(April), pp.394–403.

Sun, Y., Zhou, B., Lin, Y., Wang, W., Fernando, K.A.S., Pathak, P., Meziani, M.J., Harruff, B.A., Wang, X., Wang, H., Luo, P.G., Yang, H., Kose, M.E., Chen, B., Veca, L.M., Xie, S. and Carolina, S., 2006. Quantum-Sized Carbon Dots for Bright and Colorful Photoluminescence. (Figure 2), pp.7756–7757.

Tabish, T.A. and Zhang, S., 2019. *Graphene quantum dots: Syntheses, properties, and biological applications. Comprehensive Nanoscience and Nanotechnology*, Elsevier Ltd.

Tadesse, A., Hagos, M., RamaDevi, D., Basavaiah, K. and Belachew, N., 2020. Fluorescent-Nitrogen-Doped Carbon Quantum Dots Derived from Citrus Lemon Juice: Green Synthesis, Mercury(II) Ion Sensing, and Live Cell Imaging. *ACS Omega*, 5(8), pp.3889–3898.

Tajik, S., Dourandish, Z., Zhang, K., Beitollahi, H., Le, Q. Van, Jang, H.W. and Shokouhimehr, M., 2020. Carbon and graphene quantum dots: a review on syntheses, characterization, biological and sensing applications for neurotransmitter determination. *RSC Advances*, 10(26), pp.15406–15429.

Tsuru, T., Sasaki, S., Kamada, T., Shintani, T., Ohara, T., Nagasawa, H., Nishida, K., Kanezashi, M. and Yoshioka, T., 2013. Multilayered polyamide membranes by spray-assisted 2-step interfacial polymerization for increased performance of trimesoyl chloride (TMC)/m-phenylenediamine (MPD)-derived polyamide membranes. *Journal of Membrane Science*, 446, pp.504–512.

Vatanpour, V., Madaeni, S.S., Rajabi, L., Zinadini, S. and Derakhshan, A.A., 2012. Boehmite Nanoparticles as A New Nanofiller for Preparation of Antifouling Mixed Matrix Membranes. *J. Membr. Sci.*, 401–402, p.132.

Wang, J.-J., Yang, H.-C., Wu, M.-B., Zhang, X. and Xu, Z.-K., 2017. Nanofiltration membranes with cellulose nanocrystals as an interlayer for unprecedented performance. *Journal of Materials Chemistry A*, 5(31), pp.16289–16295.

Wang, J., Liu, G., Leung, K., Loffroy, R., Lu, P.-X. and J. Wáng, Y., 2015. Opportunities and Challenges of Fluorescent Carbon Dots in Translational Optical Imaging. *Current Pharmaceutical Design*, 21(37), pp.5401–5416.

Wang, X., Feng, Y., Dong, P. and Huang, J., 2019. A Mini Review on Carbon Quantum Dots : Preparation , Properties , and Electrocatalytic Application. 7(October), pp.1–9.

Wang, X. lei, Wei, J. fu, Dai, Z., Zhao, K. yin and Zhang, H., 2012. Preparation and characterization of negatively charged hollow fiber nanofiltration membrane by plasma-induced graft polymerization. *Desalination*, 286, pp.138–144.

Wang, Y. and Hu, A., 2014. Carbon quantum dots: Synthesis, properties and applications. *Journal of Materials Chemistry C*, 2(34), pp.6921–6939.

Wei, W., Xu, C., Wu, L., Wang, J., Ren, J. and Qu, X., 2014. Non-enzymatic-browning-reaction: A versatile route for production of nitrogen-doped carbon dots with tunable multicolor luminescent display. *Scientific Reports*, 4(SREP03564).

- Wei, Y., Liu, H., Jin, Y., Cai, K., Li, H., Liu, Y., Kang, Z. and Zhang, Q., 2013. Carbon nanoparticle ionic liquid functionalized activated carbon hybrid electrode for efficiency enhancement in supercapacitors. *New Journal of Chemistry*, 37(4), pp.886–889.
- Wen, X., Yu, P., Toh, Y.-R., Ma, X. and Tang, J., 2014. On the upconversion fluorescence in carbon nanodots and graphene quantum dots. *Chem. Commun.*, 50, pp.4703–4706.
- Wenten, I.G. and Khoiruddin, 2016. Reverse osmosis applications: Prospect and challenges. *Desalination*, 391, pp.112–125.
- Wiles, L. and Peirtsegaale, E., 2018. Reverse Osmosis: A History and Explanation of the Technology and How It Became So Important for Desalination. In: *79th International Water Conference, Scottsdale*. pp.18–49.
- Woo, Y.C., Kim, S.-H., Shon, H.K. and Tijing, L.D., 2019. Introduction: Membrane Desalination Today, Past, and Future. In: *Current Trends and Future Developments on (Bio-) Membranes*. Elsevier. pp.xxv–xlvi.
- World Economic Forum, 2020. *The Global Risks Report 2020*. Geneva.
- Wu, C., Xie, Q., Hong, Z., Shen, L. and Yu, T., 2021. Thin-film nanocomposite nanofiltration membrane with enhanced desalination and antifouling performance via incorporating L-aspartic acid functionalized graphene quantum dots. *Desalination*, 498(June 2020), p.114811.
- Wu, X., Liu, S., Cui, X., Lin, J., Zhang, H., Zhang, J. and Wang, J., 2020. Manipulating microenvironments of nanochannels in lamellar membranes by quantum dots for highly enhanced nanofiltration performance. *Chemical Engineering Science*, 228, p.116001.
- Wu, X., Zhang, Y., Han, T., Wu, H., Guo, S. and Zhang, J., 2014. Composite of graphene quantum dots and Fe₃O₄ nanoparticles: peroxidase activity and application in phenolic compound removal. *RSC Advances*, 4(7), pp.3299–3305.
- Xie, W., Geise, G.M., Freeman, B.D., Lee, H.S., Byun, G. and McGrath, J.E., 2012. Polyamide interfacial composite membranes prepared from m-phenylene diamine, trimesoyl chloride and a new disulfonated diamine. *Journal of Membrane Science*, 403–404, pp.152–161.
- Xu, H. mei, Wei, J. fu and Wang, X. lei, 2014. Nanofiltration hollow fiber membranes with high charge density prepared by simultaneous electron beam radiation-induced graft polymerization for removal of Cr(VI). *Desalination*, 346, pp.122–130.

Xu, P., Hong, J., Xu, Z., Xia, H. and Ni, Q., 2021. Novel aminated graphene quantum dots (GQDs-NH₂)-engineered nanofiltration membrane with high Mg²⁺ / Li⁺ separation efficiency. *Separation and Purification Technology*, 258(P2), p.118042.

Xu, Q., Gong, Y., Zhang, Z., Miao, Y., Li, D. and Yan, G., 2019. Preparation of graphene oxide quantum dots from waste toner, and their application to a fluorometric DNA hybridization assay. *Microchimica Acta*, 186(7), p.483.

Xue, J., Shen, J., Zhang, R., Wang, F. and Liang, S., 2020. High-flux nanofiltration membranes prepared with β -cyclodextrin and graphene quantum dots. *Journal of Membrane Science*, 612(July), p.118465.

Xue, S.-M., Xu, Z.-L., Tang, Y.-J. and Ji, C.-H., 2016. Polypiperazine-amide Nanofiltration Membrane Modified by Different Functionalized Multiwalled Carbon Nanotubes (MWCNTs). *ACS Applied Materials & Interfaces*, 8(29), pp.19135–19144.

Yan, X., Li, Q. and Li, L., 2012. Formation and Stabilization of Palladium Nanoparticles on Colloidal Graphene Quantum Dots. *Journal of the American Chemical Society*, 134(39), pp.16095–16098.

Yang, W.J., Shao, D.D., Zhou, Z., Xia, Q.C., Chen, J., Cao, X.L., Zheng, T. and Sun, S.P., 2020. Carbon quantum dots (CQDs) nanofiltration membranes towards efficient biogas slurry valorization. *Chemical Engineering Journal*, 385(October 2019), p.123993.

Yang, Y., Wu, D., Han, S., Hu, P. and Liu, R., 2013. Bottom-up fabrication of photoluminescent carbon dots with uniform morphology via a soft-hard template approach. *Chemical Communications*, 49(43), pp.4920–4922.

Yang, Y., Zhang, H., Wang, P., Zheng, Q. and Li, J., 2007. The influence of nano-sized TiO₂ fillers on the morphologies and properties of PSF UF membrane. *Journal of Membrane Science*, 288(1), pp.231–238.

Yao, S., Hu, Y. and Li, G., 2014. A one-step sonoelectrochemical preparation method of pure blue fluorescent carbon nanoparticles under a high intensity electric field. *Carbon*, 66, pp.77–83.

Yi, Z., Shao, F., Yu, L., Song, N., Dong, H., Pang, B., Yu, J., Feng, J. and Dong, L., 2020. Chemical grafting N-GOQD of polyamide reverse osmosis membrane with improved chlorine resistance, water flux and NaCl rejection. *Desalination*, 479(January), p.114341.

Yin, J., Kim, E.S., Yang, J. and Deng, B.L., 2012. Fabrication of a Novel Thin-Film Nanocomposite (TFN) Membrane Containing MCM-41 Silica Nanoparticles (NPs) for Water Purification. *J. Membr. Sci.*, 423–424, p.238.

- Yuan, Z., Wu, X., Jiang, Y., Li, Y., Huang, J., Hao, L., Zhang, J. and Wang, J., 2018. Carbon dots-incorporated composite membrane towards enhanced organic solvent nanofiltration performance. *Journal of Membrane Science*, 549, pp.1–11.
- Zeng, Z., Yu, D., He, Z., Liu, J., Xiao, F.X., Zhang, Y., Tan, T.T.Y., Wang, R. and Bhattacharyya, D., 2016. Graphene Oxide Quantum Dots Covalently Functionalized PVDF Membrane with Significantly-Enhanced Bactericidal and Antibiofouling Performances. *Sci. Rep.*, 6, p.20142.
- Zhang, C., Cui, Y., Song, L., Liu, X. and Hu, Z., 2016a. Microwave assisted one-pot synthesis of graphene quantum dots as highly sensitive fluorescent probes for detection of iron ions and pH value. *Talanta*, 150, pp.54–60.
- Zhang, C., Wei, K., Zhang, W., Bai, Y., Sun, Y. and Gu, J., 2017. Graphene Oxide Quantum Dots Incorporated into a Thin Film Nanocomposite Membrane with High Flux and Antifouling Properties for Low-Pressure Nanofiltration. *ACS Applied Materials & Interfaces*, 9(12), pp.11082–11094.
- Zhang, L., Gu, J., Song, L., Chen, L., Huang, Y., Zhang, J. and Chen, T., 2016b. Underwater superoleophobic carbon nanotubes/core-shell polystyrene@Au nanoparticles composite membrane for flow-through catalytic decomposition and oil/water separation. *Journal of Materials Chemistry A*, 4(28), pp.10810–10815.
- Zhao, D.L. and Chung, T.S., 2018. Applications of carbon quantum dots (CQDs) in membrane technologies: A review. *Water Research*, 147, pp.43–49.
- Zhao, G., Hu, R., He, Y. and Zhu, H., 2019a. Physically Coating Nanofiltration Membranes with Graphene Oxide Quantum Dots for Simultaneously Improved Water Permeability and Salt/Dye Rejection. *Advanced Materials Interfaces*, 6(5), pp.1–11.
- Zhao, G., Hu, R., Li, J. and Zhu, H., 2019b. Graphene oxide quantum dots embedded polysulfone membranes with enhanced hydrophilicity, permeability and antifouling performance. *Science China Materials*, 62(8), pp.1177–1187.
- Zhao, S. and Wang, Z., 2017. A loose nano-filtration membrane prepared by coating HPAN UF membrane with modified PEI for dye reuse and desalination. *Journal of Membrane Science*, 524, pp.214–224.
- Zhong, P.S., Widjojo, N., Chung, T.S., Weber, M. and Maletzko, C., 2012. Positively charged nanofiltration (NF) membranes via UV grafting on sulfonated polyphenylenesulfone (sPPSU) for effective removal of textile dyes from wastewater. *Journal of Membrane Science*, 417–418, pp.52–60.

Zhu, H., Wang, X., Li, Y., Wang, Z., Yang, F. and Yang, X., 2009. Microwave synthesis of fluorescent carbon nanoparticles with electrochemiluminescence properties. *Chemical Communications*, (34), pp.5118–5120.

Zhu, J., Qin, L., Uliana, A., Hou, J., Wang, J., Zhang, Y., Li, X., Yuan, S., Li, J., Tian, M., Lin, J. and Van der Bruggen, B., 2017. Elevated Performance of Thin Film Nanocomposite Membranes Enabled by Modified Hydrophilic MOFs for Nanofiltration. *ACS Applied Materials & Interfaces*, 9(2), pp.1975–1986.

Zhu, S., Meng, Q., Wang, L., Zhang, J., Song, Y., Jin, H., Zhang, K., Sun, H., Wang, H. and Yang, B., 2013. Highly Photoluminescent Carbon Dots for Multicolor Patterning , Sensors , and Bioimaging. pp.1–6.

Zong, J., Zhu, Y., Yang, X., Shen, J. and Li, C., 2011. Synthesis of photoluminescent carbogenic dots using mesoporous silica spheres as nanoreactors. *Chemical Communications*, 47(2), pp.764–766.

Zuo, P., Lu, X., Sun, Z., Guo, Y. and He, H., 2016. A review on syntheses, properties, characterization and bioanalytical applications of fluorescent carbon dots. *Microchimica Acta*, 183(2), pp.519–542.